USAAML TECHNICAL REPORT 65-34

AN INVESTIGATION OF THE BEHAVIOR OF FLOATING RING DAMPERS AND THE DYNAMICS OF HYPERCRITICAL SHAFTS ON FLEXIBLE SUPPORTS

FINAL REPORT
UVA Report No. CE-3340-104-65U

By

J. A. Friedericy
R. T. Eppink
Y. N. Liu
A. Cetiner

June 1965

U. S. ARMY AVIATION MATERIEL LABORATORIES
FORT EUSTIS, VIRGINIA

GRANT DA-AMC-44-177-63-G10

UNIVERSITY OF VIRGINIA

DDC Availability Notices

Qualified requesters may obtain copies of this report from DDC.

This report has been furnished to the Department of Commerce for sale to the public.

Disclaimers

The findings in this report are not to be construed as an official Department of the Army position, unless so designated by other authorized documents.

When Government drawings, specifications, or other data are used for any purpose other than in connection with a definitely related Government procurement operation, the United States Government thereby incurs no responsibility nor any obligation whatsoever; and the fact that the Government may have formulated, furnished, or in any way supplied the said drawings, specifications, or other data is not to be regarded by implication or otherwise as in any manner licensing the holder or any other person or corporation, or conveying any rights or permission, to manufacture, use, or sell any patented invention that may in any way be related thereto.

Trade names cited in this report do not constitute an official indorsement or approval of the use of such commercial hardware or software.

Disposition Instructions

Destroy this report when it is no longer needed. Do not return it to the originator.

DEPARTMENT OF THE ARMY
U. S. ARMY AVIATION MATERIEL LABORATORIES
FORT EUSTIS, VIRGINIA 23604

This report represents a part of a USAAML research program to develop design criteria for power transmission shafts which will operate safely at or above many of their lateral critical speeds. The objective of this specific investigation was to augment the studies reported in ASD-TDR 62-728, Parts I and II, "Design Criteria For High-Speed Power Transmission Shafts", and to include an analysis of a floating multiring-type damper for application to a CH-47A helicopter drive system.

This Command concurs with the contractor's recommendations and conclusions reported herein. It is anticipated that a future analysis will be conducted to determine the allowable shaft unbalance for the establishment of fabrication tolerances.

Task 1P125901A01403
Grant DA-AMC-44-177-63-G10
USAAML Technical Report 65-34

June 1965

AN INVESTIGATION OF THE BEHAVIOR OF FLOATING RING DAMPERS AND THE DYNAMICS OF HYPERCRITICAL SHAFTS ON FLEXIBLE SUPPORTS

Final Report
UVA Report No. CE-3340-104-65U

Prepared by
J. A. Friedericy, R. T. Eppink
Y. N. Liu, A. Cetiner

Research Laboratories for the Engineering Sciences
University of Virginia
Charlottesville, Virginia

for
U. S. ARMY AVIATION MATERIEL LABORATORIES
FORT EUSTIS, VIRGINIA

ABSTRACT

This report deals with the development of two different analyses for the vibration responses in supercritical shafts: one especially suited for the determination of support impedances (mass, spring, damping coefficients) for minimum vibration response in the criticals; the other for direct vibration response in terms of statically measured shaft defects. The traveling wave concept is extensively discussed. Presented is a preliminary parameter study of the simply supported rotating shaft with one flexible intermediate support subjected to a half sine wave defects distribution. The effects of end masses are studied also. Several conceptual designs of multiring damping assemblies which can accommodate the damping requirements of hypercritical shafts are included in the report.

PREFACE

The following constitutes the final technical report concerned with research accomplished under a grant awarded by the U. S. Army Aviation Materiel Laboratories (formerly U. S. Army Transportation Research Command), Fort Eustis, Virginia, under grant no. DA-AMC-44-177-63-G10 to the Research Laboratories for the Engineering Sciences, University of Virginia, Charlottesville, Virginia. The contract was monitored by Mr. D. Kane; the principal investigators were Dr. R. T. Eppink and J. A. Friedericy. The program was initiated 1 July 1963 and terminated 15 September 1964.

CONTENTS

ILLUSTRATIONS

SYMBOLS

a	=	subscript indicating left-end support of shaft
a_j	=	distance from origin to jth driving force
A	=	area of shaft cross section
A_{k_1}, A_{k_2}, A_{k_3}, A_{k_4}	=	arbitrary integration constants to the solution of the equation of motion in the (ℓ_{k-1}, ℓ_k) span of the shaft
A_k	=	vector representation of A_{k_1}, A_{k_2}, A_{k_3}, A_{k_4}
b	=	subscript indicating right-end support of shaft
C_+, C_-	=	functions defined in Appendix I
C_y, C_f	=	functions defined in Appendix I
C_{11}, C_{12}, C_{21}, C_{22}	=	functions defined in Appendix I
C_1, C_2, -----, C_n	=	translational damping coefficients, respectively, at intermediate supports 1, 2, ---, n
E	=	vector related to distributed driving forces evaluated at $x = 0$ and $x = \ell$
e_1, e_2, e_3	=	functions defined in Appendix I
e^1	=	$\frac{1}{K^1}\left(\frac{E_y}{E_s}\right)$
E_s	=	shear modulus for shaft material
E_y	=	Young's modulus for shaft material

F_{11}, F_{12}	=	normalized components of internal force along the X_2, X_3 axes, respectively
F_{21}, F_{22}	=	normalized components of internal moment along the $-X_3$, X_2 axes, respectively
F_1, F_2	=	internal force and moment vectors, respectively
G_k	=	coefficient matrix related to the impedance at the (k - 1)st support
H(x)	=	Heavyside function
H_a, H_b	=	characteristic coefficient matrices at the left- and right-end supports, respectively
I	=	moment of inertia of shaft cross section; also used to denote the identity matrix
j	=	subscript indicating jth driving force
k	=	subscript indicating kth intermediate support
K^1	=	shape factor for shaft cross section
K_1, K_2, ----, K_n	=	translational spring coefficients, respectively, at intermediate supports, 1, 2, -------, n
ℓ	=	length of shaft
ℓ_n	=	distance from origin of shaft to location of nth intermediate support, also used as the distance measuring the location of the single intermediate support in the transmission line analogy analysis

m	=	superscript indicating a modified deflection wave traveling through the intermediate support
N	=	total number of driving forces
n	=	total number of intermediate supports, also used as an arbitrary real constant in the reformulation of the integration coefficients A, B, C, and D
$P(x)$	=	normalized single driving force vector at location x
Q	=	normalized force vector
q_1, q_2	=	arbitrary constants used in the reformulation of the integration constants A, B, C, and D
r_1, r_2	=	arbitrary constants used in the reformulation of the integration constants A, B, C, and D
$R(x)$	=	propagation matrix of a traveling wave evaluated at x
R_k	=	coefficient matrix related to the impedance at the (k - 1)st support
s	=	$-i\omega$
$U^{>}(x)$, $U^{<}(x)$	=	incident wave functions, respectively, traveling to the right and left
$U^{>>}(x)$, $U^{<<}(x)$	=	reflection wave functions, respectively, traveling to the right and left
$U^{>>>}(x)$, $U^{<<<}(x)$	=	total wave functions, respectively, traveling to the right and left

X_1, X_2, X_3	=	right-handed orthogonal coordinate axes
x	=	distance from origin to a generic point on X_1 axis
Y_{11}, Y_{12}	=	normalized projections of the deflections of elastic curve of shaft on the X_1X_2 and X_1X_3 planes, respectively
Y_{21}, Y_{22}	=	normalized projections of the angles of inclination of elastic curve of shaft on the X_1X_2 and X_1X_3 planes, respectively
Z_a, Z_b, Z_k	=	Impedances at left- and right-end supports and kth intermediate support, respectively
β	=	$\sqrt[4]{\rho \frac{A\ell^4}{E_y I} \omega^2}$
$\Gamma_a(x)$, $\Gamma_b(x)$, $\Gamma_{bn}(x)$	=	reflection matrices at left- and right-end supports, and the intermediate support, respectively
$\epsilon(x)$	=	normalized vector distance of mass center from axis of rotation of shaft evaluated at a distance x from the origin
ϵ_o	=	amplitude of the half sine wave defects curve
$\phi_r(x)$	=	rth normal mode of vibration for a free-free beam
ω	=	angular velocity of shaft and driving forces
ω_o	=	natural frequency of the simply supported shaft
ρ	=	mass density of the shaft material

SUMMARY

This report deals with an efficient approach leading to the direct optimization of support conditions for the hypercritical shaft flexibly supported on two mass-spring-damper units at the ends and one mass-spring-damper unit at the interior. It is based on the traveling wave concept as used in electrical transmission line theory. The governing differential equation used in this analogy includes terms which account for the effects of rotating inertia, gyroscopic motion, and shear deformations.

The terminating impedance corresponding to minimum vibration response of a rotating shaft is the characteristic impedance of the shaft. This condition is termed a "matched" condition. For the shaft with both end impedances matched, no additional intermediate support is needed for further minimization of vibration response. However, when the shaft and end support impedances are not matched, the closer the matched intermediate support is placed to one of the ends, the more effectively it will minimize the vibration response of the shaft.

Included also in this report is the development of an analysis which predicts the vibration response in terms of given initial defects for the hypercritical shaft on multiple translational mass-spring-damper supports. The solution in this case is obtained by applying the vibrating beam equation to each individual span between supports and correlating the responses between consecutive spans by the use of appropriate boundary and continuity conditions at the supports.

A computational procedure of the resulting simultaneous equations has been programmed for the University of Virginia Burroughs B5000 digital computer. A limited parameter study has been performed for a simply supported 4.5-inch-outside-diameter, 28-foot-long aluminum shaft with one intermediate support. The results tend to agree with the major conclusion of the transmission line analogy studies which states that the closer the intermediate support is located to one of the end supports, the more effectively it will minimize the vibration response of the shaft. Another important conclusion reached in the parameter study is concerned with the observation that the vibration responses tend to decrease with increased damping, provided that the spring stiffness of the

intermediate support is negligible. The effects of end masses on the natural frequencies of shafts supported on two flexible exterior supports have been studied also.

Several conceptual designs for multiring damping assemblies to provide the required damping for the Battelle model shaft and the proposed Chinook hypercritical drive shaft have been developed with existing computer programs. It was found that dampers having frequency dependent characteristics are too massive for practical application. However, by sacrificing these characteristics, lightweight dampers using low viscosity fluids are feasible.

CONCLUSIONS

The studies in this report lead to the following conclusions:

1. The transmission line analogy can be extended to shafts having one interior support. For shafts having more than one interior support, simplifying assumptions should be introduced into the analysis.

2. For the shaft with both end impedances matched with the characteristic impedance of the shaft, no intermediate support is needed to assist in the minimization of vibration response.

3. When the shaft and end support impedances are not matched, the closer the matched intermediate support is placed to one of the ends, the more effectively it will minimize the vibration response of the shaft.

4. The vibration response of a simply supported shaft with one flexible intermediate support tends to decrease with increased damping, provided that the spring stiffness of the intermediate support is negligible. Changes in damping of the intermediate support do not significantly affect critical frequencies; on the other hand, changes in spring cause appreciable shifts in the critical frequencies. Massiveness of end supports will affect the mode shape and critical frequencies of flexibly supported shafts.

5. The effects of dropping the rotational inertia, gyroscopics, and shear deformation terms from the equations of motion of hypercritical shafts are negligible for the frequency ranges in which hypercritical helicopter drive shafts are expected to operate.

6. Frequency dependent multiring dampers which accommodate the damping requirements for hypercritical shafts on a one-to-one basis are too massive for practical application to the Chinook drive shaft. However, by sacrificing variable damping characteristics, a lightweight damper using the less temperature sensitive, low viscosity fluids is feasible.

RECOMMENDATIONS

Work on the transmission line analogy should be extended to shafts on many supports. However, in view of the complexity of the ensuing algebra, it is suggested that the simpler vibrating equation (which leaves out rotational inertia, gyroscopic motion, and shear deformation terms) be used in the derivations of the wave forms. In addition, studies are needed to investigate the effectiveness of supports having either translational or rotational characteristics not both, as is required for an exact match of the shaft and support impedances. Mathematically, the use of translational or rotational supports only leads to the selection of conditions in which only the predominant Γ_{11} term of the reflection matrix vanishes. It can be shown that as $\exp(e_2\sqrt{\omega \ell_n})$ tends to zero (i.e., as ω increases), the reflection matrix tends to approach

$$\Gamma_{bn}(\ell_n) \approx \Gamma_{bn_{11}}(\ell_n),$$

such that either a translational or a rotational support may just as effectively suppress vibration response. This type of match is called a "quasi-match" and could lead to the development of simple design formulas which predict the "best" impedance values in terms of frequency for a given shaft and support configuration.

Work on the vibrating beam analogy requires additional results to complete the support parameter study. One should be able to eventually establish the "best" intermediate support spring and damping coefficients and location for a shaft having a number of different end support conditions. Furthermore, the analysis should be generalized to account also for supports having rotational spring and damping characteristics. Eventually, optimum support values as obtained by the transmission line analogy should be verified in a parameter study with the vibrating beam analogy. Another use for the computer programs of the vibrating beam analogy would involve a numerical study of permissible runouts in terms of maximum mass unbalance values for a number of realistic shaft defects configurations. Such a study would be very useful in establishing fabrication tolerances.

INTRODUCTION

OBJECTIVES

The theoretical study of the performance of rotating flexible drive shafts presently under investigation as a means of transmitting power in Chinook helicopters has the primary objective of arriving at analytical tools which will evaluate performance in terms of physical quantities in a satisfactory manner. Analytical behavior studies are usually undertaken to aid experimental programs in providing direction and testing guidelines. At times they will eliminate the need for an elaborate and expensive test program. Moreover, a complete understanding of hypercritical behavior of shafts is necessary in the development of techniques for operation at and between "critical speeds" without detrimental effects.

Successful operation of flexible shafts is usually achieved by balancing to reduce dynamic forces and also by introducing support conditions (spring, damping, mass) which tend to minimize runout amplitudes and/or bearing loads at the important critical frequencies. Both of these techniques should be employed simultaneously to bring about smooth shaft operation through the criticals. Although the provision of appropriate spring, damping, and mass coefficients (impedance) at the supports, by itself, may permit the rotor to negotiate the criticals in an acceptable manner, the ease with which this may be accomplished will be greater for the better balanced (less crooked) shaft. Balancing of a hypercritical shaft may be achieved by either the proper attachment of counterweights or the placement of greater restrictions on the fabrication tolerances of the shaft.

Different mathematical procedures have to be developed for an effective study of the relative merits of each of the techniques. The analysis of a flexible shaft supported at various points along the length by flexible damping bearings is represented with reasonable accuracy by the steady state solution of the equation of motion for the beam vibrating in two mutually perpendicular planes. This solution of the "vibrating beam analog" is worked to simulate the performance of the rotating shaft under actual running conditions in which the shaft defects provide a distributed forcing function. On the other hand, the solution can be interpreted also in terms of a "transmission line analog." This approach is based on the recognition of the existence of an analog between the amplitude response of the vibrating beam and the voltage

variation in electrical transmission lines. Performing rather lengthy but straightforward algebraic manipulations to the solution, the dynamic responses are expressed in traveling wave form along the lines of electrical response waves in transmission line theory.

While the vibrating beam analogy solution provides a means of theoretically studying the effects of imperfections and balancing in the form of physically observable quantities (amplitude runouts and phase shifts) allowing a direct comparison with experimental measurement, the transmission line analogy solution is particularly useful for the direct establishment of the support conditions needed for optimum shaft operation through the criticals.

The purpose of this report is to present the development of analyses for the rotating hypercritical shaft in terms of the vibrating beam and transmission line analogs and to indicate the usefulness of these tools in terms of representative qualitative and/or quantitative results. Presented also are conceptual designs of squeeze film dampers which could provide the support impedances required for successful operation of certain hypercritical shafts. It is anticipated that the computer program and the damper designs which resulted from this work will be of use in the experimental studies of hypercritical helicopter drive shafts conducted by the Vertol Division of the Boeing Company, Morton, Pennsylvania, and the Machine Dynamics Group, Battelle Memorial Institute, Columbus, Ohio.

SCOPE

The studies covered in this report were concerned with:

1. An extension of the University of Virginia electrical transmission line analog for hypercritical shafts to include the effects of an intermediate support.
2. The development of a computer program based on the vibrating beam analog which calculates the amplitude runouts of hypercritical shafts on multiple flexible supports at given frequencies in terms of statically measured defects (initial bow, ovality, wall thickness variations).

3. The selection of two-ring squeeze film dampers to accommodate the damping requirements in both the Battelle shaft model and the 4.5-inch-outside-diameter, 28-foot-long Chinook helicopter drive shaft.

In particular, this report presents the analyses associated with the work developed under items 1 and 2. The significance of these analyses is discussed in detail. Numerical results are presented with the work of item 2 which represents a preliminary parameter study in terms of several different dampers and spring coefficients for the 4.5-inch-outside-diameter, 28-foot-long flexibly supported Chinook drive shaft with one intermediate support. The work accomplished under item 3 has been presented in earlier reports [References 1, 3, and 4]. References 2 through 4 also deal with preliminary work performed under items 1 and 2. Additional work performed under item 2 is a numerical study on the effects of end support masses on the critical frequencies of shafts on two exterior spring supports. This work has been reported in Reference 5.

The analysis based on the transmission line analogy is concerned with the specific development of the traveling wave forms for the uniform shaft flexibly supported on two rotational and translational mass-spring-damper units at the ends and one such unit in the interior. No attempt has been made to consider multiple interior supports because of the complexity of the algebra. The wave forms for the simple interior support problem are already the result of extensive algebraic labor. However, the solution is kept in as general a form as possible; that is, the rotary inertia, gyroscopics, and shear deformation terms have been retained. On the other hand, the analysis based on the vibrating beam analogy applies to the rotating shaft on multiple flexible supports, and in the governing differential equation the extra inertia and shear terms have been neglected. In addition, the flexible supports are strictly translational in character; they do not resist any rotational motion of the shaft. Computations show that the effects of rotary inertia, gyroscopics, and shear deformation terms on natural frequencies and runout amplitudes are negligible for the frequency range in which hypercritical helicopter drive shafts are expected to operate. Therefore, the simplified equations of the vibrating beam analog should represent a reasonably accurate model of hypercritical shaft behavior.

The transmission line analogy was first developed in 1961 by Nelson [Reference 6] on end supports only. Independent of the University of Virginia work, Voorhees et al [Reference 7] of the Battelle Memorial Institute, Columbus, Ohio, formulated their version of the transmission line analogy. Although founded on the same concept of relating a supercritical shaft performance to a firmly established and well-understood electrical problem, the two approaches are quite different.

The Battelle analogy is a direct analog in which the fourth-order differential equation of motion has been reduced to an approximating second-order equation without the gyroscopic motion, rotary inertia, and shear deformation terms. To make this reduction in order possible, a one-to-one relation between moments and deflections of the beam is assumed which necessitates a compromise in the representation of boundary conditions. The approach has the advantage that all of the terminology and computational aids developed for the electrical transmission line problem can be utilized directly in the design of supports for supercritical shafts.

The University of Virginia transmission line analogy on the other hand, is not a direct analog, but rather a mathematical analog. The fourth-order differential equation which governs supercritical shaft behavior is solved in an exact manner. The various component terms to the solution are then reformulated in such a manner that these terms are mathematically analogous to the standing wave terms in the solution of the less complex transmission line equations. In this form, the solution to the fourth-order equation can be interpreted in terms of the same physical concepts used for the electrical transmission line problem. Thus the shaft runout is treated as a series of deflection waves (voltage waves) traveling along the shaft (transmission line). These waves are in part absorbed and in part reflected at the supports (load).

TRANSMISSION LINE ANALOGY SOLUTION OF THE HYPERCRITICAL SHAFT WITH ONE INTERMEDIATE SUPPORT

THEORY

1. Assumptions and Notations

It is shown in Figure 1 that the mathematical model of a prismatic shaft is embedded in a right-handed orthogonal normalized space coordinate system with axes X_1, X_2, and X_3. Let S_0 represent the shaft with elastic curve S. Let A_0 and B_0, where the end supports are attached, represent the end bodies with elastic curves A and B, respectively. The intermediate support is attached to the shaft at $x = \ell_n$, where $0 < \ell_n < \ell$. Force, torque, and motion along the X_1 axis is assumed to be zero. Constant angular velocity, small transverse motion, axial symmetry, and linearity are assumed throughout.

For points on the elastic curves, A, S, and B define "position" as the vector

$$Y^* = \begin{bmatrix} Y_1^* \\ Y_2^* \end{bmatrix} = \begin{bmatrix} Y_{11}^* + i\, Y_{12}^* \\ Y_{21}^* + i\, Y_{22}^* \end{bmatrix}$$

where Y_{11}^* and Y_{12}^* are the projections of the deflections of the elastic curves A, S, and B on the $X_1 X_2$ and $X_1 X_3$ planes, respectively. Y_{21}^* and Y_{22}^* are, respectively, the angles of inclination of A, S, and B on the planes $X_1 X_2$ and $X_1 X_3$ (see Figures 2 and 3).

Similarly, define "force" as a vector

$$Q^* = \begin{bmatrix} Q_1^* \\ Q_2^* \end{bmatrix} = \begin{bmatrix} Q_{11}^* + i\, Q_{12}^* \\ Q_{21}^* + i\, Q_{22}^* \end{bmatrix}$$

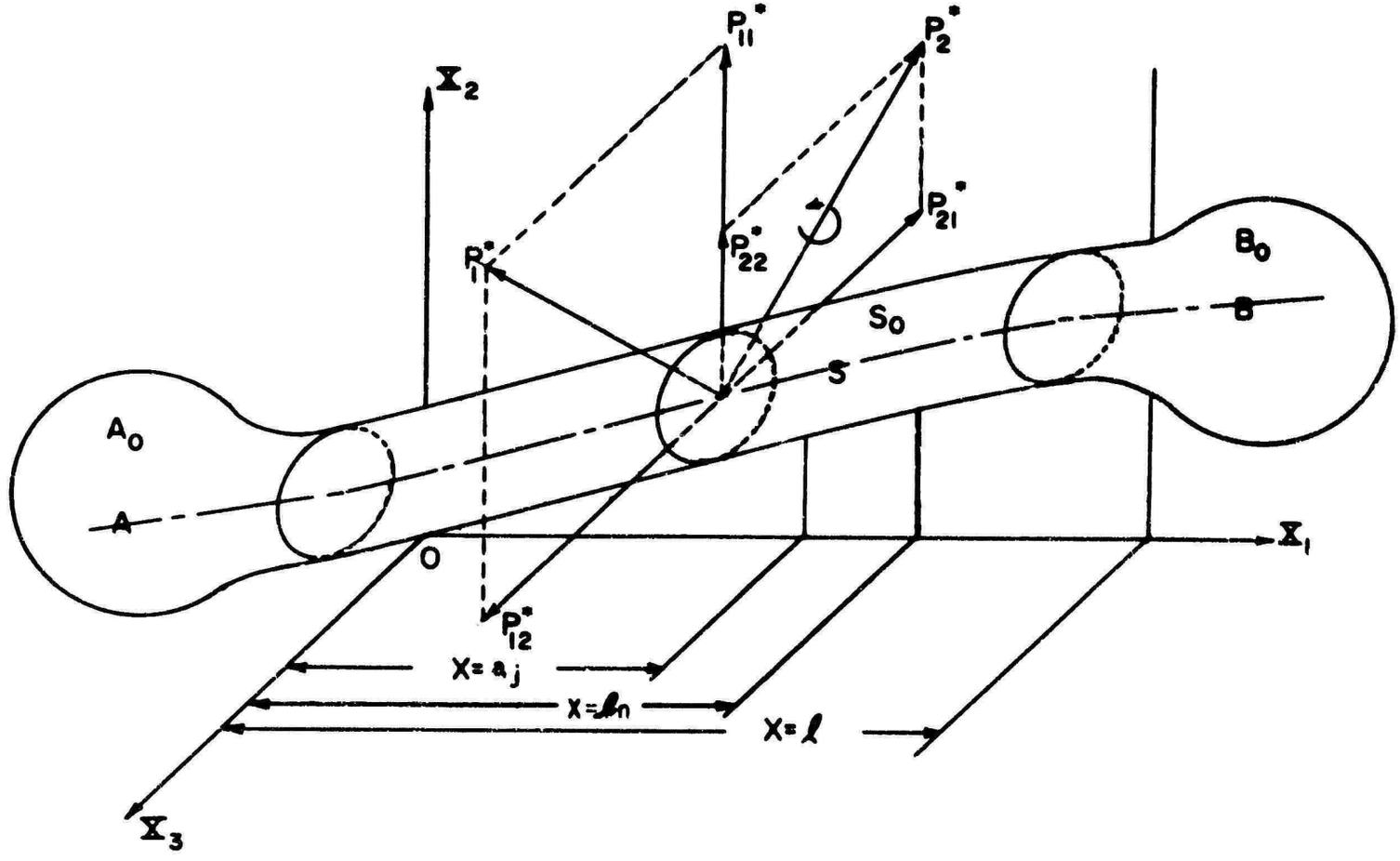

Figure 1. Pictorial Representation of A_0, S_0, B_0 Embedded in X_1, X_2, X_3 With a Driving Force $P^*(aj)$.

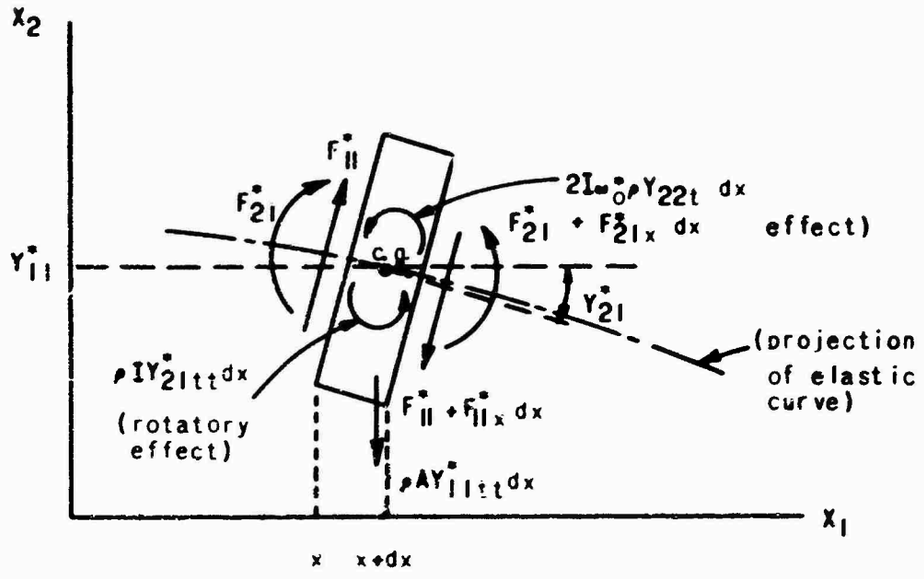

Figure 2. Projection of a Differential Shaft Element Upon X_1X_2 Plane With Acting Forces.

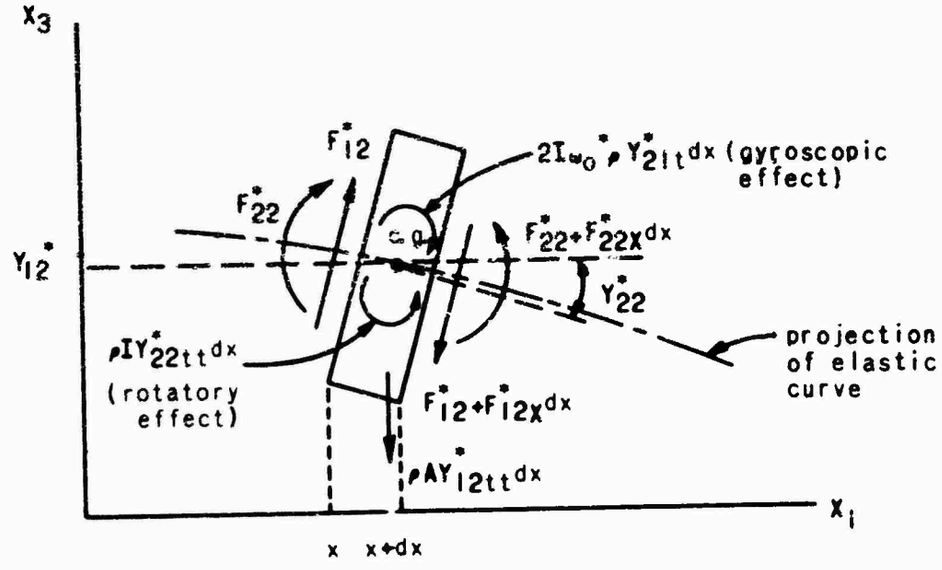

Figure 3. Projection of a Differential Shaft Element Upon X_1X_3 Plane With Acting Forces.

where the Q^*_{11} and Q^*_{12} are the components of force along the X_2 and X_3 axes, respectively, and Q^*_{21} and Q^*_{22} are the components of torque along the $-X_3$ and X_2 axes, respectively.

The force vector P^* denotes the "driving force" which can be related to lack of straightness and balance in the shafts. The driving forces are applied on the shaft at a finite set of points $x = a_j$, $j = 1, 2, \ldots N$ and x is an element of $(0, \ell)$, an open interval with end points $0, \ell$.

Similarly, let the force vector F^* denote the "internal force" which applies to the differential mass element (see Figures 2 and 3).

2. Equations of Motion for the Shaft

The equations which govern the behavior of rotating shafts include the effects of gyroscopic motion, rotational inertia, and shear deformations. The projections of an infinitesimal element of the shaft of length dx with all the forces acting on it are shown in Figures 2 and 3. The symbols used in these two figures are listed as follows:

"*" denotes the unnormalized variable
ω = angular velocity of the rotating shaft
I = moment of inertia of the shaft cross section area
ρ = mass density of the shaft material
A = area of the shaft cross section

Considering the projection on the $X_1 X_2$- plane only for the time being, one may obtain the following two equations by applying equilibrium conditions (see Figure 2).

By summing moments,

$$F^*_{11} - F^*_{21x} - \rho I Y^*_{21\,tt} - 2 I \omega \; Y^*_{22t} = 0. \tag{1}$$

By summing forces,

$$F^*_{11x} + A Y^*_{11\,tt} = 0. \tag{2}$$

By applying the shear relationship,

$$F_{11}^{*} = K^{1}AE_{s}\,(-Y_{11x}^{*} - Y_{21}^{*})$$

where

K^{1}	= numerical factor depending on the shape of cross section
E_{s}	= shear modulus for shaft material
Y_{11x}^{*}	= slope of deflection curve
Y_{21}^{*}	= slope of deflection curve when shearing force is neglected
$-Y_{11x}^{*} - Y_{21}^{*}$	= change of slope deflection curve due to shearing force only

The above equation may be rearranged as

$$F_{11}^{*} + K^{1}AE_{s}(Y_{11x}^{*} + Y_{21}^{*}) = 0. \qquad (3)$$

By applying the bending relationship,

$$-F_{21}^{*} = \frac{X_{21x}^{*}}{E_{y}I},$$

where

F_{21}^{*}	= moment on the differential section
Y_{21x}^{*}	= change of slope of deflection curve
E_{y}	= Young's modulus for shaft material

The above equation may be rearranged as

$$F_{21}^{*} + E_{y}IY_{21x}^{*} = 0. \qquad (4)$$

Similarly, considering the projection on the X_1X_3 plane which is an imaginary plane, using the same arguments as before, one may obtain the following four equations (see Figure 3).

$$F^*_{12} - F^*_{22x} - \rho I Y^*_{22tt} + 2\rho I\omega \; Y^*_{21t} = 0. \tag{1'}$$

$$F^*_{12x} + \rho A Y^*_{12tt} = 0. \tag{2'}$$

$$F^*_{12} + K'AE_s (Y^*_{12x} + Y^*_{22}) = 0. \tag{3'}$$

$$F^*_{22} + E_y I Y^*_{22x} = 0. \tag{4'}$$

Combining each pair of equations such that equation (k) + i equation (k') where k = 1, 2, 3, 4, one may obtain the corresponding four equations as follows:

$$(F^*_{11} + iF^*_{12}) - (F^*_{21x} + iF^*_{22}) - \rho I (Y^*_{21tt} + iY^*_{22tt}) + 2i\rho\omega (Y^*_{21ti} Y^*_{22t}) = 0.$$

$$(F^*_{11x} + iF^*_{12x}) + \rho A(Y^*_{11tt} + iY^*_{12tt}) = 0.$$

$$(F^*_{11} + iF^*_{12}) + K'AE_s \left[(Y^*_{11x} + iY^*_{12x}) + (Y^*_{21} + iY^*_{22})\right] = 0.$$

$$(F^*_{21} + iF^*_{22}) + E_y I (Y_{21x} + iY^*_{22x}) = 0.$$

Applying the notations for position vector and force vector as defined at the beginning of the section, one may rewrite the above equations in more compact forms.

$$F_1^* - F_{2x}^* - \rho I Y_{2tt}^* + 2i\rho I\omega \quad Y_{2t}^* = 0.$$

$$F_{1x}^* + \rho A Y_{1tt}^* = 0 .$$

$$F_1^* + K'AE_s (Y_{1x}^* + Y_2^*) = 0.$$

$$F_2^* + E_y I Y_{2x}^* = 0.$$

For normalizing these equations of motion, R_b, $E_y A$, and R_b/C_s are used corresponding to unit length, unit force, and unit time, respectively. R_b and C_s are, respectively, radius of gyration in bending and the velocity of sound for the shaft material. Note that $C_s = \sqrt{\frac{E_y}{\rho}}$. Applying the standard procedures for normalization, one may obtain the differential equations of motion in the following forms:

$$\left.\begin{aligned} F_1 - F_{2x} - Y_{2tt} + 2i\omega \quad Y_{2t} &= 0 \\ F_{1x} + Y_{1tt} &= 0 \\ F_2 + Y_{2x} &= 0 \\ e'F_1 + Y_{1x} + Y_2 &= 0 \end{aligned}\right\} \qquad (5)$$

where $e' = (\frac{1}{K'}) \frac{E_y}{E_s}$.

The above motion equations in Laplace transform form are:

$$\left.\begin{aligned} &\tilde{F}_1 - \tilde{F}_{2x} + s(2i\omega - s)\,\tilde{Y}_2 = 0 \\ &\tilde{F}_{1x} + s^2\tilde{Y}_1 = 0 \\ &\tilde{F}_2 + \tilde{Y}_{2x} = 0 \\ &e'\tilde{F}_1 + \tilde{Y}_{1x} + \tilde{Y}_2 = 0 \end{aligned}\right\} \qquad (6)$$

where Y_1 and Y_2 are, respectively, the transverse position and the inclination of normal of the elastic curve of shaft.

In equation 5, eliminating F_1, F_2, and Y_2, one may obtain the governing differential equation of the system in the following form:

$$Y_{1xxxx} + Y_{1tt} - (1 + e')\,Y_{1\,xxtt} + e'Y_{1tttt} + 2i\omega\,(Y_{1xxtt} - e'\,Y_{1ttt}) = 0. \qquad (7)$$

With concentrated driving forces acting on the shaft, the steady state solution to this differential equation may be represented in the form

$$Y_1 = y(x)\,e^{i\omega t}$$

where ω = angular velocity of driving force and y(x) is of the form

$$y(x) = Ae^{r_1 x} + Be^{r_2 x} + Ce^{r_3 x} + De^{r_4 x}$$

where r_1, r_2, r_3 and r_4 are the roots of the characteristic equations of the governing differential equation. A, B, C, and D are the arbitrary integration constants.

3. Solutions for the Equations of Motion

A more physical model of shaft which corresponds to the mathematical model in Figure 1 is represented in Figure 4. The shaft end conditions and the condition of the intermediate support are described as impedances or mobilities, and $P(a_j)$ is the jth driving force in the open interval $(0, \ell)$. The impedances are denoted, respectively, as $Z_a(0)$, $Z_b(\ell)$ and $Z_n(\ell_n)$ for the left end support, right end support, and intermediate support.

Because of axial symmetry, the relation between the force vector $\tilde{Q}$ and the position vector $\tilde{Y}$ may be written in either of the two following forms:

$$\tilde{Q} = sZ\tilde{Y} \qquad \text{or} \qquad \tilde{Y} = \frac{1}{s} M\tilde{Q},$$

where "~" denotes the Laplace transformation and s is the Laplace transformation variable. Z and M are, respectively, called impedance and mobility in 2 by 2 matrices with complex entries. It will be assumed that the impedance or mobility of the supports is known or can be calculated.

Taking the Laplace transformation of equation 7,

$$\tilde{Y}_{1xxxx} + s\left[2i\omega - s(1 + e')\right]\tilde{Y}_{1xx} + s^2\left[1 + se'(s - 2i\omega)\right]\tilde{Y}_1 = 0.$$

Let $\tilde{Y}_1 = Ae^{r_1 x} + Be^{r_2 x} + Ce^{r_3 x} + De^{r_4 x}$, then

$$r^4 + s\left[2i\omega - s(1 + e')\right]r^2 + s\left[1 + se'(s - 2i\omega)\right] = 0,$$

which yields

$$r_1, r_2 = \pm i e_1 \sqrt{\omega}$$

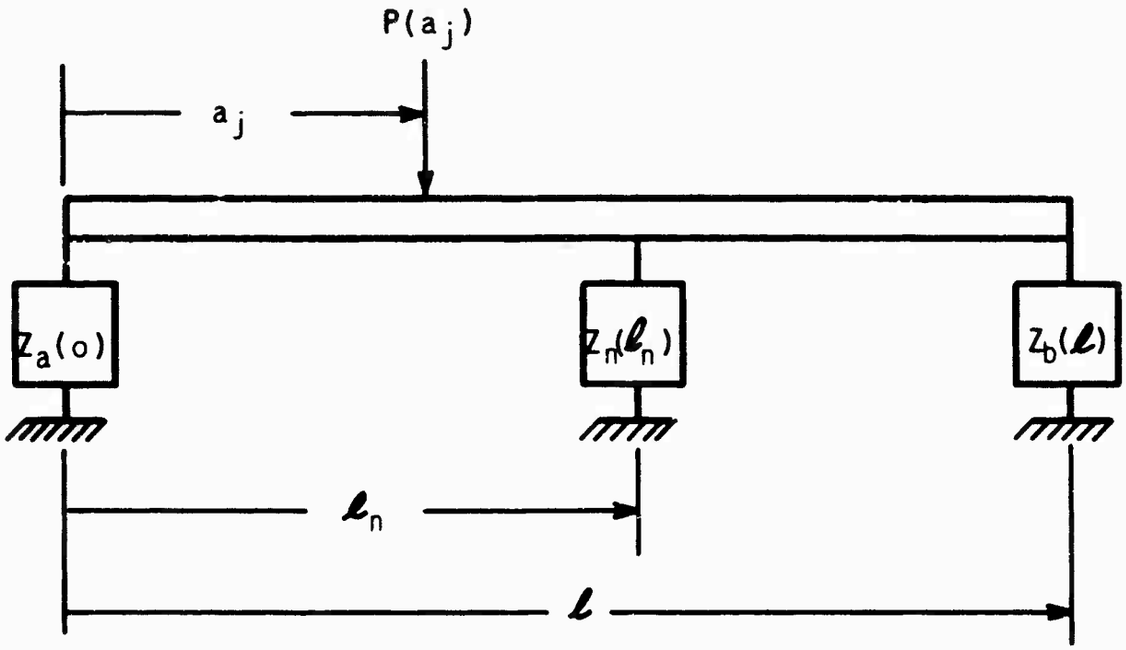

Figure 4. Shaft With Intermediate Support.

where

$$\omega = is$$

$$e_1 = \sqrt{\frac{1}{e_3} + e'\omega}$$

$$e_3 = \sqrt{1 + \alpha^2} + \alpha$$

$$\alpha = \omega - \frac{1}{2} is\,(e' - 1),$$

and gives

$$r_3,\ r_4 = \pm e_2\sqrt{\omega}$$

where

$$e_2 = \sqrt{e_3 - e'\omega}\ .$$

By applying the relationships in equation 6, one may derive the expressions for $\tilde{Y}_2$, $\tilde{F}_1$, and $\tilde{F}_2$:

$$\tilde{Y}_2 = \sqrt{\omega}\left[-\frac{i}{e_1 e_3} Ae^{r_1 x} + \frac{i}{e_1 e_3} Be^{r_2 x} - \frac{e_3}{e_2} Ce^{r_3 x} + \frac{e_3}{e_2} De^{r_4 x}\right].$$

$$\tilde{F}_1 = \omega^{3/2}\left[-\frac{i}{e_1} Ae^{r_1 x} + \frac{i}{e_1} Be^{r_2 x} + \frac{1}{e_2} Ce^{r_3 x} - \frac{1}{e_2} De^{r_4 x}\right].$$

$$\tilde{F}_2 = \omega\left[-\frac{1}{e_3} Ae^{r_1 x} - \frac{1}{e_3} Be^{r_2 x} + e_3 Ce^{r_3 x} + e_3 De^{r_4 x}\right].$$

Introducing another arbitrary set of constants, q_1, q_2, r_1, r_2, such that

$$A = -\frac{i}{s}\omega^{n+1} e_1 e_3 r_1$$

$$B = -\frac{i}{s}\omega^{n+1} e_3 q_1$$

$$C = -\frac{i}{s}\omega^{n+1} e_2 r_2$$

$$D = -\frac{i}{s}\omega^{n+1} e_2 q_2,$$

one may rewrite the expressions for $\tilde{Y}_1$, $\tilde{Y}_2$, $\tilde{F}_1$, $\tilde{F}_2$ as follows:

$$\left.\begin{aligned}
\tilde{Y}_1 &= \frac{1}{s}\omega^n [-e_1 e_3 \omega e^{-ie_1\sqrt{\omega}x} q_1 - ie_2\omega e^{-e_2\sqrt{\omega}x} q_2 - ie_1 e_3 \omega e^{ie_1\sqrt{\omega}x} r_1 - ie_2\omega e^{e_2\sqrt{\omega}x} r_2] \\
\tilde{Y}_2 &= \frac{1}{s}\omega^n [\omega^{3/2} e^{-ie_1\sqrt{\omega}x} q_1 - ie_3\omega^{3/2} e^{-e_2\sqrt{\omega}x} q_2 - \omega^{3/2} ie_1\sqrt{\omega}x r_1 + ie_3\omega^{3/2} e^{e_2\sqrt{\omega}x} r_2] \\
\tilde{F}_1 &= \omega^n [-ie_3\omega^{3/2} e^{-ie_1\sqrt{\omega}x} q_1 + \omega^{3/2} e^{-e_2\sqrt{\omega}x} q_2 + ie_3\omega^{3/2} ie_1\sqrt{\omega}x r_1 - \omega^{3/2} e^{e_2\sqrt{\omega}x} r_2] \\
\tilde{F}_2 &= \omega^n [e_1\omega e^{-ie_1\sqrt{\omega}x} q_1 - e_2 e_3 \omega e^{-e_2\sqrt{\omega}x} q_2 + e_1\omega e^{ie_1\sqrt{\omega}x} r_1 - e_2 e_3 \omega e^{e_2\sqrt{\omega}x} r_2]
\end{aligned}\right\} \quad (3)$$

Defining $q = \begin{bmatrix} q_1 \\ q_2 \end{bmatrix}$ and $r = \begin{bmatrix} r_1 \\ r_2 \end{bmatrix}$, two arbitrary constant vectors in a two-dimensional complex vector space, the above four equations may be written in the following compact form.

$$\begin{bmatrix} \tilde{Y} \\ \tilde{F} \end{bmatrix} = \begin{bmatrix} \frac{1}{s} C_y & 0 \\ 0 & C_f \end{bmatrix} \begin{bmatrix} C_{11} & C_{12} \\ C_{21} & C_{22} \end{bmatrix} \begin{bmatrix} R(x) & 0 \\ 0 & R(x) \end{bmatrix} \begin{bmatrix} q \\ r \end{bmatrix} \qquad (9)$$

where C_y, C_f, C_{11}, C_{12}, C_{21}, and C_{22} are given in Appendix I. The "propagation matrix" R(x) is a function of the real numbers defined by

$$R(x) = \begin{bmatrix} \text{cis}\,(e_1\sqrt{\omega}x) & 0 \\ 0 & \exp(-e_2\sqrt{\omega}x) \end{bmatrix},$$

where

$$\text{cis}\theta = e^{i\theta} = \cos\theta + i\sin\theta$$

$$\exp\theta = e^{\theta}.$$

Simply by expanding the matrix form of equation 9, one may verify this equation to be the same as equation 8.

4. Boundary Conditions

Applying the boundary conditions at $x = 0$, a_j, ℓ_n, ℓ on the X_1 axis, one may determine the integration constants appearing in the lution of the differential equation (see equation 9).

The boundary conditions employed here are:

at $x = 0$, $\quad -\tilde{F}(0) = sZ_a(0)\,\tilde{Y}(0)$;

at $x = a_j$, $\quad \tilde{Y}(a_j - 0) = \tilde{Y}(a_j + 0)$,

$$\tilde{F}(a_j - 0) + \tilde{P}(a_j + 0) = 0;$$

at $x = \ell_n$ $\quad \tilde{Y}(\ell_n - 0) = \tilde{Y}(\ell_n + 0)$,

$$\tilde{F}(\ell_n - 0) - \tilde{F}(\ell_n + 0) = sZ_n(\ell_n)\,\tilde{Y}(\ell_n - 0);$$

at $x = \ell$ $\quad \tilde{F}(\ell) = sZ_b(\ell)\,\tilde{Y}(\ell)$;

where -0, +0 denote, respectively, the limit from the left and the limit from the right.

5. Reflection Matrices at Supports in Terms of Characteristic Impedances

Several functions are useful for the process of evaluating boundary conditions. At $x = 0$ on the X_1 axis, the reflection matrix $\Gamma_a(0)$ is defined in terms of end impedance by

$$\Gamma_a(0) = [-C_{22} + \overset{\Delta}{z}_a(0)\, C_{12}]^{-1} [C_{21} - \overset{\Delta}{z}_a(0)\, C_{11}], \qquad (10)$$

where

$$\overset{\Delta}{z} = \overset{\#}{E}\, Z\, \overset{\#}{E},\ \overset{\#}{E} = \begin{bmatrix} 1 & 0 \\ 0 & -1 \end{bmatrix}.$$

At $x = \ell$ on the X_1 axis, the reflection matrix $\Gamma_b(\ell)$ is defined by

$$\Gamma_b(\ell) = [-C_{22} + z_b(\ell) C_{12}]^{-1} [C_{21} - z_b(\ell)\, C_{11}], \qquad (11)$$

where

$$z = \frac{1}{\sqrt{\omega}} \overset{\#\#\#}{F}\, Z\, \overset{\#}{F},\ \overset{\#}{F} = \begin{bmatrix} 1 & 0 \\ 0 & \sqrt{\omega} \end{bmatrix}.$$

At $x = \ell_n$ on the X_1 axis, the reflection matrix $\Gamma_{bn}(\ell_n)$ is defined in terms of $Z_b(\ell)$ and $Z_n(\ell_n)$ by

$$\Gamma_{bn}(\ell_n) = [-C_{22} + z_{bn}(\ell_n) C_{12}]^{-1} [C_{21} - z_{bn}(\ell_n) C_{11}], \qquad (12)$$

where

$$z_{bn}(\ell_n) = z_b(\ell_n) + z_n(\ell_n)$$

$$z_b(\ell_n) = [C_{21} + C_{22}\Gamma_b(\ell_n)][C_{11} + C_{12}\Gamma_b(\ell_n)]^{-1}.$$

On the closed interval $[0, \ell]$ reflection matrices $\Gamma_a(x)$, $\Gamma_b(x)$ and $\Gamma_{bn}(x)$ are defined, respectively, in terms of $\Gamma_a(0)$, $\Gamma_b(\ell)$ and $\Gamma_{bn}(\ell_n)$ by

$$\begin{aligned}
\Gamma_a(x) &= R(x)\Gamma_a(0)R(x) \\
\Gamma_b(x) &= R(\ell - x)\Gamma_b(\ell)R(\ell - x) \qquad (13) \\
\Gamma_{bn}(x) &= R(\ell_n - x)\Gamma_{bn}(\ell_n)\, R(\ell_n - x).
\end{aligned}$$

6. Impedances in Terms of Reflection Matrices

On $[0, \ell]$ it can be shown that $\overset{\Delta}{z}_a(x)$ is related to $\Gamma_a(x)$ by the equation

$$\overset{\Delta}{z}_a(x) = [C_{21} + C_{22}\Gamma_a(x)][C_{11} + C_{12}\Gamma_a(x)]^{-1} \qquad (14)$$

Similarly, for $z_b(x)$ and $\Gamma_b(x)$ on $(0, \ell)$,

$$z_b(x) = [C_{21} + C_{22}\Gamma_b(x)][C_{11} + C_{12}\Gamma_b(x)]^{-1} \qquad (15)$$

and, for $z_{bn}(x)$, $\Gamma_{bn}(x)$ on $(0, \ell)$,

$$z_{bn}(x) = [C_{21} + C_{22}\Gamma_{bn}(x)][C_{11} + C_{12}\Gamma_{bn}(x)]^{-1} \qquad (16)$$

Thus, Z_a, Z_b and Z_{bn} may be calculated on $[0, \ell]$.

Let

$$z_0 = C_{21} C_{11}^{-1} \tag{17}$$

z_0 is called the characteristic impedance of a semi-infinite shaft looked at from the right. Similarly, $\overset{\Delta}{z}_0$ is called the characteristic impedance of a semi-infinite shaft looked at from the left.

7. Solutions in Wave Form

After determining the integration constants in terms of support conditions and proceeding with a lengthy algebraic manipulation of the resulting equations, one may express equation 9 in the following traveling wave forms for N concentrated driving forces $P(a_j)$ on $[0, \ell_n]$, applied at $x = a_1, a_2, \ldots, a_j, \ldots a_N$ on the X_1 axis.

$$\begin{bmatrix} \tilde{Y} \\ \tilde{F} \end{bmatrix} = \begin{bmatrix} \frac{1}{s} C_y & 0 \\ 0 & C_f \end{bmatrix} \begin{bmatrix} C_{11} & C_{12} \\ C_{21} & C_{22} \end{bmatrix} \begin{bmatrix} \overset{>>>}{U(x)} \\ \overset{<<<}{U(x)} \end{bmatrix} \tag{18}$$

where

$$\overset{>>>}{U(x)} = \overset{>>}{U(x)} + \overset{>}{U(x)}$$

$$\overset{<<<}{U(x)} = \overset{<<}{U(x)} + \overset{<}{U(x)}.$$

For $0 < x < \ell_n$,

$$\overset{>}{U}(x) = \sum_{j=1}^{N} R(x - a_j) C_+ C_f^{-1} \tilde{P}(a_j) [\, H(x - a_j) - H(x - \ell_n)]\,.$$

(exists only in $a_j < x < \ell_n$)

$$\overset{<}{U}(x) = \sum_{j=1}^{N} R(a_j - x) C_- C_f^{-1} \tilde{P}(a_j) H(a_j - x).$$

(exists only in $0 < x < a_j$)

$$\overset{>>}{U}(x) = R(x)[\, I - \Gamma_a(0)\,\Gamma_{bn}(0)]^{-1}\,\Gamma_a(0)\,[\, R(\ell_n)\Gamma_{bn}(\ell_n)\overset{>}{U}(\ell_n) + \overset{<}{U}(0)]\,H(\ell_n - x).$$

(exists only in $0 < x < \ell_n$)

$$\overset{<<}{U}(x) = R(\ell_n - x)[\, I - \Gamma_{bn}(\ell_n)\Gamma_a(\ell_n)]^{-1}\,\Gamma_{bn}(\ell_n)[\, \overset{>}{U}(\ell_n) + R(\ell_n)\Gamma_a(0)\overset{<}{U}(0)]\,H(\ell_n - x).$$

(exists only in $0 < x < \ell_n$)

For $\ell_n < x < \ell$,

$$\overset{>}{U}(x) = \overset{>}{U}^m(x) = R(x - \ell_n)[\, I + C_{11}^{-1} C_{12} \Gamma_b(\ell_n)]^{-1}\,[\, I + C_{11}^{-1} C_{12} \Gamma_{bn}(\ell_n)]\,\overset{>}{U}(\ell_n - 0)\,H(x - \ell_n).$$

(exists only in $\ell_n > x > \ell$)

$$\overset{>>}{U}(x) = \overset{>>}{U}^m(x) = R(x - \ell_n)[\, I + C_{11}^{-1} C_{12} \Gamma_b(\ell_n)]^{-1}[\, I + C_{11}^{-1} C_{12} \Gamma_{bn}(\ell_n)]\,\overset{>>}{U}(\ell_n - 0)\,H(x - \ell_n).$$

(exists only in $\ell_n < x < \ell$)

$$\overset{<}{U}(x) = \overset{<}{U}^m(x) = R(\ell - x)\Gamma_b(\ell)\overset{>}{U}^m(\ell)H(x - \ell_n).$$ (exists only in $\ell_n < x < \ell$)

$$\overset{<<}{U}(x) = \overset{<<}{U}^m(x) = R(\ell - x)\Gamma_b(\ell)\overset{>>}{U}^m(\ell)H(x - \ell_n).$$ (exists only in $\ell_n < x < \ell$)

$$H(p) = \begin{cases} 0 & p < 0 \\ 1 & p > 0 \end{cases}$$ and I = Identity matrix.

DISCUSSION OF RESULTS

1. The Traveling Wave Concept

The steady state wave interpretation of the solution of equation 18 provides a means toward visualizing the effects of support parameters (mass, spring, damping) on hypercritical shaft behavior.

Incident waves traveling along the shaft are considered as being initiated by the action of a single driving force $P(a_j)$ located at $x = a_j$. $\overset{>}{U}_j(x)$ and $\overset{<}{U}_j(x)$ are defined, respectively, as "incident waves" traveling to the right and left from $x = a_j$. They are independent of all support conditions.

$$\overset{>}{U}_j(x) = R(x - a_j)\, C_+ C_f^{-1} \tilde{P}(a_j)[\, H(x - a_j) - H(x - \ell_n)\,].$$

$$\overset{<}{U}_j(x) = R(a_j - x) C_- C_f^{-1} \tilde{P}(a_j) H(a_j - x).$$

The propagation of the wave from the point of application, $x = a_j$, of the driving force $\tilde{P}(a_j)$ is described by the "propagation matrix," $R(x - a_j)$ or $R(a_j - x)$, as the wave is traveling to the right or left, respectively. Thus, at $x = \ell_n$, $\overset{>}{U}_j(x)$ has traveled a distance $(\ell_n - a_j)$ to the intermediate support of the system. The quantities $[\, H(x - a_j) - H(x - \ell_n)\,]$ and $H(a_j - x)$ simply indicate the regions in which the waves exist. The quantities $C_+ C_f^{-1}$ and $C_- C_f^{-1}$ perform elementary transformations or operations on the applied forces and are associated with frequency and shaft characteristics.

A similar interpretation may be given to the quantities $\overset{>>}{U}_j(x)$ and $\overset{<<}{U}_j(x)$, which are regarded as "reflected waves" traveling to the right and left, respectively. They may be expressed as follows:

$$\overset{>>}{U_j}(x) = R(x)[\,I - \Gamma_a(0)\Gamma_{bn}(0)]^{-1}\Gamma_a(0)[\,R(\ell_n)\Gamma_{bn}(\ell_n)\overset{>}{U_j}(\ell_n) + \overset{<}{U_j}(0)\,]H(\ell_n - x).$$

$$\overset{<<}{U_j}(x) = R(\ell_n - x)[\,I - \Gamma_{bn}(\ell_n)\Gamma_a(\ell_n)]^{-1}\Gamma_{bn}(\ell_n)[\,\overset{>}{U_j}(\ell_n) + R(\ell_n)\Gamma_a(0)\overset{<}{U_j}(0)\,]H(\ell_n - x).$$

The second term in each expression may be restated as an infinite series:

$$[\,I - \Gamma_a(0)\Gamma_{bn}(0)\,]^{-1} = I + \Gamma_a(0)\Gamma_{bn}(0) + \Gamma_a(0)\Gamma_{bn}(0)\Gamma_a(0)\Gamma_{bn}(0)$$
$$+ \Gamma_a(0)\Gamma_{bn}(0)\Gamma_a(0)\Gamma_{bn}(0)\Gamma_a(0)\Gamma_{bn}(0) + \cdots$$

$$[\,I - \Gamma_{bn}(\ell_n)\Gamma_a(\ell_n)\,]^{-1} = \underset{i}{I} + \underset{ii}{\Gamma_{bn}(\ell_n)\Gamma_a(\ell_n)} + \underset{iii}{\Gamma_{bn}(\ell_n)\Gamma_a(\ell_n)\Gamma_{bn}(\ell_n)\Gamma_a(\ell_n)}$$
$$+ \Gamma_{bn}(\ell_n)\Gamma_a(\ell_n)\Gamma_{bn}(\ell_n)\Gamma_a(\ell_n)\Gamma_{bn}(\ell_n)\Gamma_a(\ell_n) + \cdots$$
$$\underset{iv}{\phantom{\Gamma_{bn}(\ell_n)\Gamma_a(\ell_n)\Gamma_{bn}(\ell_n)\Gamma_a(\ell_n)}}$$

Calling the first term i, the second term ii, etc., as noted above, one gets for $\overset{>>}{U_j}(x)\,|_i$ (again $H(\ell_n - x)$ restricts the range of the waves to the open interval $(0, \ell_n)$):

$$\overset{>>}{U_j}(x)\,|_i = R(x)\Gamma_a(0)R(\ell_n)\Gamma_{bn}(\ell_n)\overset{>}{U_j}(\ell_n) + R(x)\Gamma_a(0)\overset{<}{U_j}(0).$$

The last quantity, $\overset{<}{U_j}(0)$, represents an incident wave traveling to the left at the point $x = 0$; i.e., the left end of the system. If the quantity $\Gamma_a(0)$ signifies that this wave has been reflected at $x = 0$, then the reflected wave now traveling to the right has propagated the distance x, as indicated by R(x). Similarly, the last quantity of the first term, $\overset{>}{U_j}(\ell_n)$, represents an incident wave which is traveling to the right and is located at $x = \ell_n$; i.e., the intermediate support of the system. The quantity $\Gamma_{bn}(\ell_n)$ signifies reflection of this wave at the intermediate support, $x = \ell_n$. The next term, $R(\ell_n)$, signifies propagation of the

reflected wave to the left through the distance ℓ_n which locates it at the left end, x = 0. The wave is now reflected again to the right as indicated by $\Gamma_a(0)$, and R(x) signifies propagation through the distance x to the point under investigation. Thus the term $\overset{>>}{U_j}(x)\,|_i$ represents the contributions of two reflected waves to the right immediately following the initiation of the incident waves. This is illustrated in Figure 5.

Now, consider the second term, ii, of the expansion for $[\,I - \Gamma_a(0)\Gamma_{bn}(0)\,]^{-1}$,

$$\overset{>>}{U_j}(x)\,|_{ii} = R(x)\Gamma_a(0)\Gamma_{bn}(0)\Gamma_a(0)R(\ell_n)\Gamma_{bn}(\ell_n)\overset{>}{U_j}(\ell_n) + R(x)\Gamma_a(0)\Gamma_{bn}(0)\Gamma_a(0)\overset{<}{U_j}(0),$$

which may also be written as

$$\overset{>>}{U_j}(x)\,|_{ii} = R(x)\Gamma_a(0)R(\ell_n)\Gamma_{bn}(\ell_n)R(\ell_n)\Gamma_a(0)R(\ell_n)\Gamma_{bn}(\ell_n)\overset{>}{U_j}(\ell_n)$$
$$+ R(x)\Gamma_a(0)R(\ell_n)\Gamma_{bn}(\ell_n)R(\ell_n)\Gamma_a(0)\overset{<}{U_j}(0).$$

Following the same reasoning used for the analysis of $\overset{>>}{U_j}(x)\,|_i$, one may observe that the added terms correspond to the wave propagating and reflecting an additional two times with the reflected wave again traveling to the right. This is shown in Figure 6. The addition of the rest of the terms in the series, i.e., $\overset{>>}{U_j}(x)\,|_{iii}$, $\overset{>>}{U_j}(x)\,|_{iv}$, etc., accounts for all of the reflected waves traveling to the right. The summation of all of the waves traveling to the right is complete if the incident wave is added to the above; i.e.,

$$\overset{>>>}{U_j}(x) = \overset{>}{U_j}(x) + \overset{>>}{U_j}(x)\,|_i + \overset{>>}{U_j}(x)\,|_{ii} + \overset{>>}{U_j}(x)\,|_{iii} + \cdots$$
$$= \overset{>}{U_j}(x) + \overset{>>}{U_j}(x)\,.$$

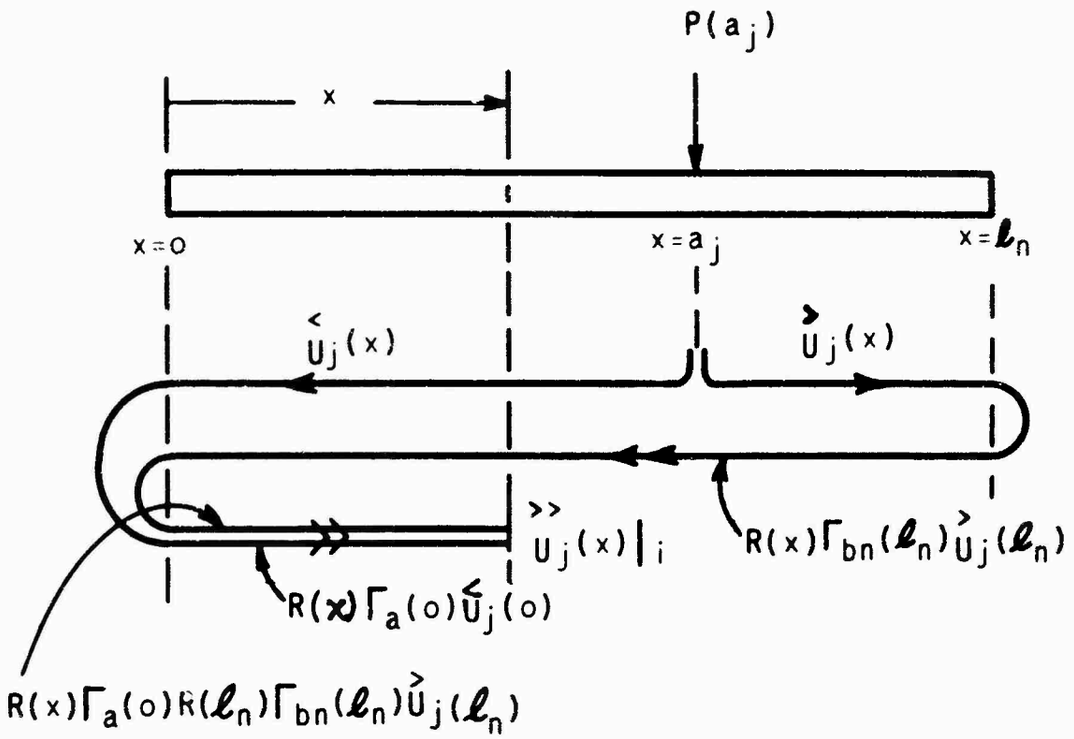

Figure 5. First-Term Propagation of Waves in the (o, ℓ_n) Portion of the Shaft.

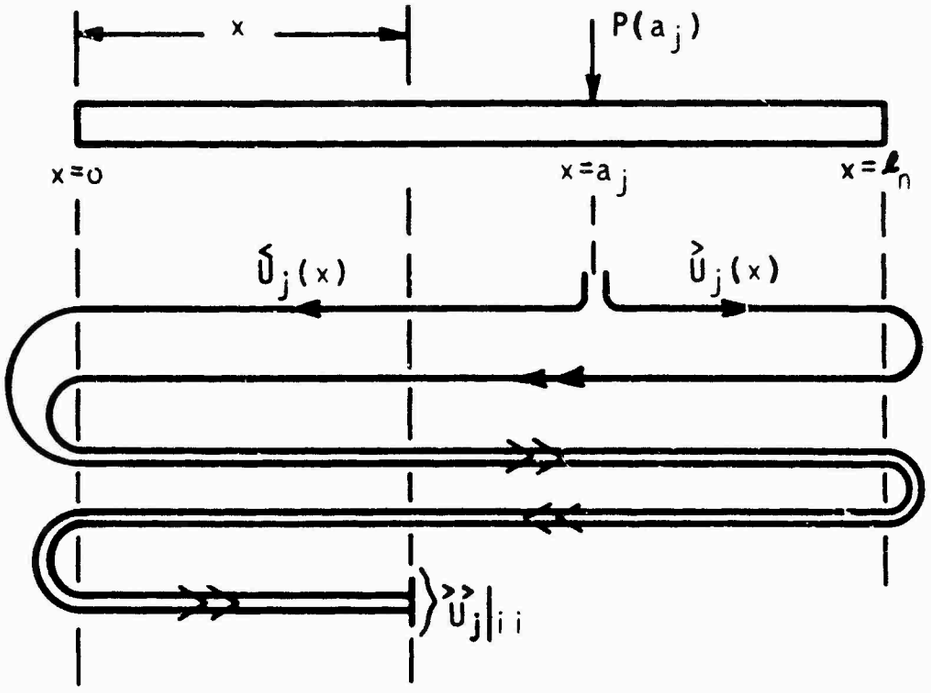

Figure 6. First- and Second-Term Propagation of Waves in the (o,ℓ_n) Portion of the Shaft.

Similar results may be obtained for $\overset{<<}{U_j}(x)$. That is,

$$\overset{<<}{U_j}(x) = \overset{<<}{U_j}(x)\big|_i + \overset{<<}{U_j}(x)\big|_{ii} + \overset{<<}{U_j}(x)\big|_{iii} + \cdots$$

The summation of $\overset{<<}{U_j}(x)$, the reflected wave to the left, with $\overset{<}{U_j}(x)$, the incident wave to the left, includes all of the waves traveling to the left as they are observed passing point x on the shaft.

The complete response on the open interval $(0, \ell_n)$ at point x may be determined by properly combining all of the waves traveling past point x in both the left and right directions. The expansion of equation 18 for $\tilde{Y}$ in terms of N driving forces $P(a_j)$ at $x = a_1, a_2, \cdots a_j, \cdots a_N$,

$$\tilde{Y} = \frac{1}{s} C_y [\, C_{11} \overset{>>>}{U}(x) + C_{12} \overset{<<<}{U}(x)\,],$$

indicates the relatively direct manner in which the waves are combined to obtain the total response at point x.

In examining the portion of the shaft (ℓ_n, ℓ) in terms of a single driving force $P(a_j)$, $\overset{>m}{U_j}(x)$ may be thought of as a "modified incident wave" which is initiated by the driving force at $x = a_j$ traveling to the right, as indicated by $\overset{>}{U_j}(x)$ on $(0, \ell_n)$:

$$\overset{>m}{U_j}(x) = R(x - \ell_n)[\, I + C_{11}^{-1} C_{12} \Gamma_b(\ell_n)\,]^{-1} [\, I + C_{11}^{-1} C_{12} \Gamma_{bn}(\ell_n)\,] \overset{>}{U_j}(\ell_n - 0) H(x - \ell_n).$$

After propagating to $x = \ell_n$, $\overset{>}{U_j}(x)$ becomes $\overset{>}{U_j}(\ell_n - 0)$ and then partly passes through the intermediate support after being modified by $[\, I + C_{11}^{-1} C_{12} \Gamma_{bn}(\ell_n)\,]$, a characteristic matrix of the intermediate support. The other part of the wave is reflected back to the left from the intermediate support, as shown in Figure 7. The second term of the above expression may be written as an infinite series:

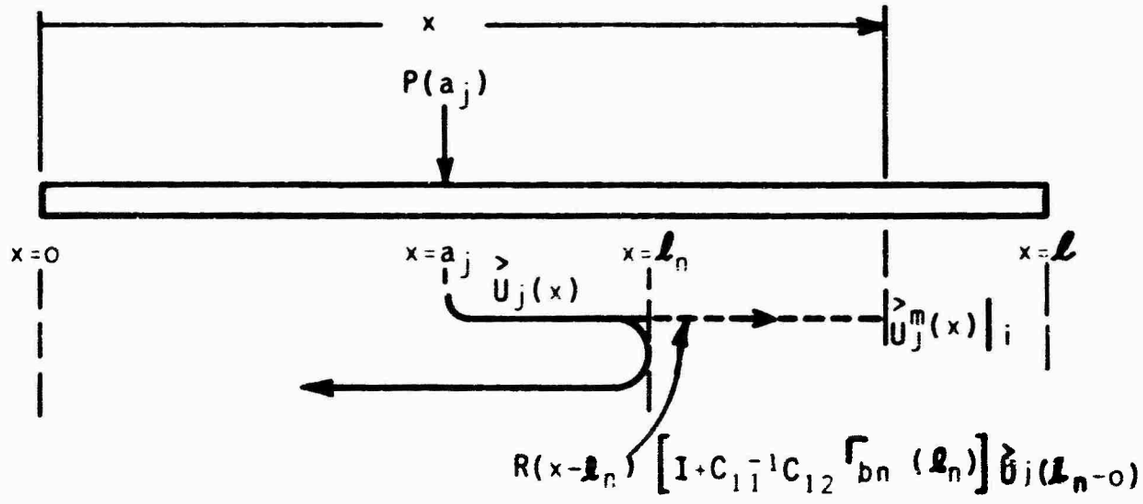

Figure 7. First-Term Propagation of Modified Incident Wave in the (ℓ_n, ℓ) Portion of the Shaft.

$$[I + C_{11}^{-1} C_{12}\Gamma_b(\ell_n)]^{-1} = \underbrace{I}_{i} + \underbrace{(-C_{11}^{-1}C_{12})\Gamma_b(\ell_n)}_{ii} + \underbrace{(-C_{11}^{-1}C_{12})(-C_{11}^{-1}C_{12})\Gamma_b(\ell_n)}_{iii}$$

$$+ \underbrace{(-C_{11}^{-1}C_{12})(-C_{11}^{-1}C_{12})(-C_{11}^{-1}C_{12})\Gamma_b(\ell_n)}_{iv} + \cdots .$$

Again, the order of the terms is indicated by i, ii, iii, etc. Considering $\overset{>}{U}_j^m(x)$ and taking, for the time being only the first term i of the above expression,

$$\overset{>}{U}_j^m(x)\,|_i = R(x - \ell_n)[I + C_{11}^{-1} C_{12}\Gamma_{bn}(\ell_n)]\,\overset{>}{U}_j(\ell_n - 0)$$

which signifies the wave passes through the intermediate support and has propagated a distance $(x - \ell_n)$, as indicated by $R(x - \ell_n)$. This is also illustrated in Figure 7.

Consider now the second term, ii, of the expression for $[I + C_{11}^{-1}C_{12}\Gamma_b(\ell_n)]^{-1}$,

$$\overset{>}{U}_j^m(x)\,|_{ii} = R(x - \ell_n)(-C_{11}^{-1}C_{12})\Gamma_b(\ell_n)[I + C_{11}^{-1}C_{12}\Gamma_{bn}(\ell_n)]\,\overset{>}{U}_j(\ell_n - 0),$$

which may be rewritten as

$$\overset{>}{U}_j^m(x)\,|_{ii} = R(x - \ell_n)(-C_{11}^{-1}C_{12})R(\ell - \ell_n)\Gamma_b(\ell)R(\ell - \ell_n)[I + C_{11}^{-1}C_{12}\Gamma_{bn}(\ell_n)]\,\overset{>}{U}_j(\ell_n - 0).$$

Following the same reasoning as before, one may observe that the added terms correspond to the wave propagating to the right after being reflected twice, first at the right end support and then at the intermediate support. It is shown in Appendix II that the term $(-C_{11}^{-1}C_{12})$ corresponds to a reflection matrix of a fixed support. This means that the intermediate support acts as a fixed support, which reflects the modified waves coming from the right after being reflected at $x = \ell$ and will not permit these waves to pass through. This is illustrated in Figure 8. The same analysis may be applied to the

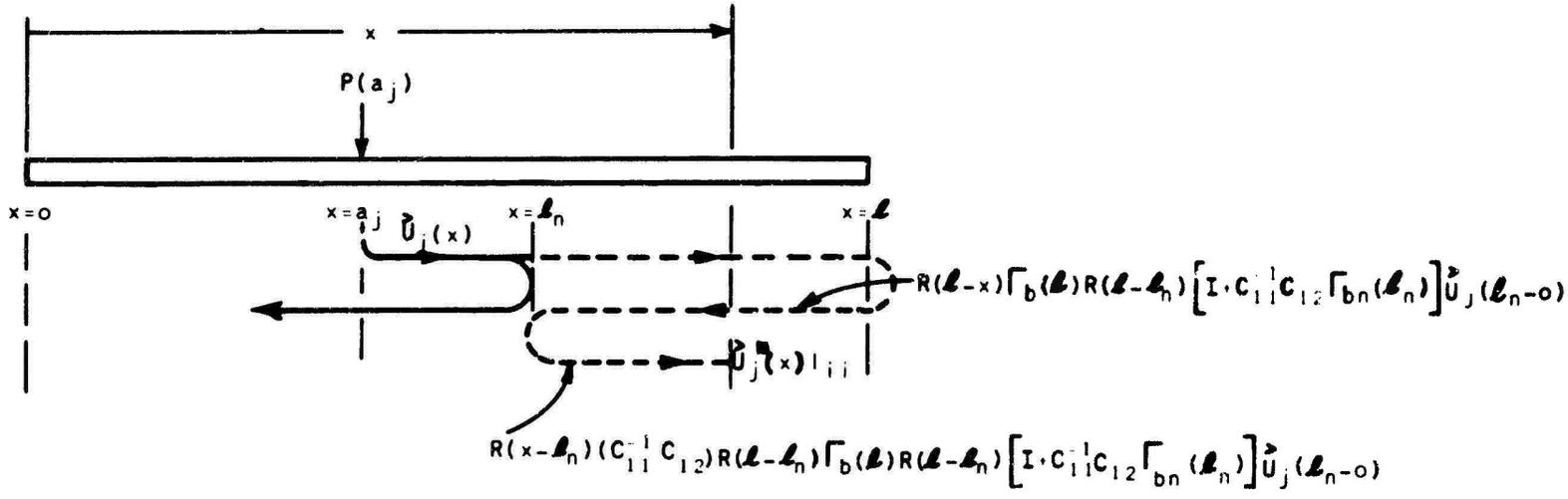

Figure 8. First- and Second-Term Propagation of Modified Incident Waves in the (ℓ_n, ℓ) Portion of the Shaft.

remaining terms of the series. Similar reasoning may be applied to $\overset{>>}{U}{}_j^m(x)$, which has the same form as $\overset{>}{U}{}_j^m(x)$.

$$\overset{>>}{U}{}_j^m(x) = R(x - \ell_n)[I + C_{11}^{-1}C_{12}\Gamma_b(\ell_n)]^{-1}[I + C_{11}^{-1}C_{12}\Gamma_{bn}(\ell_n)\overset{>>}{U}_j(\ell_n - 0)H(x - \ell_n).$$

The summation of all of the waves traveling to the right in $(\ell_n - \ell)$ is complete if the "modified incident wave" is added to the above expression; i.e.,

$$\overset{>>>}{U}{}_j^m(x) = \overset{>}{U}{}_j^m(x) + \overset{>>}{U}{}_j^m(x).$$

Similar results may be obtained for $\overset{<}{U}{}_j^m(x)$ and $\overset{<<}{U}{}_j^m(x)$, the waves traveling to the left. The summation of the waves in the interval (ℓ_n, ℓ) of the shaft is

$$\overset{<<<}{U}{}_j^m(x) = \overset{<}{U}{}_j^m(x) + \overset{<<}{U}{}_j^m(x)$$

$$= R(\ell - x)\Gamma_b(\ell)[\overset{>}{U}{}_j^m(\ell) + \overset{>>}{U}{}_j^m(\ell)]H(x - \ell_n).$$

The mechanics of the propagation of these waves is illustrated in Figure 9, using the first two terms of the expanded form.

The complete response at point x in (ℓ_n, ℓ) due to N single forces $P(a_j)$, at $a_1, a_2 \ldots, a_j \ldots, a_N$ may be determined by properly combining all of the waves traveling past point x in both the right and left directions.

$$\tilde{Y} = \frac{1}{s}C_y[C_{11}\overset{>>>}{U}{}^m(x) + C_{12}\overset{<<<}{U}{}^m(x)].$$

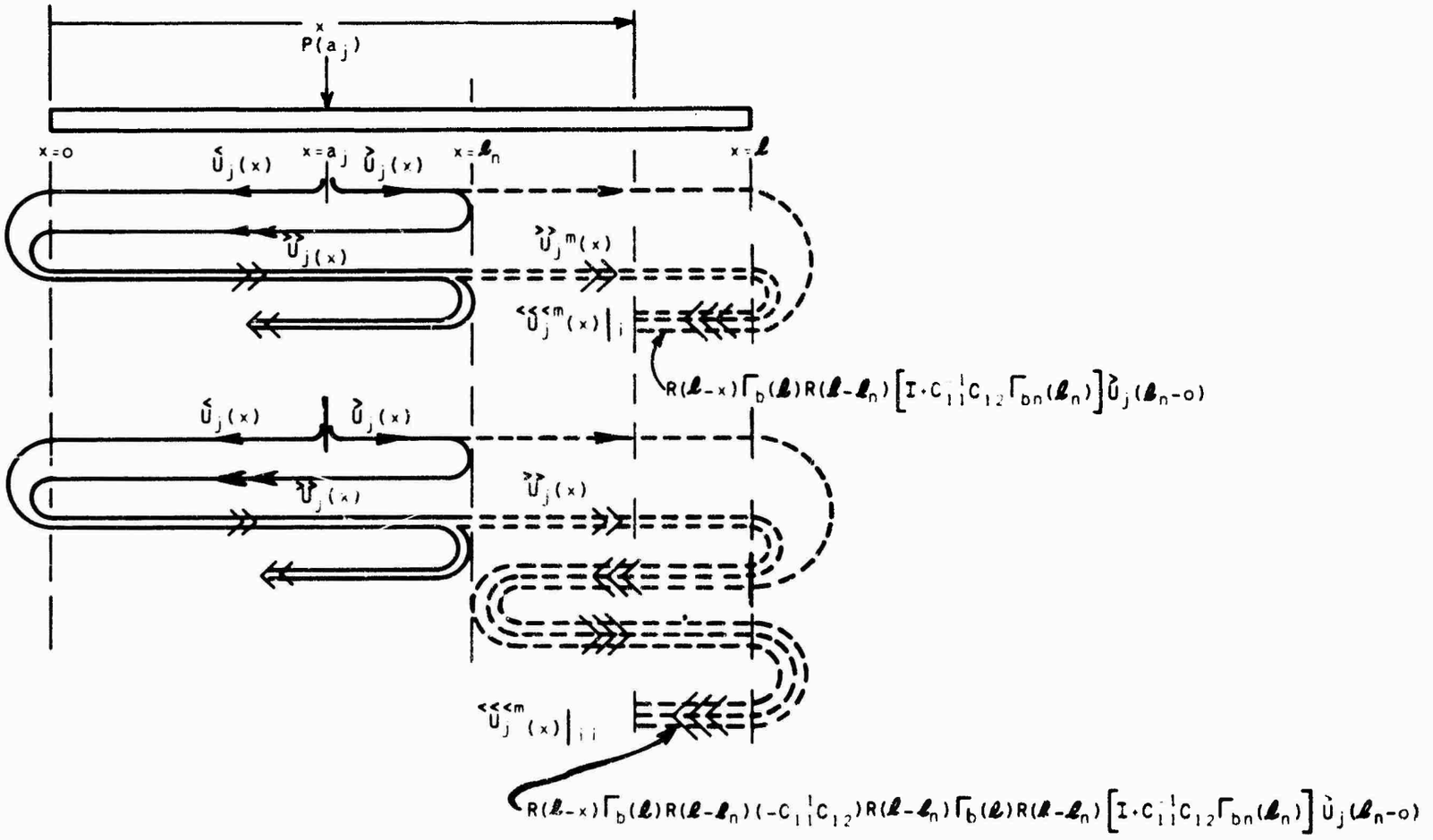

Figure 9. First- and Second-Term Propagation of Modified Waves in (ℓ_n, ℓ) Portion of the Shaft.

2. Impedance Matching

The response of the system of Figure 4 in terms of a single driving force, $P(a_j)$, is

$$\tilde{Y} = \frac{1}{s} C_y [\, C_{11} \overset{>>>}{U_j}(x) + C_{12} \overset{<<<}{U_j}(x) \,] .$$

By proper control of the conditions at both ends and the intermediate support, the reflected waves may be eliminated or at least minimized such that the response consists solely or principally of incident waves. Mathematical representation of the above statement is to set $\overset{>>>}{U_j}(x) \equiv \overset{>}{U_j}(x)$ and $\overset{<<<}{U_j}(x) \equiv \overset{<}{U_j}(x)$ or $\overset{>>}{U_j}(x) = \overset{<<}{U_j}(x) \equiv 0$. According to equation 18, in terms of a single driving force $P(a_j)$, the condition $\overset{>>}{U_j}(x) = \overset{<<}{U_j}(x) \equiv 0$ may be obtained by setting

$$\Gamma_a(0) = \Gamma_b(\ell) = \Gamma_{bn}(\ell_n) \equiv 0 .$$

Physically, this is equivalent to setting the impedance of the supports equal to the shaft characteristic impedance at those points. That is, the shaft has been "matched" at the supports.

If the above conditions are satisfied, equation 18 may be rewritten in terms of $P(a_j)$ alone as

$$\begin{bmatrix} \tilde{Y} \\ \tilde{F} \end{bmatrix} = \begin{bmatrix} \frac{1}{s} C_y & 0 \\ 0 & C_f \end{bmatrix} \begin{bmatrix} C_{11} & C_{12} \\ C_{21} & C_{22} \end{bmatrix} \begin{bmatrix} \overset{>}{U_j}(x) \\ \overset{<}{U_j}(x) \end{bmatrix}$$

where, for $0 < x \ell_n$,

$$\overset{>}{U_j}(x) = R(x - a_j) C_+ C_f^{-1} \tilde{P}(a_j) [\, H(x - a_j) - H(x - \ell_n) \,]$$

$$\overset{<}{U_j}(x) = R(a_j - x) C_- C_f^{-1} \tilde{P}(a_j) H(a_j - x) .$$

For $\ell_n < x < \ell$,

$$\overset{>}{U}_j(x) = \overset{>}{U}{}^m_j(x) = R(x - \ell_n)\overset{>}{U}_j(\ell_n - 0)H(x - \ell_n).$$

Examination of these expressions yields the following observations. The incident wave initiated from the driving force $\tilde{P}(a_j)$ at $x = a_j$ has traveled to the intermediate support; this is specified by $\overset{>}{U}_j(\ell_n - 0)$. The wave then simply passes through the intermediate support without any modification into the interval $\ell_n < x < \ell$. One may conclude from this that if both end impedances are matched with the shaft characteristic impedance, i.e., $\Gamma_a(0) = \Gamma_b(\ell) \equiv 0$, the effect of the intermediate support on the shaft's dynamic behavior is redundant. Actually, further inspection of equation 18 shows that even if the intermediate support were not optimum (the incident wave is now modified in $[\ell_n, \ell]$), its effect is redundant. Thus, from a practical point of view, if the end impedances can be matched with the shaft characteristic impedance, nothing is gained by the optimization of the intermediate support in terms of minimum vibration.

The matching of end impedances with that of the shaft is a formidable task, not only because impedances are a function of frequency, but primarily because of the uniqueness of the conditions required to control these impedances. Moreover, in practical applications, the choice in end support configurations is limited, since they usually are governed by such factors as transmission gears, couplings, and unwieldy mountings. Thus, the intermediate support has to be employed for optimization purposes, since the end impedances are not available.

Examining equation 18 in terms of $P(a_j)$ again, the waves which are reflected by the intermediate support or pass through the intermediate support with modifications are:

$$\overset{>>}{U}_j(x) = R(x)[I - \Gamma_a(0)\Gamma_{bn}(0)]^{-1}\Gamma_a(0)[R(\ell_n)\Gamma_{bn}(\ell_n)\overset{>}{U}_j(\ell_n) + \overset{<}{U}_j(0)]H(\ell_n - x).$$

$$\overset{<<}{U}_j(x) = R(\ell_n - x)[I - \Gamma_{bn}(\ell_n)\Gamma_a(\ell_n)]^{-1}\Gamma_{bn}(\ell_n)[\overset{>}{U}_j(\ell_n) + R(\ell_n)\Gamma_a(0)\overset{<}{U}_j(0)]H(\ell_n - x).$$

$$\overset{>}{U}{}^m_j(x) = R(x - \ell_n)[I + C_{11}^{-1}C_{12}\Gamma_b(\ell_n)]^{-1}[I + C_{11}^{-1}C_{12}\Gamma_{bn}(\ell_n)]\overset{>}{U}_j(\ell_n - 0)H(x - \ell_n).$$

$$\overset{>>}{U}{}^m_j(x) = R(x - \ell_n)[I + C_{11}^{-1}C_{12}\Gamma_b(\ell_n)]^{-1}[I + C_{11}^{-1}C_{12}\Gamma_{bn}(\ell_n)]\overset{>>}{U}_j(\ell_n - 0)H(x - \ell_n).$$

$$\overset{<<<}{U}{}^m_j(x) = R(\ell - x)\Gamma_b(\ell)[\overset{>}{U}{}^m_j(\ell) + \overset{>>}{U}{}^m_j(\ell)]H(x - \ell_n).$$

If the intermediate support is optimized, i.e., the support impedance is matched with the shaft characteristic impedance at that point looking to the left (see Figure 4), or $\Gamma_{bn}(\ell_n) \equiv 0$, the above expressions may be rewritten as follows:

$$\left.\begin{aligned}
&\overset{>>}{U}_j(x) = R(x)\Gamma_a(0)\overset{<}{U}_j(0)H(\ell_n - x)\\
&\overset{<<}{U}_j(x) = 0\\
&\overset{>}{U}{}^m_j(x) = R(x - \ell_n)[I + C_{11}^{-1}C_{12}\Gamma_b(\ell_n)]^{-1}\overset{>}{U}_j(\ell_n - 0)H(x - \ell_n)\\
&\overset{>>}{U}{}^m_j(x) = R(x - \ell_n)[I + C_{11}^{-1}C_{12}\Gamma_b(\ell_n)]^{-1}\overset{>>}{U}_j(\ell_n - 0)H(x - \ell_n)\\
&\overset{<<<}{U}{}^m_j(x) \quad R(\ell - x)\Gamma_b(\ell)R(\ell - \ell_n)[I \quad C_{11}^{-1}C_{12}\Gamma_b(\ell_n)]^{-1}[\overset{>}{U}_j(\ell_n - 0)\\
&\qquad\qquad\qquad\qquad\qquad\qquad\qquad\qquad + \overset{>>}{U}_j(\ell_n - 0)]H(x - \ell_n)
\end{aligned}\right\} \quad (19)$$

It may be seen from the above expressions that the only remaining reflected wave on $(0, \ell_n)$ is $\overset{>>}{U}_j(x)$ which is an unavoidable situation since the left end support is not optimized. However, since $\overset{<<}{U}_j(x) \equiv 0$, it will not be reflected at the intermediate support, and from a vibration minimization standpoint it is optimized on $(0, \ell_n)$. Examining the last three expressions, one may note that the incident wave $\overset{<}{U}_j(x)$ and reflected wave $\overset{>>}{U}_j(x)$ on $(0, \ell_n)$ will travel to $x = \ell_n$ to pass on to (ℓ_n, ℓ) and never return to $(0, \ell_n)$ again. The modified wave will propagate back and forth in the (ℓ_n, ℓ) interval to be damped out eventually by the unmatched impedance at $x = \ell$. It should be remembered that for the waves in this interval the intermediate support behaves as a fixed support and will reflect all of the incoming waves from the right. Proper interpretation of equation 19 is, then, that the intermediate support cannot be optimized to effectively suppress the waves which have propagated into the span or interval adjacent to the span in which the driving force acts.

If the driving force $P(a_j)$ were to act in the (ℓ, ℓ_n) span, $\ell_n < a_j < \ell$, the following should be observed. The equations for the resulting waves may be obtained by proper permutation of the symbols in equations 18 and 19. Again the impedance of the interior support $Z_{bn}(\ell_n)$ works as a filter; this time the incident waves traveling to the left and the reflected waves as they travel from the right end support will pass through in a modified form to $(0, \ell_n)$; and, as in the case of $P(a_j)$ acting in $(0, \ell_n)$, the modified waves will be blocked on the way back by the interior support. Eventually, they will be damped out by the impedance at the end support $x = 0$.

If an interior impedance rather than an end impedance were to be used for optimized control of the vibration amplitudes of the rotating shaft, it should be recognized that disturbing forces $P(a_j)$ in the span $\ell_n < a_j < \ell$ could upset the effectiveness of the interior impedance, due to the fact that the resulting waves in the $(0, \ell_n)$ span have to be

suppressed by the impedance at x = 0. Similarly, the waves generated by forces $P(a_j)$ in $(0, \ell)$ have to be damped out by the impedance at $x = \ell$.

One obvious way to suppress the $\overset{<<<}{U_j^m}(x)$ wave is to let $\Gamma_b(\ell)$ be identically equal to zero, i.e., optimize the end support at $x = \ell$, but it was agreed that, in general, the end conditions are such that they do not lend themselves very readily to optimization.

In view of these facts, the minimization of vibration response in a shaft by means of an intermediate support may be accomplished by letting it approach the support on the right end of the shaft as closely as possible while meeting the condition of matching the shaft impedance looking to the left. Mathematically, this is indicated in the last of equation 19, where as $\ell - \ell_n$ approaches zero, $\overset{<<<}{U_j^m}(x)$ also approaches zero. In other words,

$$\overset{<<<}{U_j^m}(x) = R(\ell - x)\Gamma_{bn}(\ell)[I + C_{11}^{-1}C_{12}\Gamma_{bn}(\ell)]^{-1}[\overset{>}{U_j}(\ell - 0) + \overset{>>}{U_j}(\ell - 0)]H(x - \ell_n) \equiv 0,$$

since $\Gamma_b(\ell)$ becomes $\Gamma_{bn}(\ell) \equiv 0$ and $R(\ell - \ell_n)$ approaches I.

It may be said, then, that the closer the matched intermediate support is placed to the end support, the more effective the amplitude suppression will be in the (ℓ_n, ℓ) portion of the shaft. If the intermediate support were to coincide with the end support, the system would behave as a shaft having only one optimized end. That is, all reflected waves would be suppressed eventually, since $\overset{<<}{U}(x) \equiv 0$. It should be noted, then, that one optimized end support will suppress all reflection waves and that the impedance will have the same value whether one or two optimized end supports are used. The only difference exists in the amplitude response; it is the larger in the case of one optimized support. How much larger it will be depends on how far the impedance value of the other support is from optimum.

In conclusion, it is recommended that the interior support be placed very closely to one of the end supports and that some sort of mounting be used in the end supports to aid in the dissipation of modified traveling waves.

3. Determination of the Matched Impedance of the Interior Support

The optimum impedance, $Z_n(\ell_n)$, of the intermediate support is determined from the condition, $\Gamma_{bn}(\ell_n) \equiv 0$. Using equation 16 and comparing the result with equation 17,

$$z_{bn}(\ell_n) = C_{21} C_{11}^{-1} = z_o.$$

If

$$z_{bn}(\ell_n) = z_b(\ell_n) + z_n(\ell_n),$$

then after establishing $z_b(\ell_n)$ experimentally and computing $z_n(\ell_n)$, the optimum impedance of the intermediate support

$$Z_n(\ell_n) = \begin{bmatrix} Z_{n_{11}} & Z_{n_{12}} \\ Z_{n_{21}} & Z_{n_{22}} \end{bmatrix}$$

may be obtained from

$$z_n(\ell_n) = \frac{1}{\sqrt{\omega}} \overset{\#}{F} Z_n(\ell_n) \overset{\#}{F},$$

where

$$\overset{\#}{F} = \begin{bmatrix} 1 & 0 \\ 0 & \sqrt{\omega} \end{bmatrix}.$$

The components $Z_{n_{11}}$, $Z_{n_{12}}$, $Z_{n_{21}}$, and $Z_{n_{22}}$ may be correlated to physical parameters in the following manner. Let a point support C_o having a mass C_m exist at ℓ_n of the shaft. r_g is the radius of gyration of C_o

about axis of symmetry, r_m is the radius of gyration of C_o about a diameter through the center of gravity of C_o, and ω is the angular velocity of C_o about X_1 axis (see Figure 1). Let a translational spring, K_1, and damper, C_1, be applied to the center of gravity of C_o in a symmetric fashion about the X_1 axis; furthermore, let K_2 and C_2, respectively, be symmetrical rotational springs and dampers applied at the center of gravity of C_o, then the impedance of $Z_n(\ell_n)$ may be written as follows:

$$Z_n(\ell_n) = C_1 \begin{bmatrix} 1 & 0 \\ 0 & \frac{C_2}{C_1} \end{bmatrix} + \frac{K_1}{s} \begin{bmatrix} 1 & 0 \\ 0 & K_2/K_1 \end{bmatrix} + C_m \begin{bmatrix} s & 0 \\ 0 & sr_m^2 - (i\omega)r_g^2 \end{bmatrix}.$$

The $Z_{n_{12}}$ and $Z_{n_{21}}$ are different from zero if the damper and springs are not applied to the center of gravity of C_o. The other two components are for the case in which the forces are applied to the center of gravity of C_o:

$$Z_{n_{11}} = C_1 + \frac{K_1}{s} + C_m s$$

and

$$Z_{n_{22}} = C_2 + \frac{K_2}{s} + C_m [sr_m^2 - (i\omega)r_g^2].$$

VIBRATING BEAM ANALOGY SOLUTION OF THE HYPERCRITICAL SHAFT ON MULTIPLE FLEXIBLE SUPPORTS

THEORY

1. Mathematical Model

The system investigated consists of a rotating shaft supported at an arbitrary number of locations along the length of the shaft on mass-spring-damper units which resist dynamic loads by translation only. The shaft rotating at angular velocity ω is forced by its mass defects distributed along the shaft length. The mass defects are obtained from statically measured quantities of initial bow, ovality, and wall thickness variation, and indicate at any given cross-sectional station along the length of the rotor the magnitude and direction by which the mass center deviates from the axis of rotation. It is assumed here that the axis of rotation coincides with the elastic line of the cross sections of the shaft.

The solution of the equation of motion is accomplished by dividing the system into a number of subsystems. These are analyzed independently and combined eventually by means of the appropriate boundary and conditions at the supports. The system is shown in schematic form in Figure 10.

2. Solutions for the Equation of Motion

The governing differential equation of the motion for any span of the rotating shaft is in its nondimensional form:

$$Y_{1xxxx} + Y_{1tt} = \omega^2 \epsilon(x) e^{i\omega t} \tag{20}$$

where

Y_1 = normalized runout amplitude in complex coordinates

x = position coordinate along axis of the shaft

ω = angular velocity of the driving forces

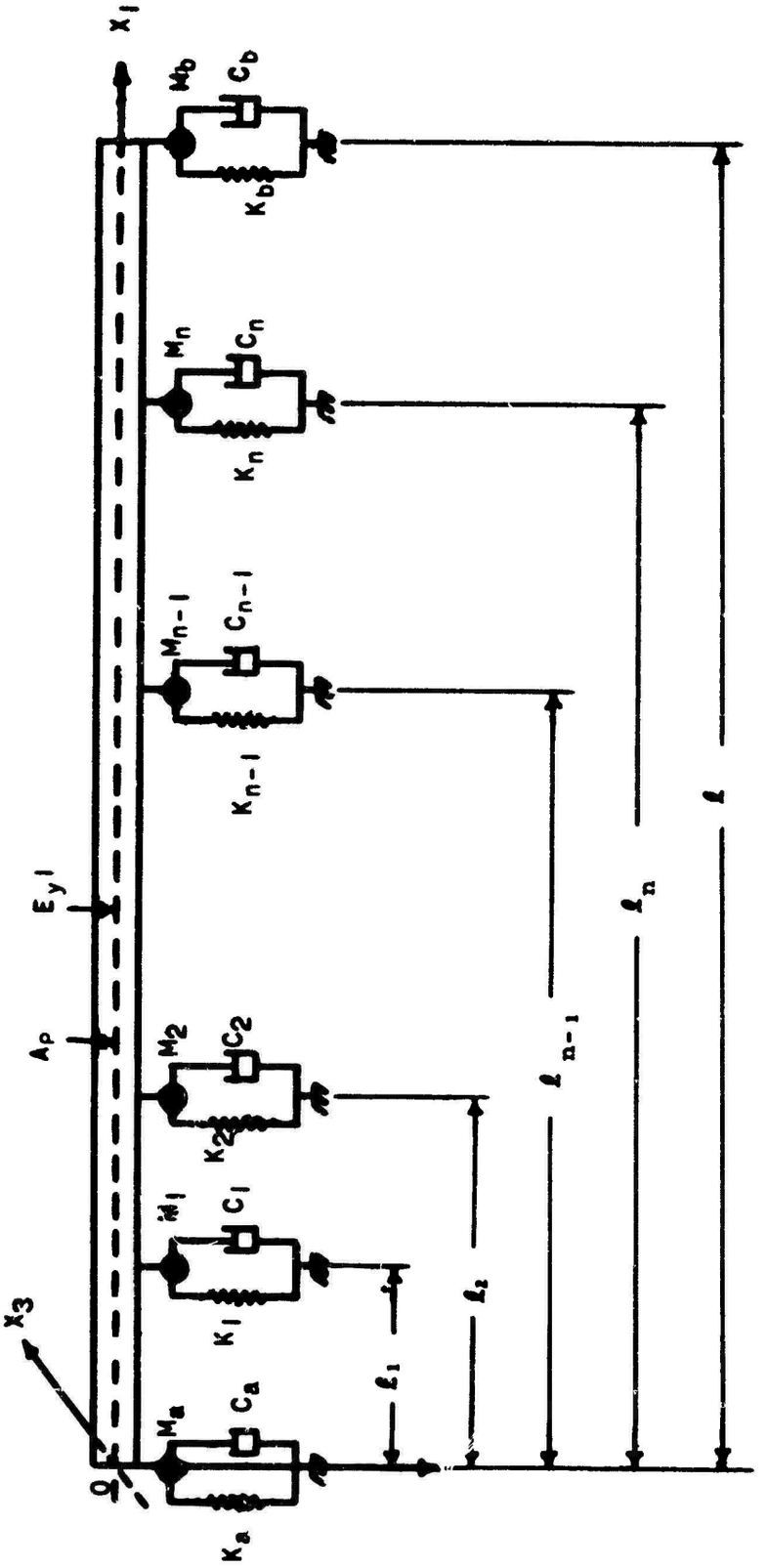

Figure 10. Uniform Shaft on Multiple Translational Supports.

$\epsilon(x)$ = normalized vector distance of mass centers from axis of rotation

The steady state solution of equation 20 for any span between two successive supports, ℓ_{k-1} and ℓ_k, is

$$Y_1 = y(x)e^{i\omega t} \tag{21}$$

where

$$y(x) = A_{k1}\cosh\beta x + A_{k2}\mathrm{Sinh}\beta x + A_{k3}\cos\beta x + A_{k4}\sin\beta x + \sum_{r=1}^{\infty} \frac{\omega^2 \epsilon_r \phi_r(x)}{\omega_r^2 - \omega^2} \text{ --- for } \ell_{k-1} \leq x \leq \ell_k .$$

A_{k1}, A_{k2}, A_{k3}, and A_{k4} are integration constants and

$$\beta = \sqrt[4]{\rho \frac{A\ell^4}{E_y I} \omega^2}$$

$$\epsilon_r = \frac{1}{\ell_k - \ell_{k-1}} \int_{\ell_{k-1}}^{\ell_k} \epsilon(x)\phi_r(x)\,dx$$

$\phi_r(x)$ = normal modes of vibration for a free-free beam

= $\cosh\sqrt{\omega}_r x + \cos\sqrt{\omega}_r x - \sigma(\sinh\sqrt{\omega}_r x + \sin\sqrt{\omega}_r x)$

in which for the first five terms,

r	$\sqrt{\omega_r}$	σ_r
1	4.7300388	0.9825022
2	7.8532045	1.0007773
3	10.995607	0.9999665
4	14.137165	1.0000015
5	17.278759	0.9999999

and for $r > 5$,

$$\sqrt{\omega_r} = \frac{\pi}{2}(2r + 1)$$

$$\sigma_r = 1 - \frac{2e^{\sqrt{\omega_r}}(\cos\sqrt{\omega_r} - \sin\sqrt{\omega_r}) - 2e^{-2\sqrt{\omega_r}}}{1 - 2e^{\sqrt{\omega_r}}\sin\sqrt{\omega_r} - e^{-2\sqrt{\omega_r}}}.$$

3. Boundary Conditions

The boundary conditions at each extreme end of the shaft are:

$$\text{at } x = 0 \qquad Y_{1xx}(0) = 0; \qquad Y_{1xxx}(0) + Z_a Y_1(0) = 0,$$

$$x = \ell \qquad Y_{1xx}(\ell) = 0; \qquad Y_{1xxx}(\ell) + Z_b Y_1(\ell) = 0,$$

where

n = number of intermediate supports

$Z_k = K_k + iC_k\omega - M_k\omega^2$ complex force per unit displacement (impedance) at kth support

K_k = spring coefficient at kth support

C_k = damping coefficient at kth support

M_k = mass of kth support

Substitution of the boundary conditions into equation 21 yields

$$A_{a_1} - A_{a_3} = 0$$

$$\frac{Z_a}{\beta^3} A_{a_1} + \frac{Z_a}{\beta^3} A_{a_3} - A_{a_4} = \frac{Z_a}{\beta^3} Y_{1p}(0)$$

$$\left[\cosh\beta\right] A_{b_1} + \left[\sinh\beta\right] A_{b_2} - \left[\cos\beta\right] A_{b_3} - \left[\sin\beta\right] A_{b_4} = 0$$

$$\left[\sinh\beta + \frac{Z_b}{\beta^3}\cosh\beta\right] A_{b_1} + \left[\cosh\beta + \frac{Z_b}{\beta^3}\sinh\beta\right] A_{b_2} + \left[\sin\beta + \frac{Z_b}{\beta^3}\cos\beta\right] A_{b_3}$$
$$+ \left[-\cos\beta + \frac{Z_b}{\beta^3}\sin\beta\right] A_{b_4} = -\frac{Z_b}{\beta^3} Y_{1p}(\ell),$$

where $Y_{1p} = \sum_{r=1}^{\infty} \frac{\omega^2 \epsilon_r \phi_r(x)}{\omega_r^2 - \omega_o^2}$.

Let

$$H_a = \begin{bmatrix} 1 & 0 & -1 & 0 \\ \frac{Z_a}{\beta^3} & 1 & \frac{Z_a}{\beta^3} & -1 \\ 0 & 0 & 0 & 0 \\ 0 & 0 & 0 & 0 \end{bmatrix}$$

and

$$H_b = \begin{bmatrix} 0 & 0 & 0 & 0 \\ 0 & 0 & 0 & 0 \\ \cosh\beta & \sinh\beta & -\cos\beta & -\sin\beta \\ \sinh\beta + \frac{Z_b}{\beta^3}\cosh\beta & \cosh\beta + \frac{Z_b}{\beta^3}\sinh\beta & \sin\beta + \frac{Z_b}{\beta^3}\cos\beta & -\cos\beta + \frac{Z_b}{\beta^3}\sin\beta \end{bmatrix} .$$

Also let

$$A_k = \begin{Bmatrix} A_{k_1} \\ A_{k_2} \\ A_{k_3} \\ A_{k_4} \end{Bmatrix} \qquad E = \begin{Bmatrix} 0 \\ -\frac{Z_a}{\beta^3} Y_{1P}(0) \\ 0 \\ -\frac{Z_b}{\beta^3} Y_{1P}(\ell) \end{Bmatrix} .$$

The boundary conditions at $x = 0$ and $x = \ell$ may be written in matrix rotation as follows:

$$H_a A_a + H_b A_b = E . \tag{22}$$

Boundary and continuity conditions at the kth intermediate support are:

$$\begin{aligned} Y_1(\ell_k + 0) &= Y_1(\ell_k - 0) \\ Y_{1x}(\ell_k + 0) &= Y_{1x}(\ell_k - 0) \\ Y_{1xx}(\ell_k + 0) &= Y_{1xx}(\ell_k - 0) \\ Y_{1xxx}(\ell_k + 0) &= Y_{1xxx}(\ell_k - 0) + Z_k Y_1(\ell_k - 0), \end{aligned}$$

where -0, +0 denote, respectively, the limit from the right and the limit from the left. When expressed in matrix rotation, these equations may be written as

$$S_k A_{k+1} = S_k A_k + \frac{Z_k}{\beta^3} T_k A_k + \frac{Z_k}{\beta^3} B_k , \tag{23}$$

where

$$S_k = \begin{bmatrix} \cosh\beta\ell_k & \sinh\beta\ell_k & \cos\beta\ell_k & \sin\beta\ell_k \\ \sinh\beta\ell_k & \cosh\beta\ell_k & -\sin\beta\ell_k & \cos\beta\ell_k \\ \cosh\beta\ell_k & \sinh\beta\ell_k & -\cos\beta\ell_k & -\sin\beta\ell_k \\ \sinh\beta\ell_k & \cosh\beta\ell_k & \sin\beta\ell_k & -\cos\beta\ell_k \end{bmatrix},$$

$$T_k = \begin{bmatrix} 0 & 0 & 0 & 0 \\ 0 & 0 & 0 & 0 \\ 0 & 0 & 0 & 0 \\ \cosh\beta\ell_k & \sinh\beta\ell_k & \cos\beta\ell_k & \sin\beta\ell_k \end{bmatrix},$$

$$B_k = \begin{Bmatrix} 0 \\ 0 \\ 0 \\ Y_{1p}(\ell_k) \end{Bmatrix}.$$

Dividing by S_k, equation 23 becomes

$$A_{k+1} = \left[I + \frac{Z_k}{\beta^3} S_k^{-1} T_k\right] A_k + \frac{Z_k}{\beta^3} S_k^{-1} B_k,$$

where I = identity matrix.

Let

$$P_k = S_k^{-1} T_k \text{ and } Q_k = S_k^{-1} B_k;$$

then from the recurrence formula,

$$A_{k+1} = \left[I + \frac{Z_k}{\beta^3} P_k \right] A_k + \frac{Z_k}{\beta^3} Q_k . \tag{24}$$

it follows that

$$A_b = R_b A_a + G_b , \tag{25}$$

where if

$$R_a = I$$
$$G_a = 0,$$

then

$$R_b = \left[I + \frac{Z_n}{\beta^3} P_n \right] R_n ,$$
$$R_n = \left[I + \frac{Z_{n-1}}{\beta^3} \right] R_{n-1} ,$$

.

.

.

$$R_1 = \left[I + \frac{Z_a}{\beta^3} \right] R_a ,$$

and

$$G_b = \frac{Z_n}{\beta^3} Q_n + \left[I + \frac{Z_n}{\beta^3} P_n \right] G_n,$$

$$G_n = \frac{Z_n - 1}{\beta^3} Q_{n-1} + \left[I + \frac{Z_{n-1}}{\beta^3} P_{n-1} \right] G_{n-1},$$

.

.

.

$$G_1 = \frac{Z_a}{\beta^3} Q_a + \left[I + \frac{Z_a}{\beta^3} P_a \right] G_a.$$

Substitution of equation 25 into equation 22 yields

$$H_a A_a + H_b \left[R_b A_a + G_b \right] = E.$$

Rearranging terms,

$$A_a = \left[H_a + H_b R_b \right]^{-1} \left[E - H_b G_b \right]. \tag{26}$$

Solving for A_a, all other coefficients, A_b, A_n, --, A_k, --, A_1, can be obtained with equations 24 and 25. The amplitude runout at any span (ℓ_{k+1}, ℓ_k) can then be computed with equation 21.

NUMERICAL RESULTS

1. Computer Program

A computational procedure based on equations 21, 24, 25, and 26 has been programmed for the University of Virginia Burroughs B 5000 high-speed digital computer. Typical numerical results are presented in the next section.

A flow diagram of the computer program is presented in Appendix III. It will compute the runout amplitudes in terms of given frequencies at an arbitrary number of points for any initial defects distribution for a shaft flexibly supported at as many points as possible from a computational standpoint. This maximum number of supports feasible for any given computer run depends on the rate of convergence of the numerical solution of equation 26, which decreases rapidly with an increasing number of supports. It is believed that a shaft having five intermediate supports represents a practical upper limit that can be processed with any reasonable speed and accuracy.

2. Presentation of Results for Parameter Study

A limited parameter study in terms of several massless spring-damper configurations has been performed for the 4.5-inch-outside-diameter, 28-foot-long Chinook drive shaft running on one intermediate support. This support is located at one of the following points: one-eighth, one-quarter, and one-half span. The end supports are assumed to possess the characteristics of a simple support, while the intermediate support has any one of the following spring-damper combinations:

Configuration	K lb./in.	C lb. sec./in.
1	0	0
2	1060	0
3	10600	0
4	0	1.954
5	1060	1.954
6	10600	1.954
7	0	5.863
8	1060	5.863
9	10600	5.863

The dimensions and input values used in the parameter study are shown in Figure 11. The results of maximum radial runouts of the shaft at given frequencies in terms of the above listed parameters are presented in graphical form in Figures 12 through 36. For the sake of simplicity, the initial defects curve is assumed to have the shape of a half sine wave lying in a plane through the axis of rotation of the shaft and having a maximum defects amplitude, ϵ_o , at midspan. The

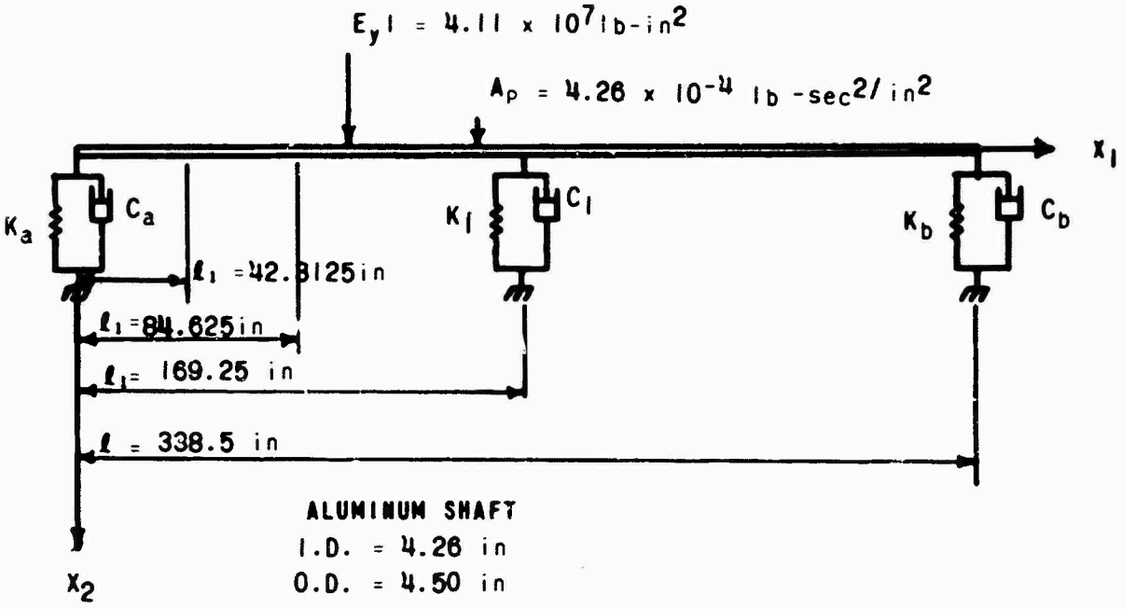

ALUMINUM SHAFT

I.D. = 4.26 in

O.D. = 4.50 in

ℓ_1 = designates the location of intermediate support

$K_a = K_b = 10^8$ lb/in

$C_a = C_b = 0$ lb-sec/i } imitates simple support characteristics

$$K_{beam} = \frac{E_y I}{\ell^3} = 1.06 \text{ lb/in}$$

$$C_{beam} = \frac{(E_y I A_\rho)^{1/2}}{\ell} = 0.39087 \text{ lb-sec/in}$$

$$\omega_o = \pi^2 \sqrt{\frac{E_y I}{\rho A \ell^4}} = 4.26 \text{ cycles/sec}$$

Figure 11. Dimensions and Input Values for the Chinook Drive Shaft.

results are given in nondimensional form; i.e., maximum runout amplitudes are indicated in terms of a unit defects amplitude, frequencies in terms of the fundamental frequency of the simply supported shaft. In this case, the fundamental frequency is $\omega_o = 4.26$ cycles per second. It is hoped that this limited study will indicate trends in shaft behavior, as the spring and damping coefficients, as well as the location of the intermediate support, are varied.

3. Discussion of Results of Parameter Study

Several comments may be made concerning trends in the behavior of shafts on one intermediate support, as presented in Figures 12 through 36.

1. An increase in the spring stiffness of the intermediate support will increase the values of the natural frequencies in accordance with the relationships shown in Figures 37, 38, and 39.
2. Appreciable changes in the damping coefficients do not induce significant shifts in critical frequencies.
3. An increase in the damping coefficients tends to decrease maximum runouts, provided that the accompanying stiffness value is low (<1060 pounds per inch).
4. Placement of the intermediate support near one of the end supports also tends to decrease maximum runouts.

The cross marks shown in Figures 12 through 28 indicate the occurrence of sudden high runout amplitudes, which corresponds with the second and fourth critical frequencies of the shaft for the case in which the support is at midspan and the third critical for the case in which it is at quarter span. In the first case, these criticals are excited by the defects distribution which is not completely symmetrical about midspan due to round-off errors in the computations of the coordinates for the forcing function. This minute asymmetry is of sufficient magnitude to cause large spikelike gains in amplitude at the antisymmetrical critical frequencies, since there is absolutely no damping available from the translational spring damper (located exactly at $\ell_1 = 0.5\ell$) to suppress these gains. In the case of the running shaft in which the intermediate support is located at quarter span, one of the node points of the third critical mode coincides with

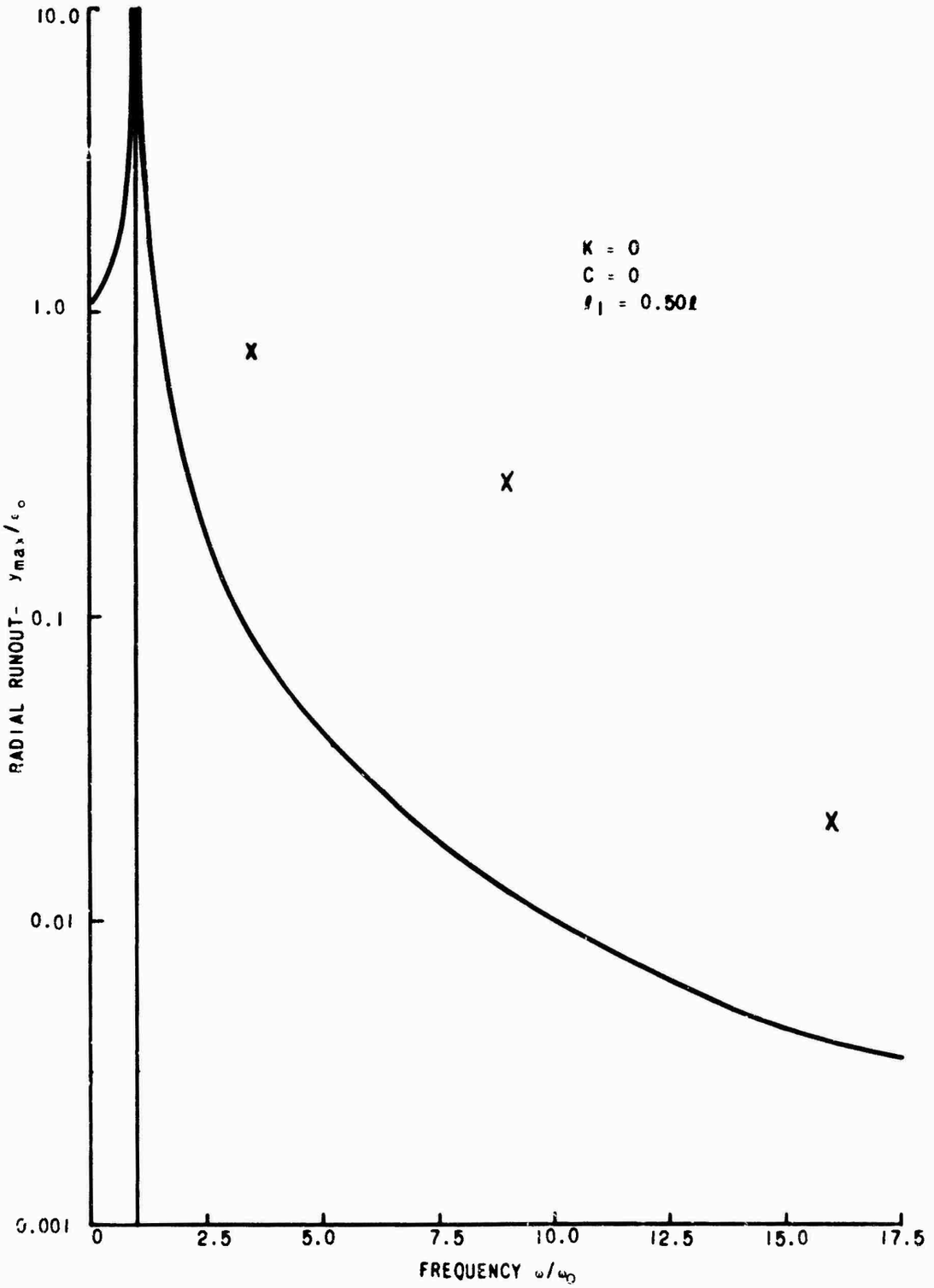

Figure 12. Runout Versus Frequency Curve of a Rotating Shaft for an Intermediate Support at Midspan.

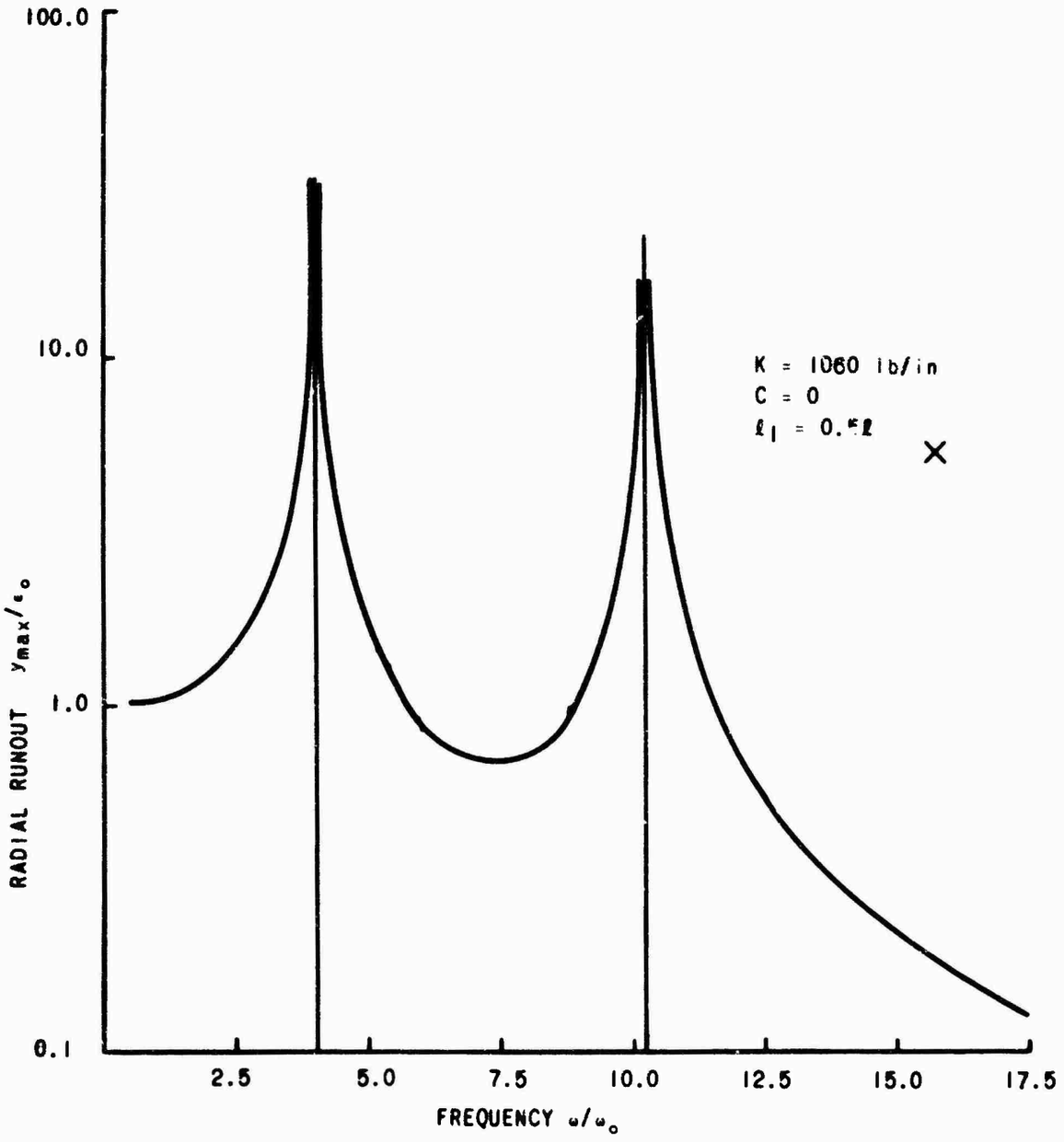

Figure 13. Runout Versus Frequency Curve of a Rotating Shaft for an Intermediate Support at Midspan.

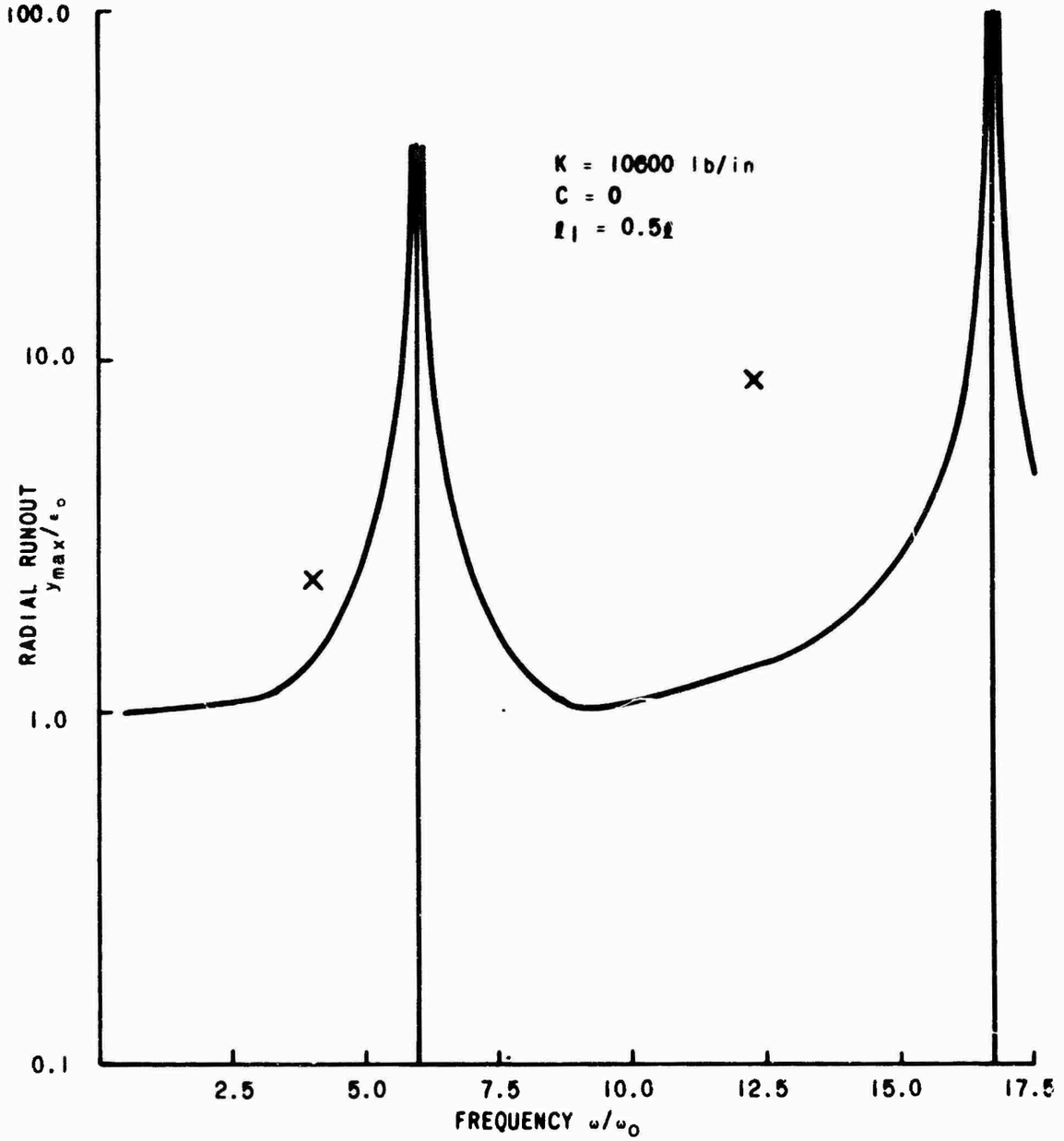

Figure 14. Runout Versus Frequency Curve of a Rotating Shaft for an Intermediate Support at Midspan.

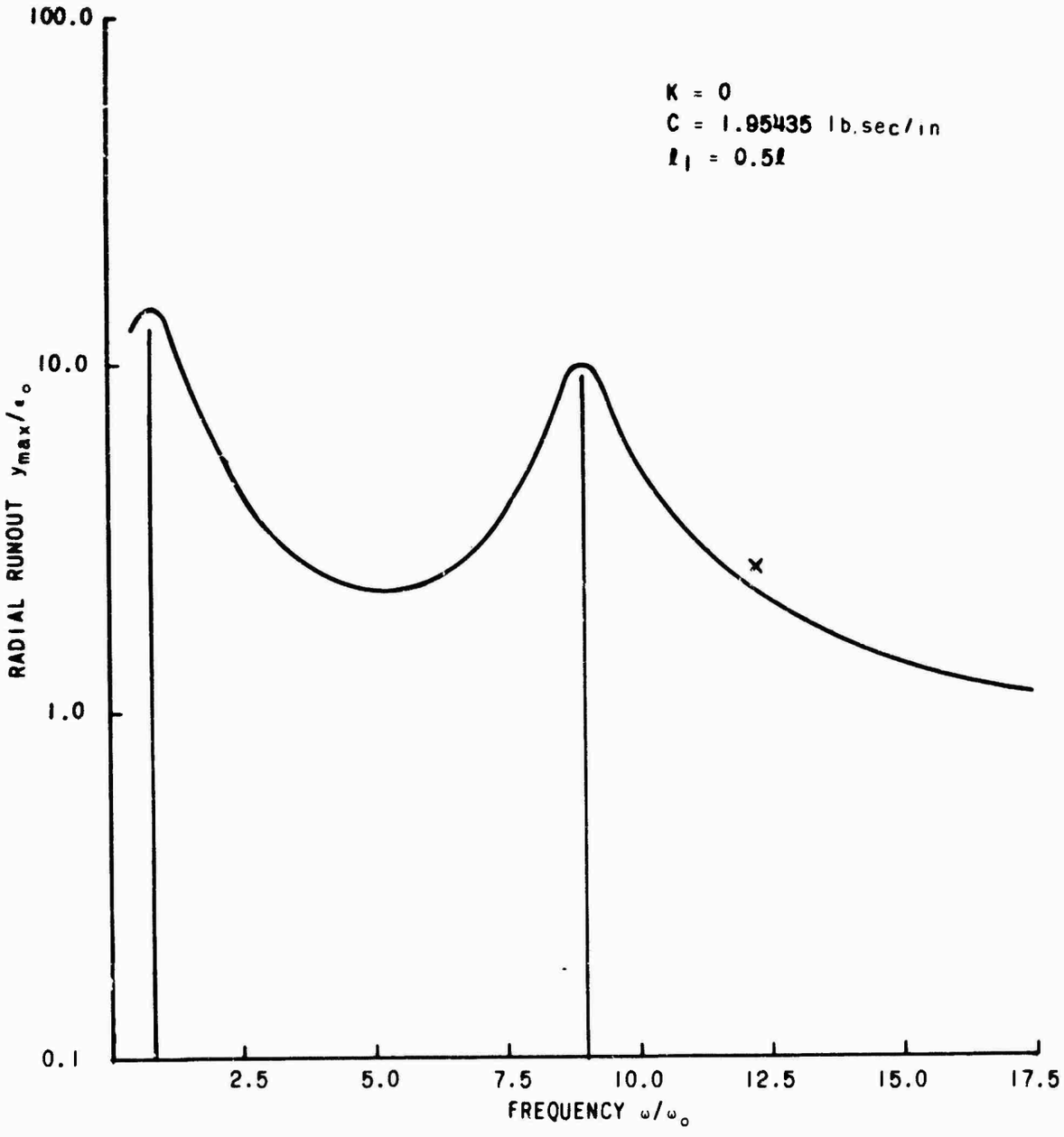

Figure 15. Runout Versus Frequency Curve of a Rotating Shaft for an Intermediate Support at Midspan.

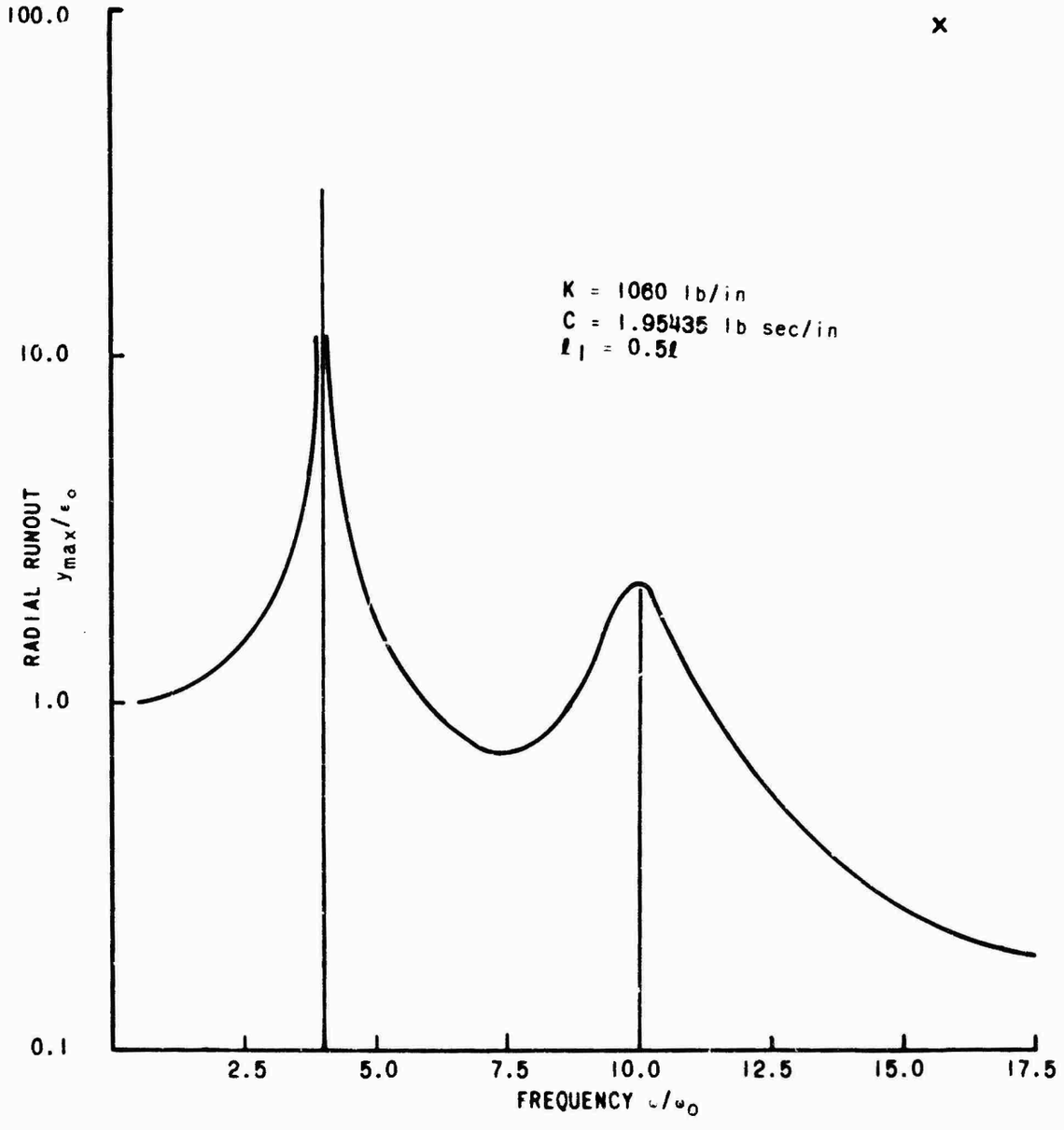

Figure 16. Runout Versus Frequency Curve of a Rotating Shaft for an Intermediate Support at Midspan.

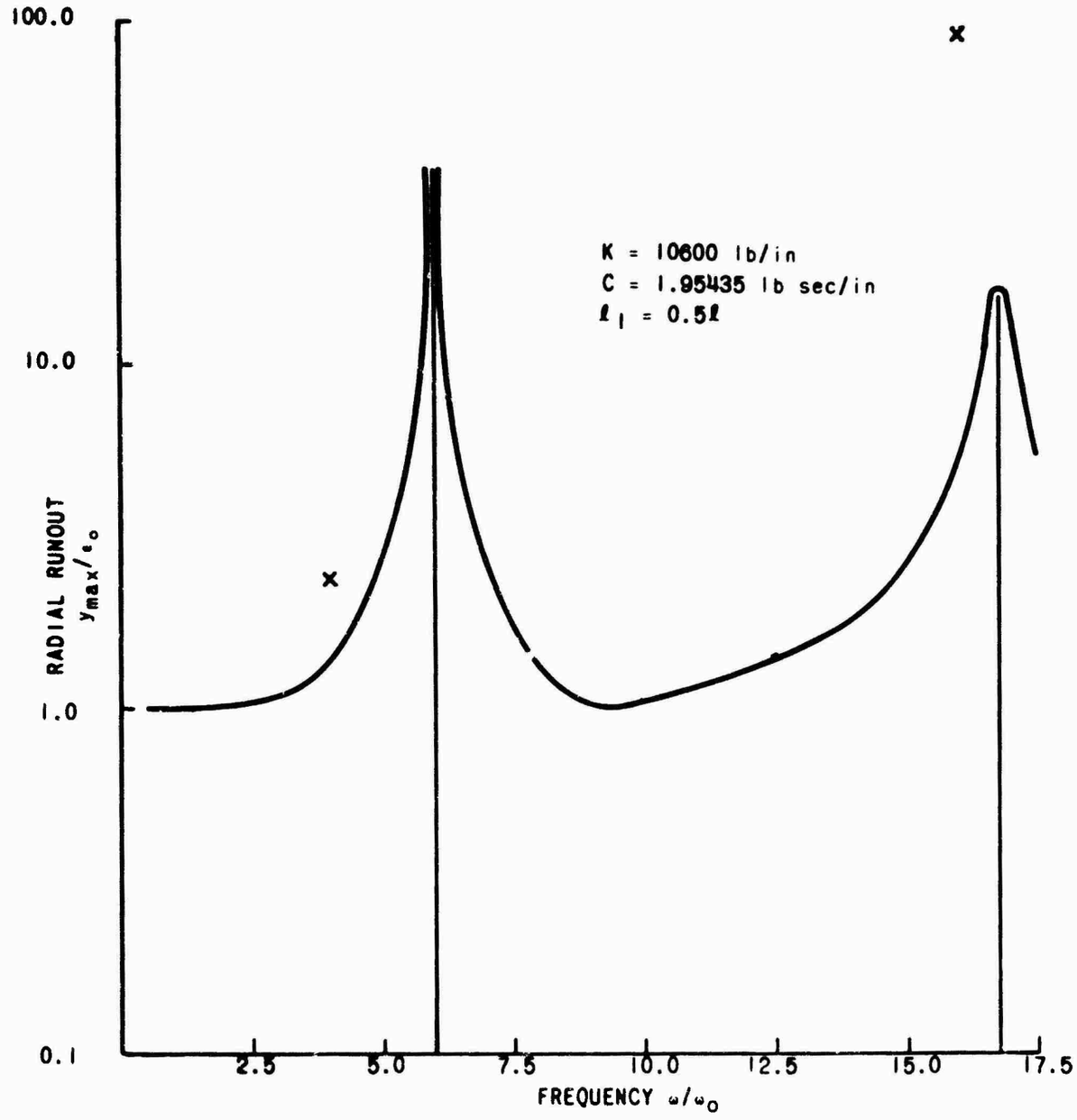

Figure 17. Frequency Curve of a Rotating Shaft for an Intermediate Support at Midspan.

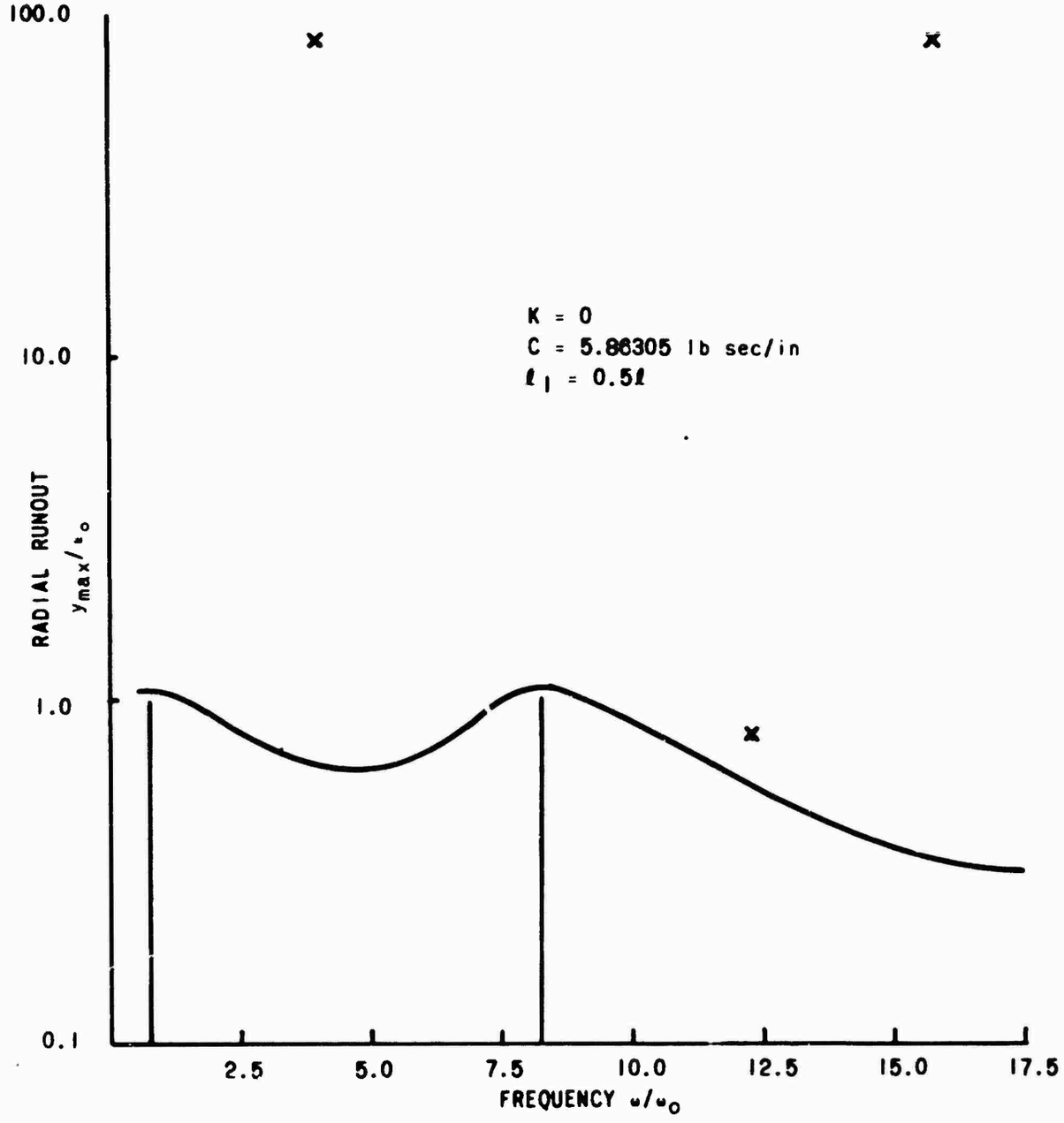

Figure 18. Runout Versus Frequency Curve of a Rotating Shaft for an Intermediate Support at Midspan.

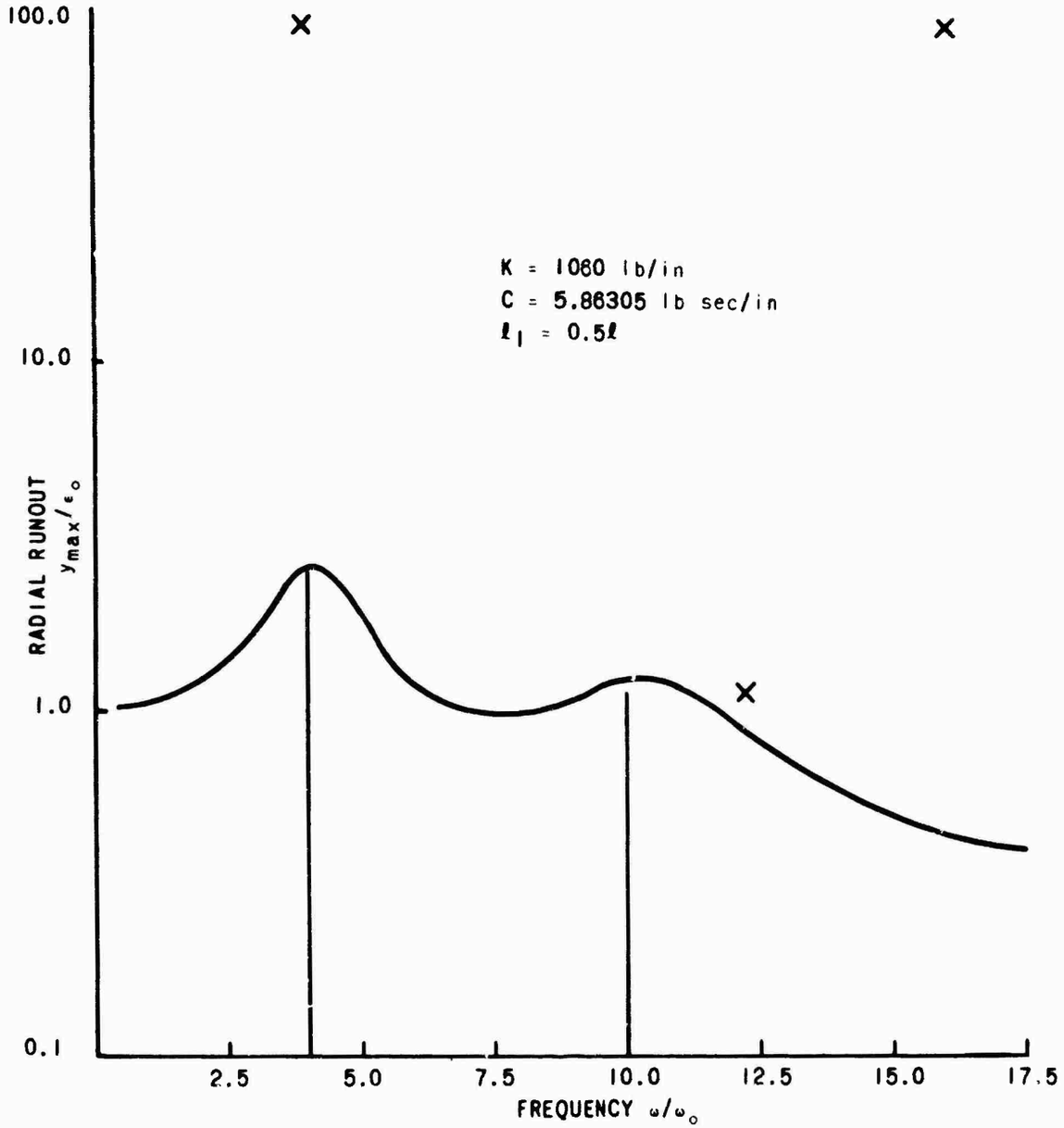

Figure 19. Runout Versus Frequency Curve of a Rotating Shaft for an Intermediate Support at Midspan.

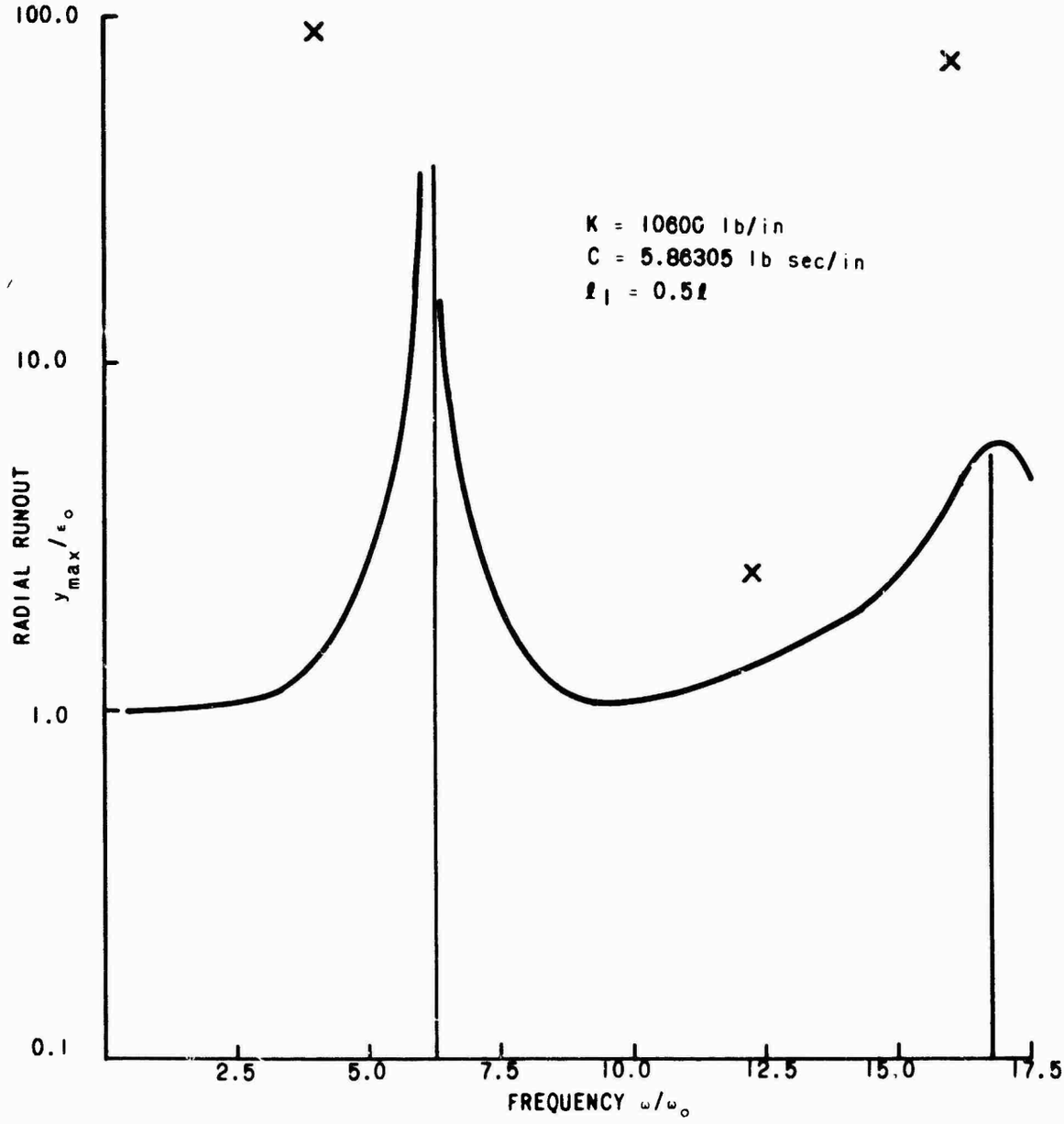

Figure 20. Frequency Curve of a Rotating Shaft for an Intermediate Support at Midspan.

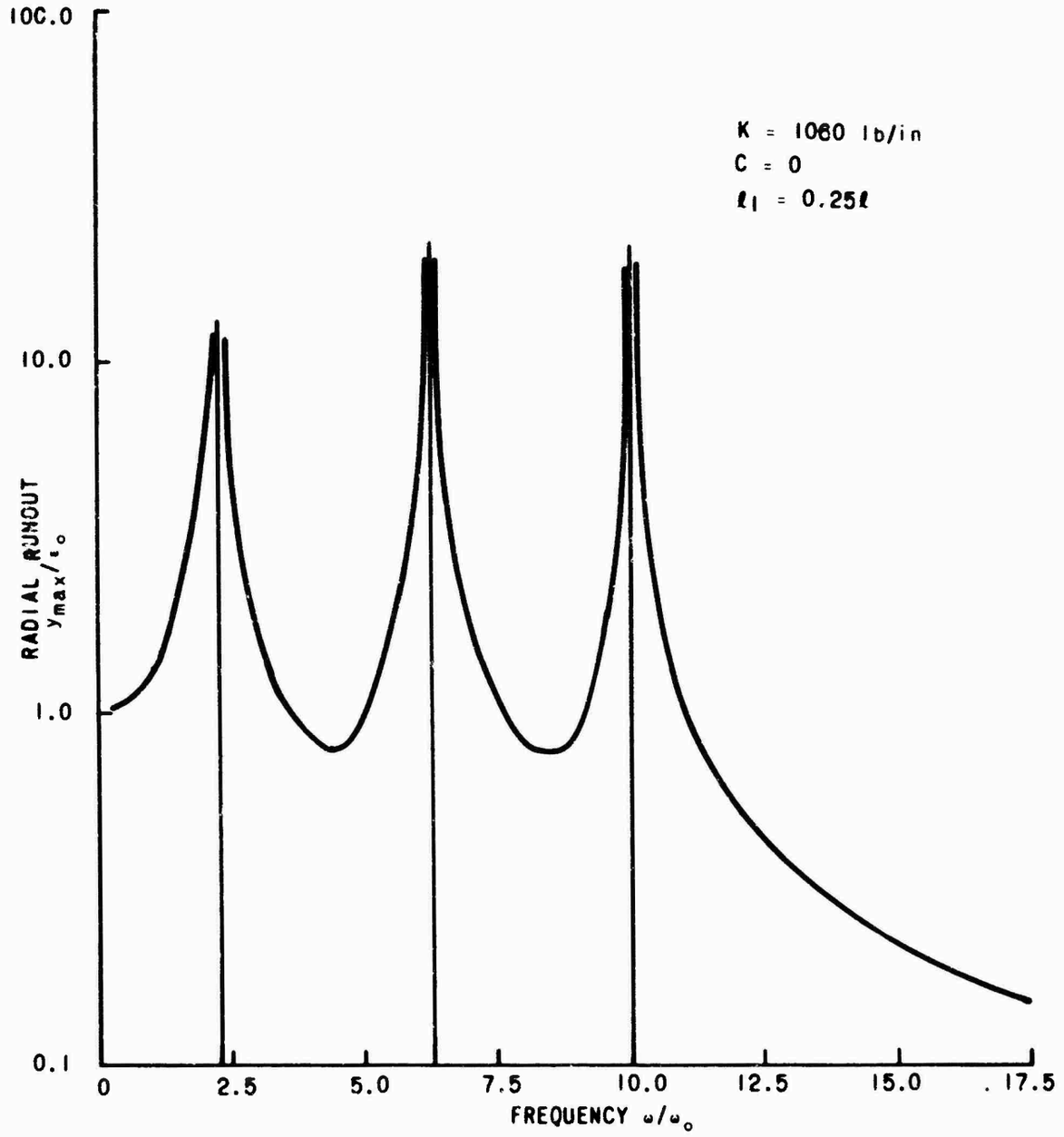

Figure 21. Runout Versus Frequency Curve of a Rotating Shaft for an Intermediate Support at Quarter Span.

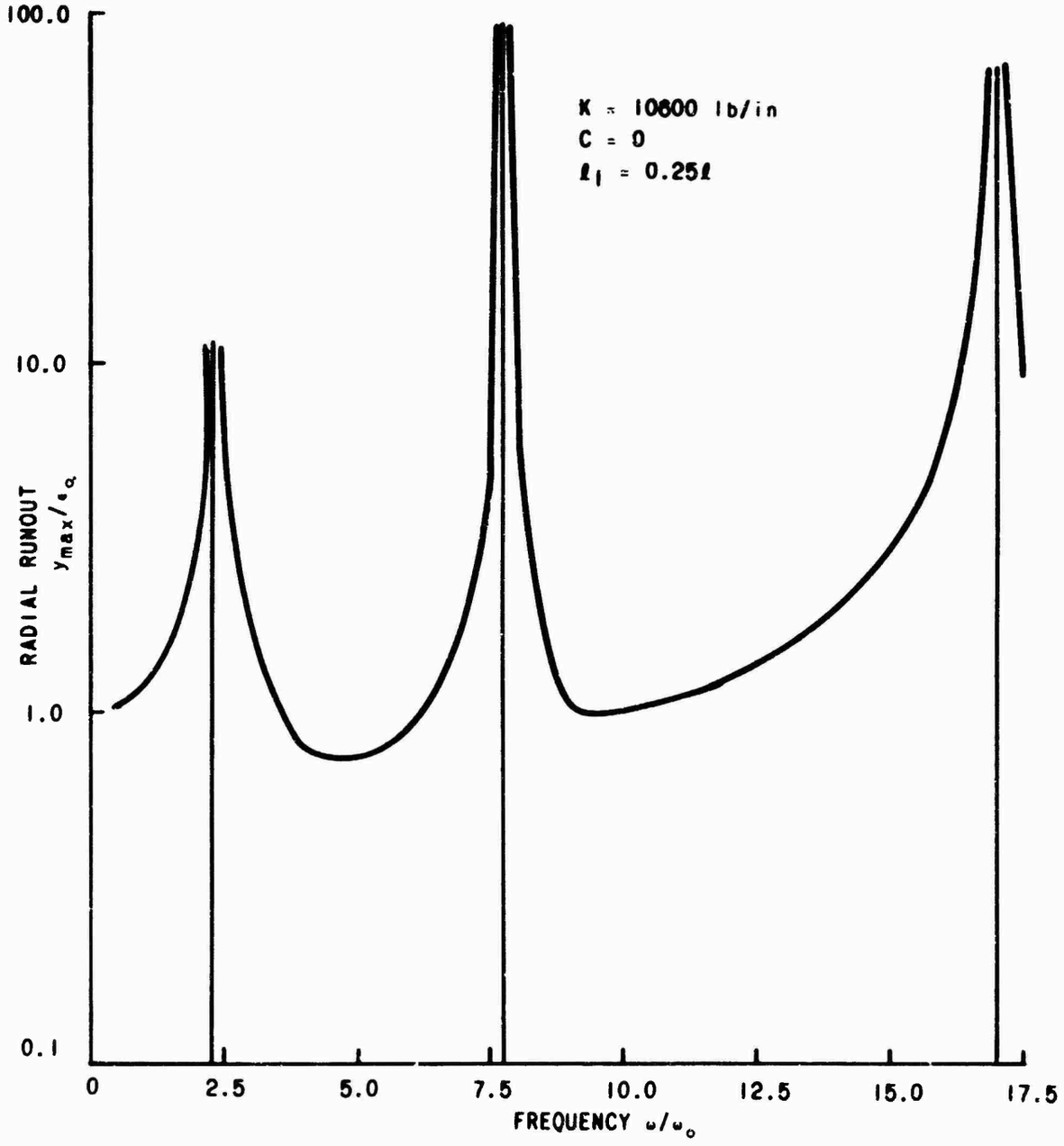

Figure 22. Runout Versus Frequency Curve of a Rotating Shaft for an Intermediate Support at Quarter Span.

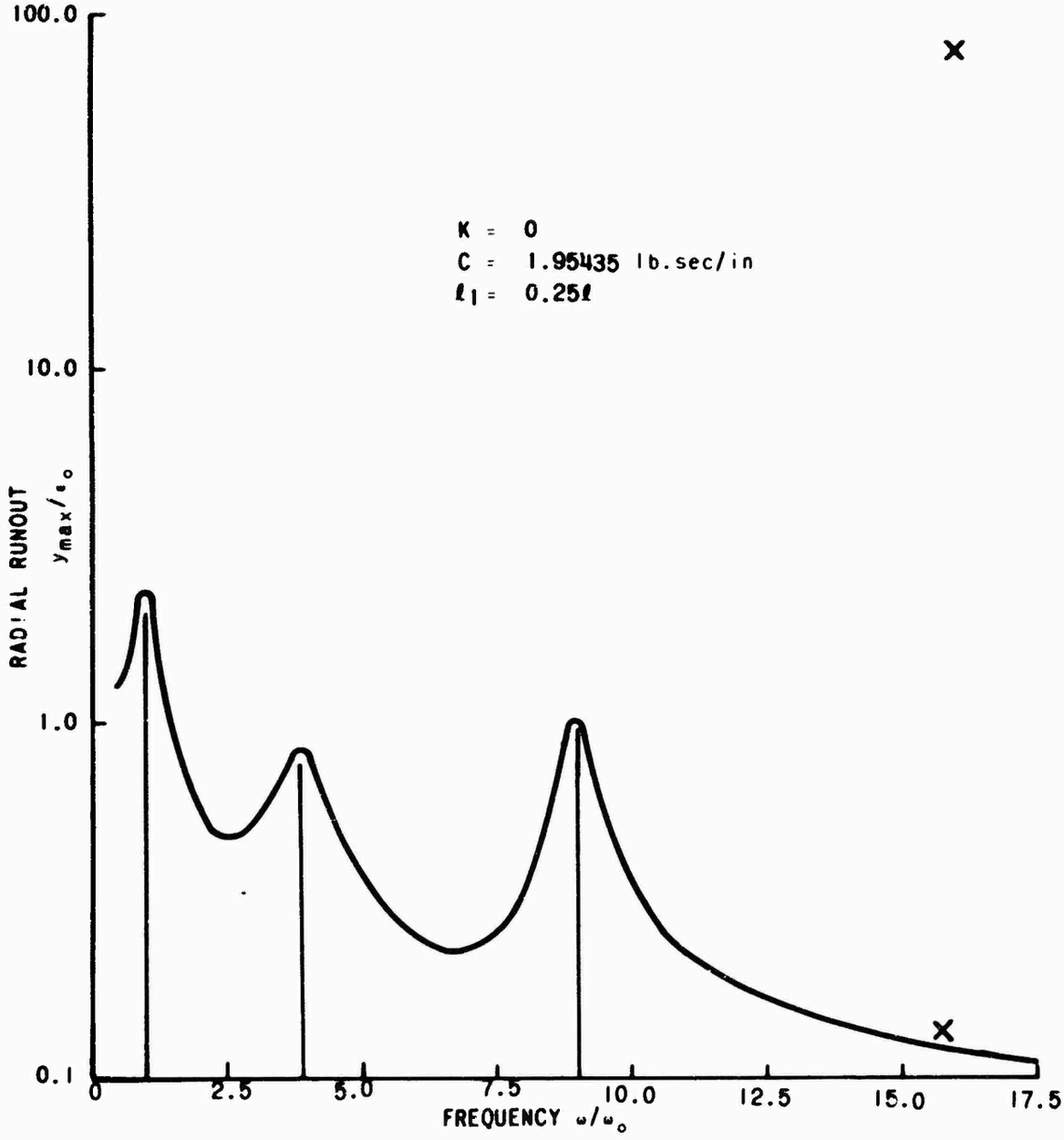

Figure 23. Runout Versus Frequency Curve of Rotating Shaft for an Intermediate Support at Quarter Span.

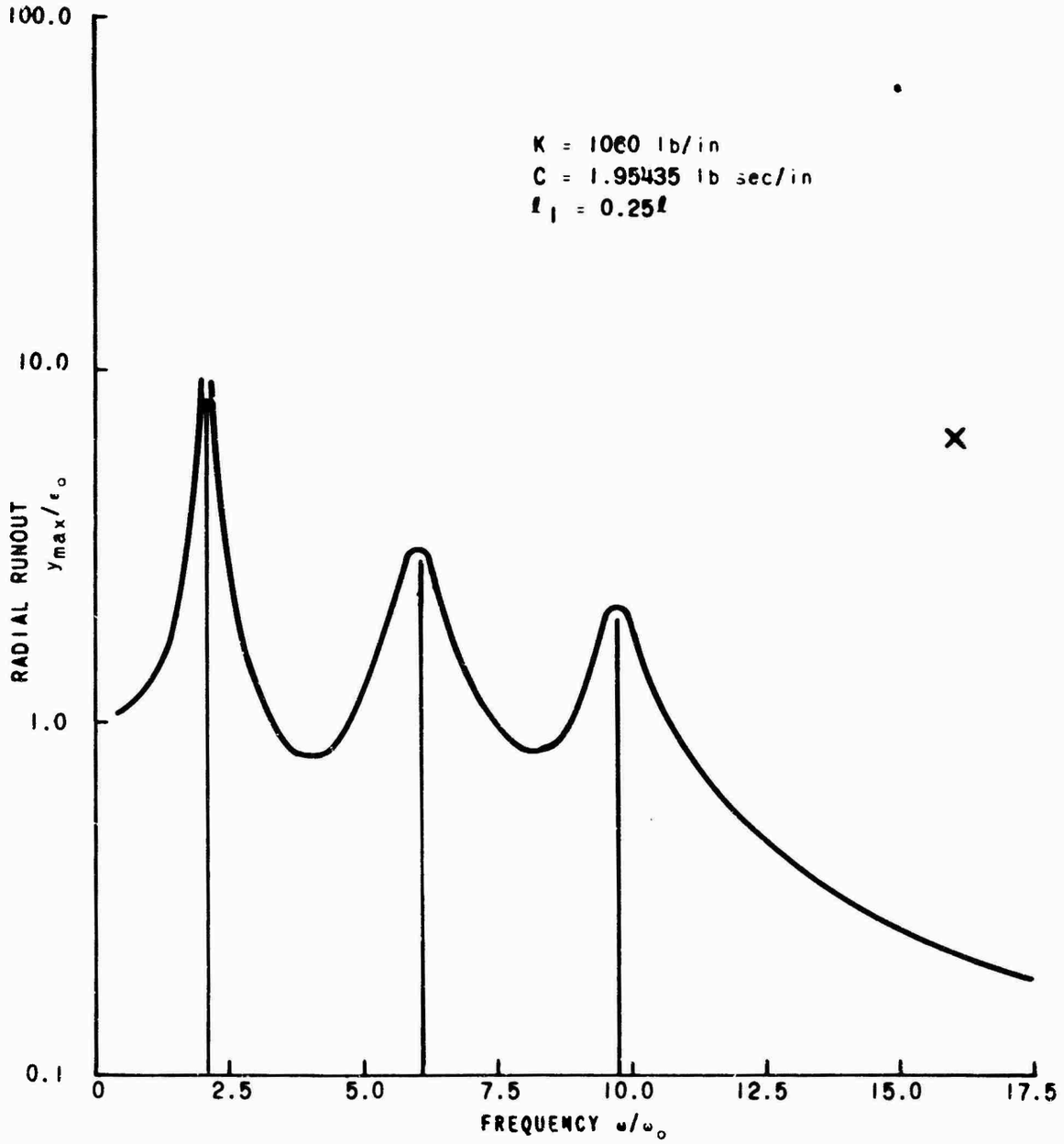

Figure 24. Runout Versus Frequency Curve of a Rotating Shaft for an Intermediate Support at Quarter Span.

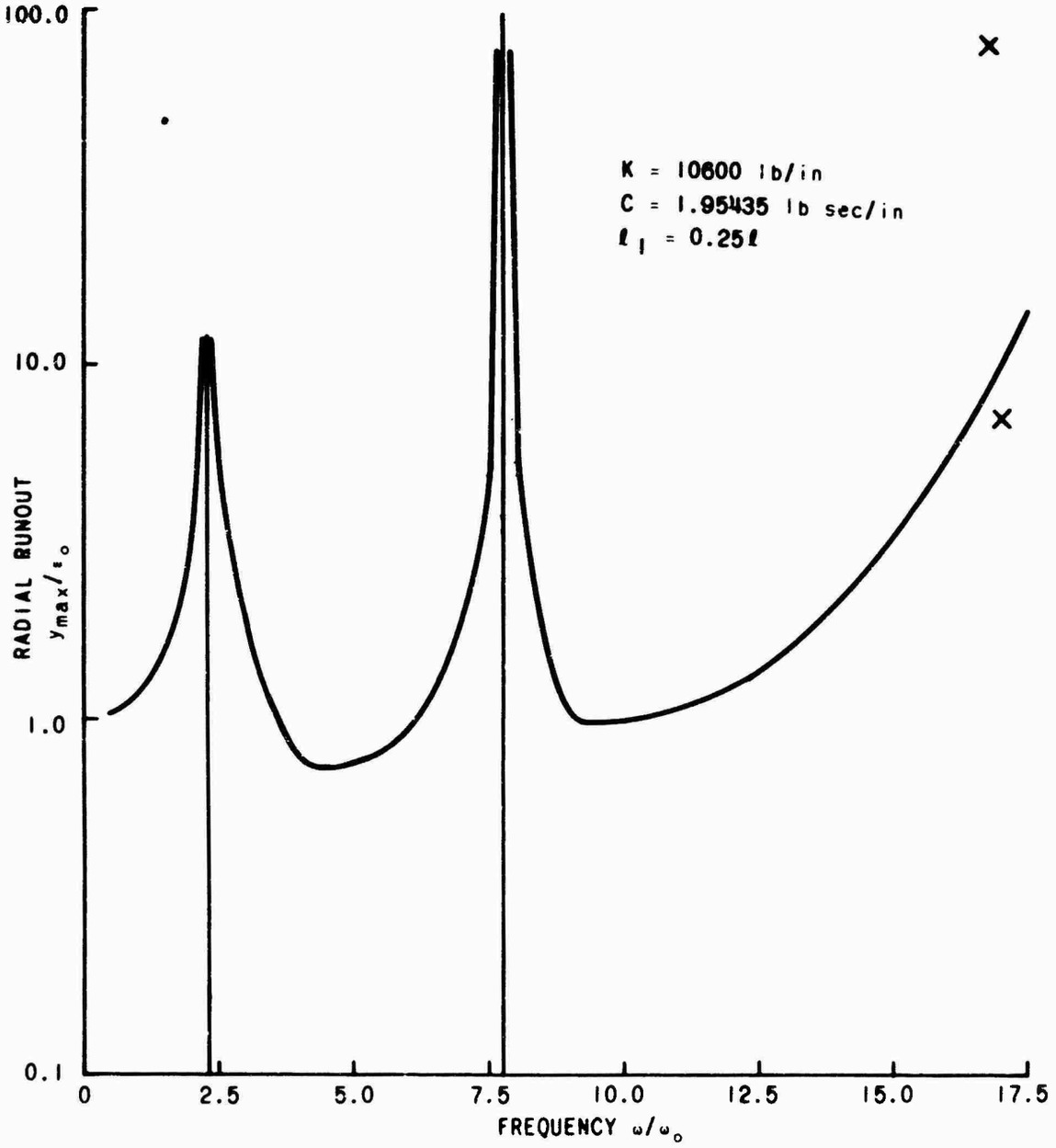

Figure 25. Runout Versus Frequency Curve of a Rotating Shaft for an Intermediate Support at Quarter Span.

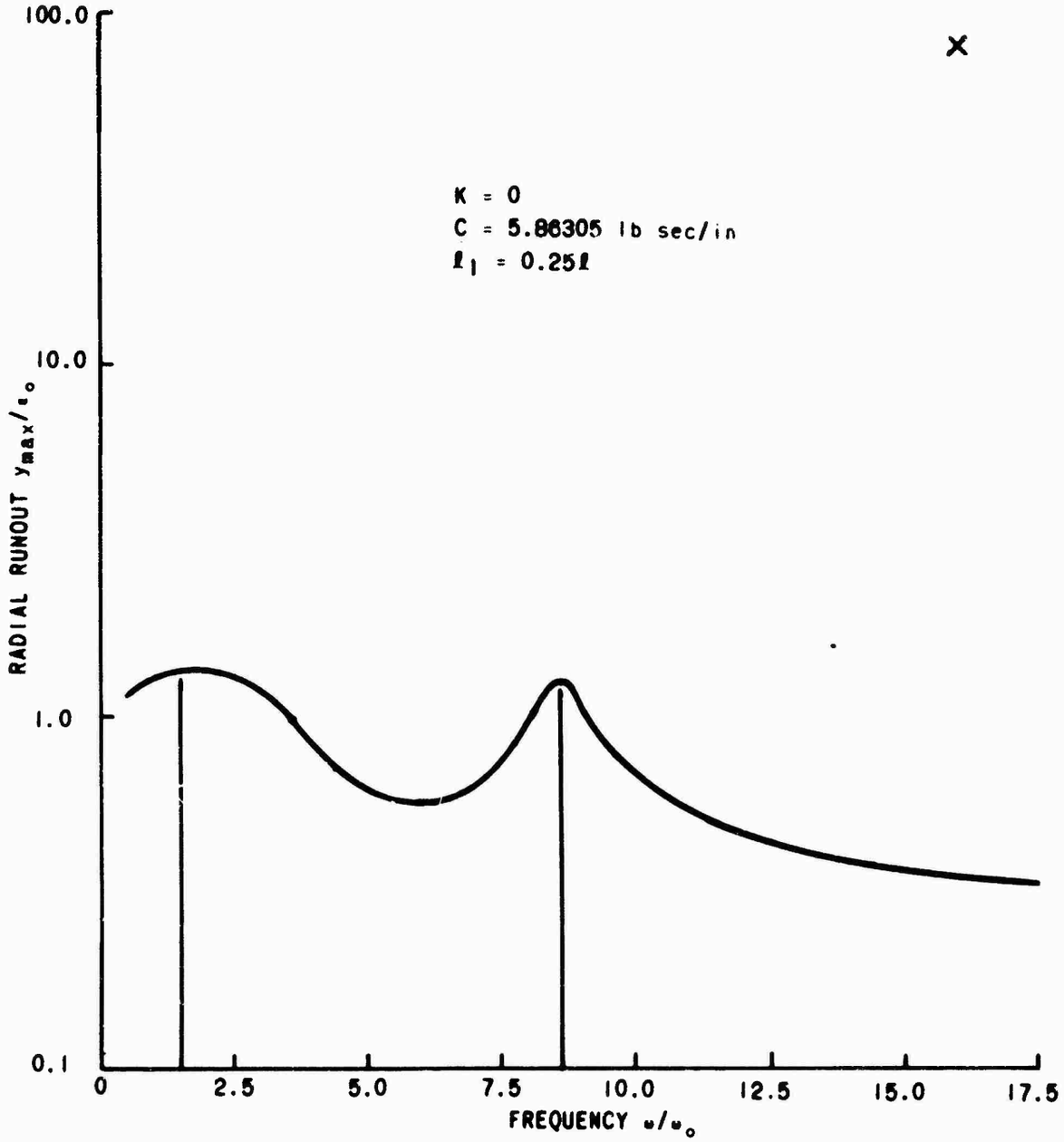

Figure 26. Runout Versus Frequency Curve of a Rotating Shaft for an Intermediate Support at Quarter Span.

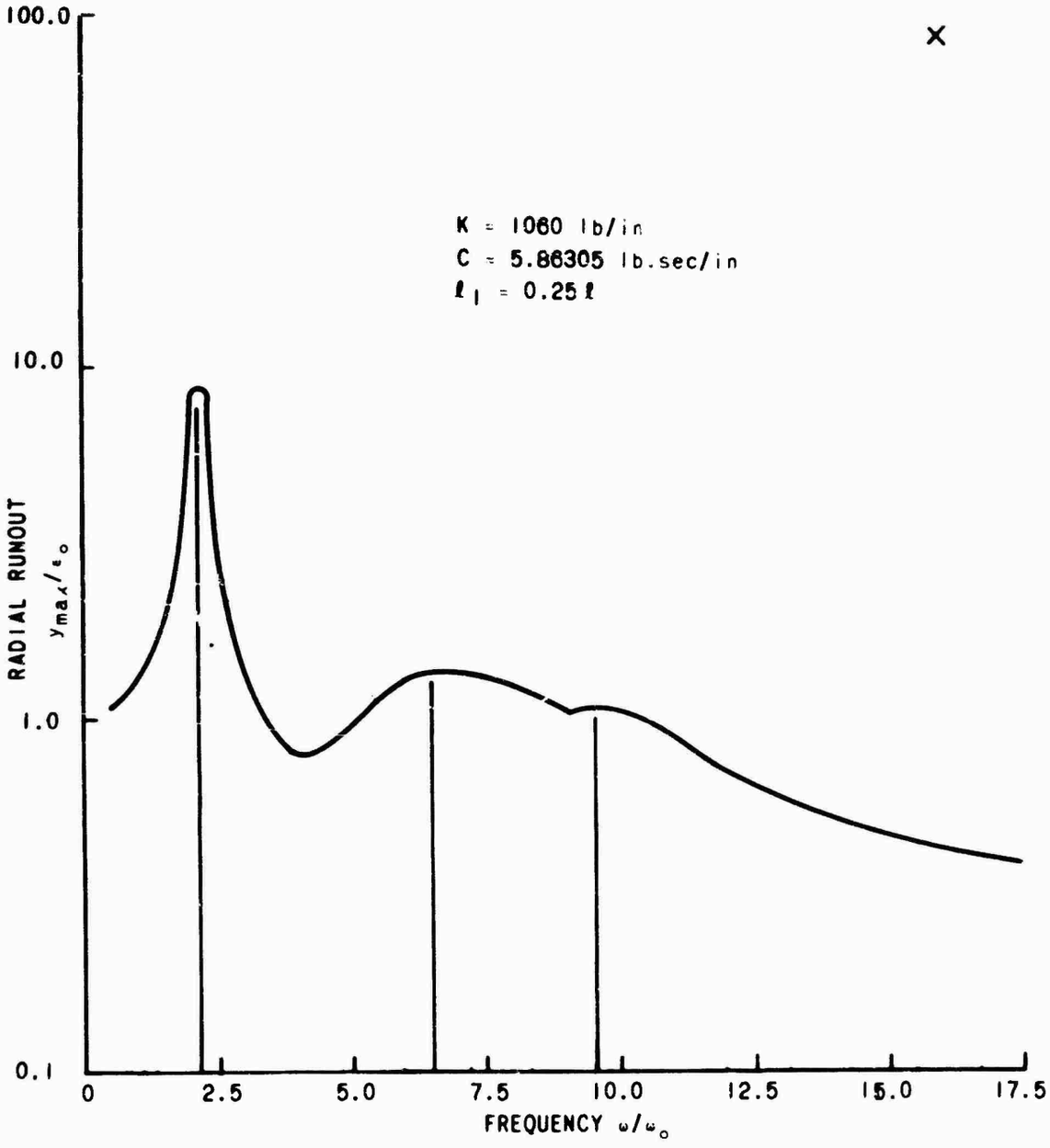

Figure 27. Runout Versus Frequency Curve of a Rotating Shaft for an Intermediate Support at Quarter Span.

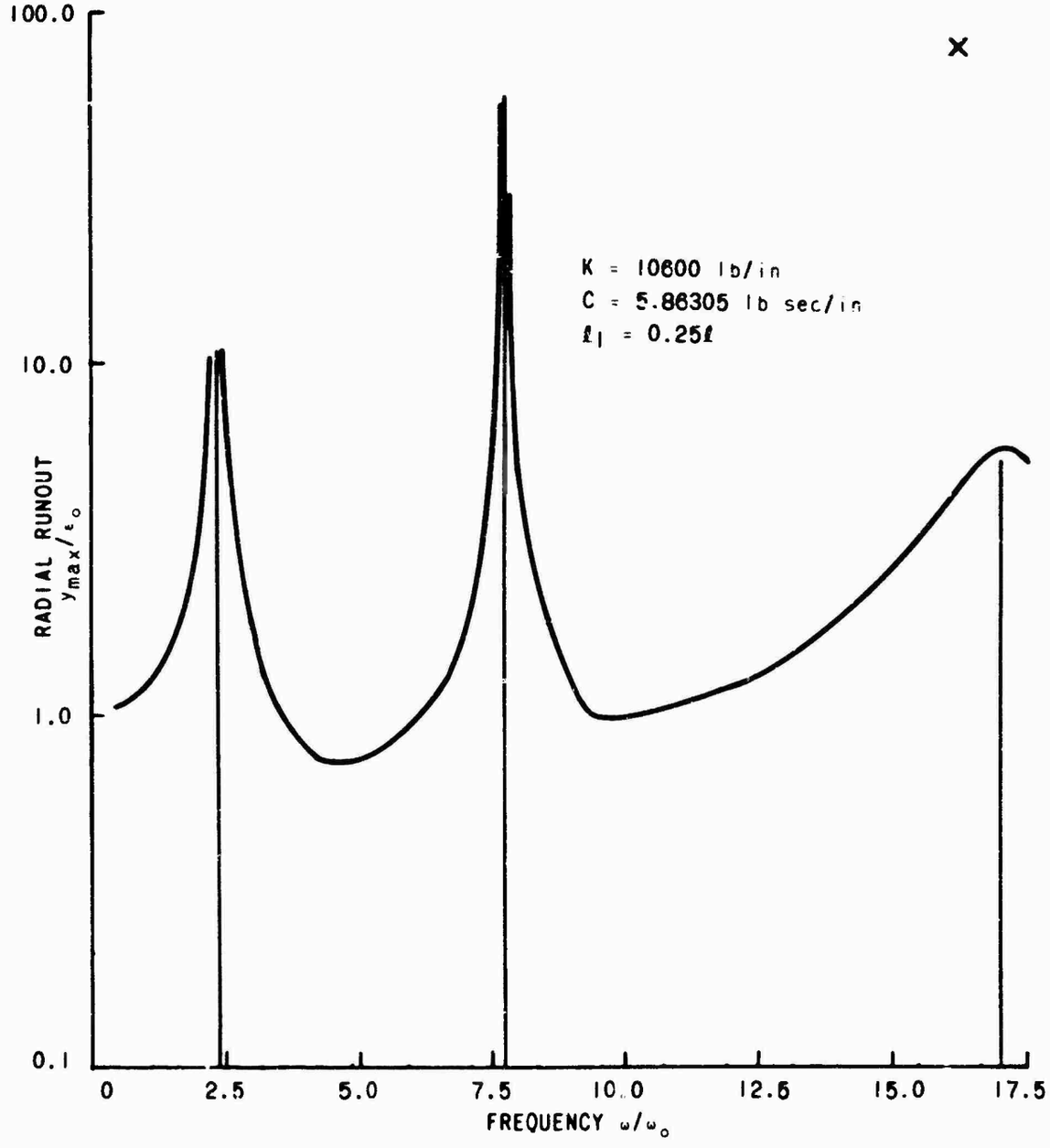

Figure 28. Runout Versus Frequency Curve of a Rotating Shaft for an Intermediate Support at Quarter Span.

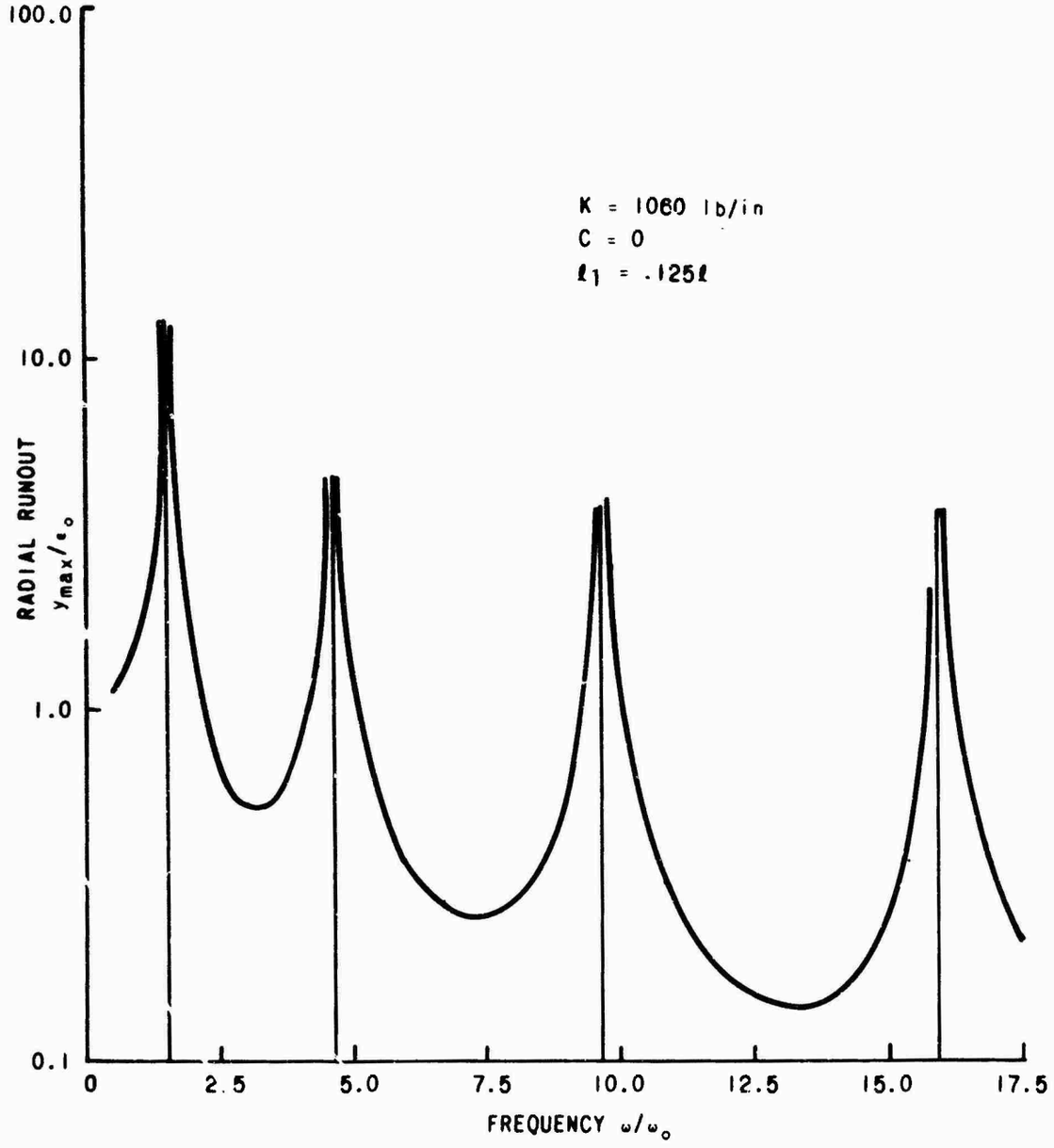

Figure 29. Runout Versus Frequency Curve of a Rotating Shaft For an Intermediate Support at 0.125 Span.

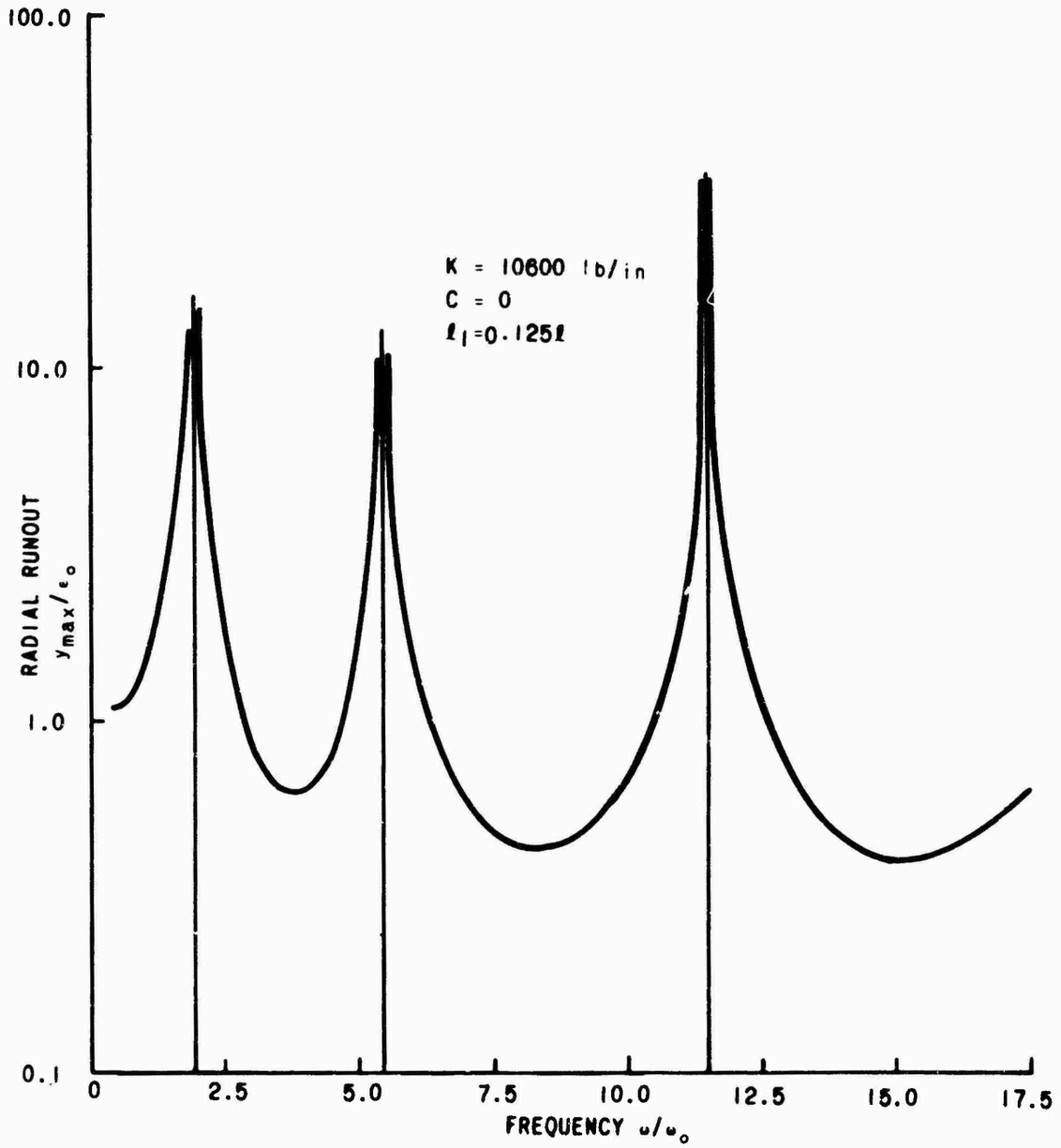

Figure 30. Runout Versus Frequency Curve of a Rotating Shaft for an Intermediate Support at 0.125 Span.

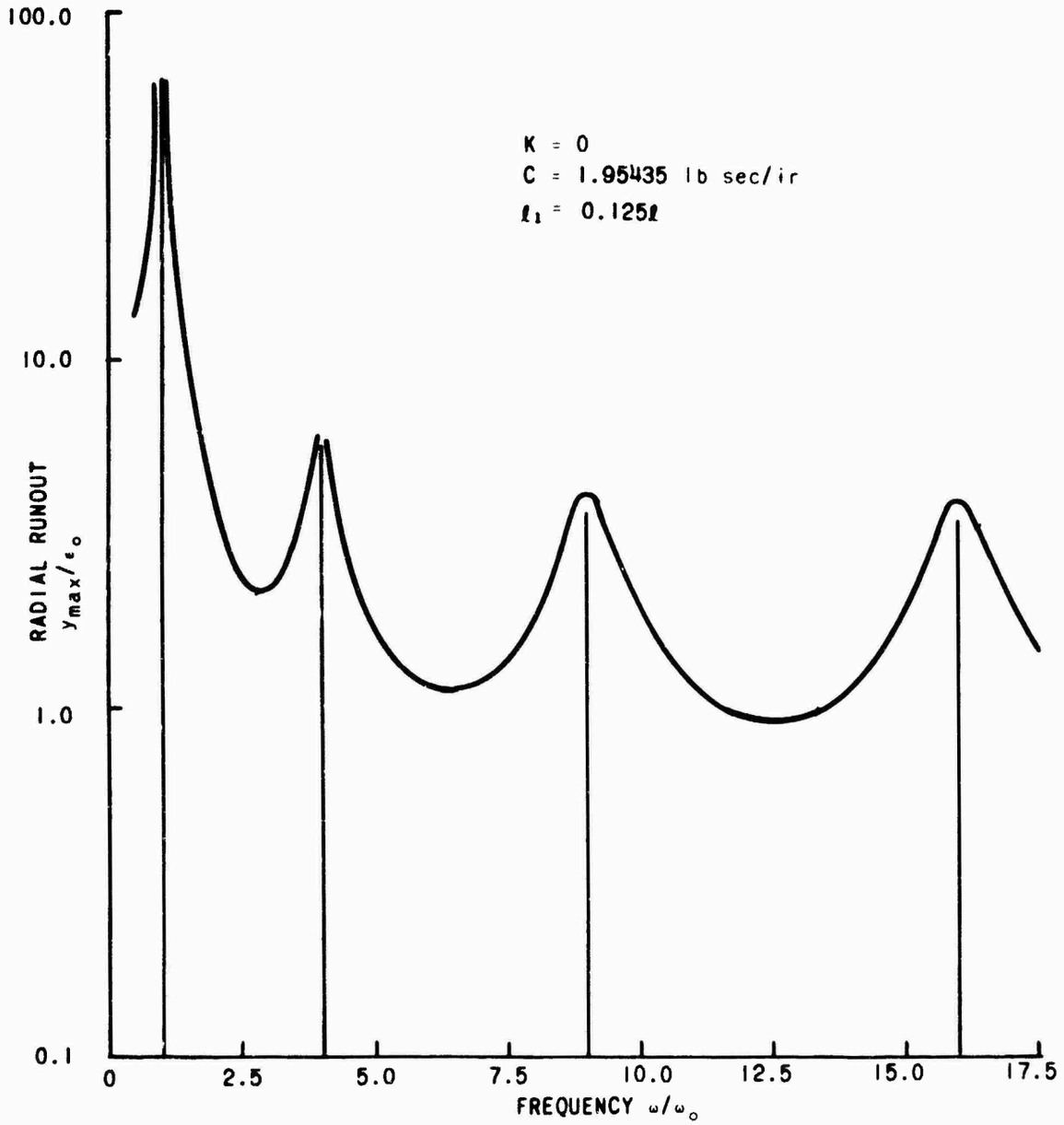

Figure 31. Runout Versus Frequency Curve of a Rotating Shaft for an Intermediate Support at 0.125 Span.

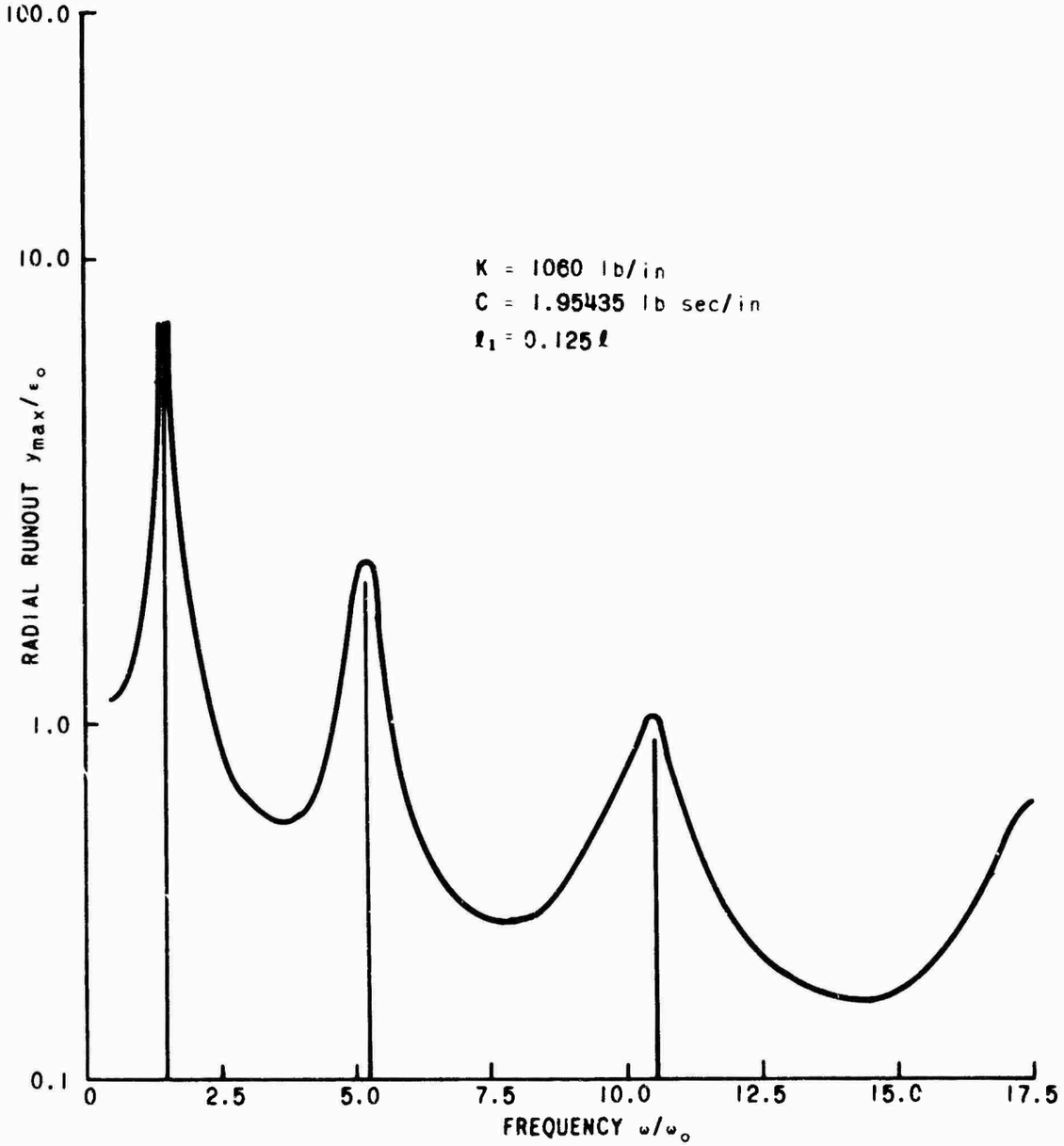

Figure 32. Runout Versus Frequency Curve of a Rotating Shaft for an Intermediate Support at 0.125 Span.

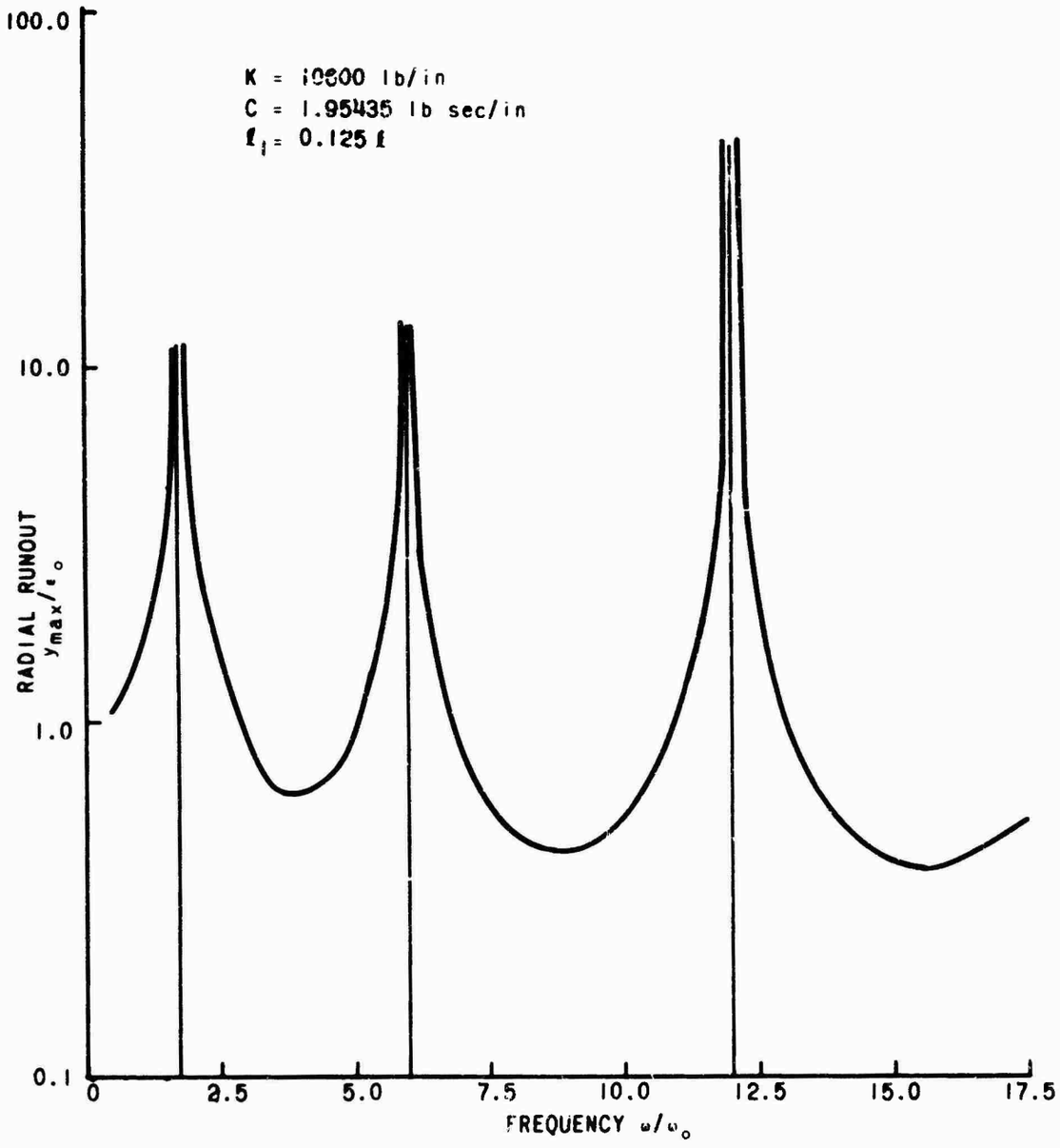

Figure 33. Runout Versus Frequency Curve of a Rotating Shaft for an Intermediate Support at 0.125 Span.

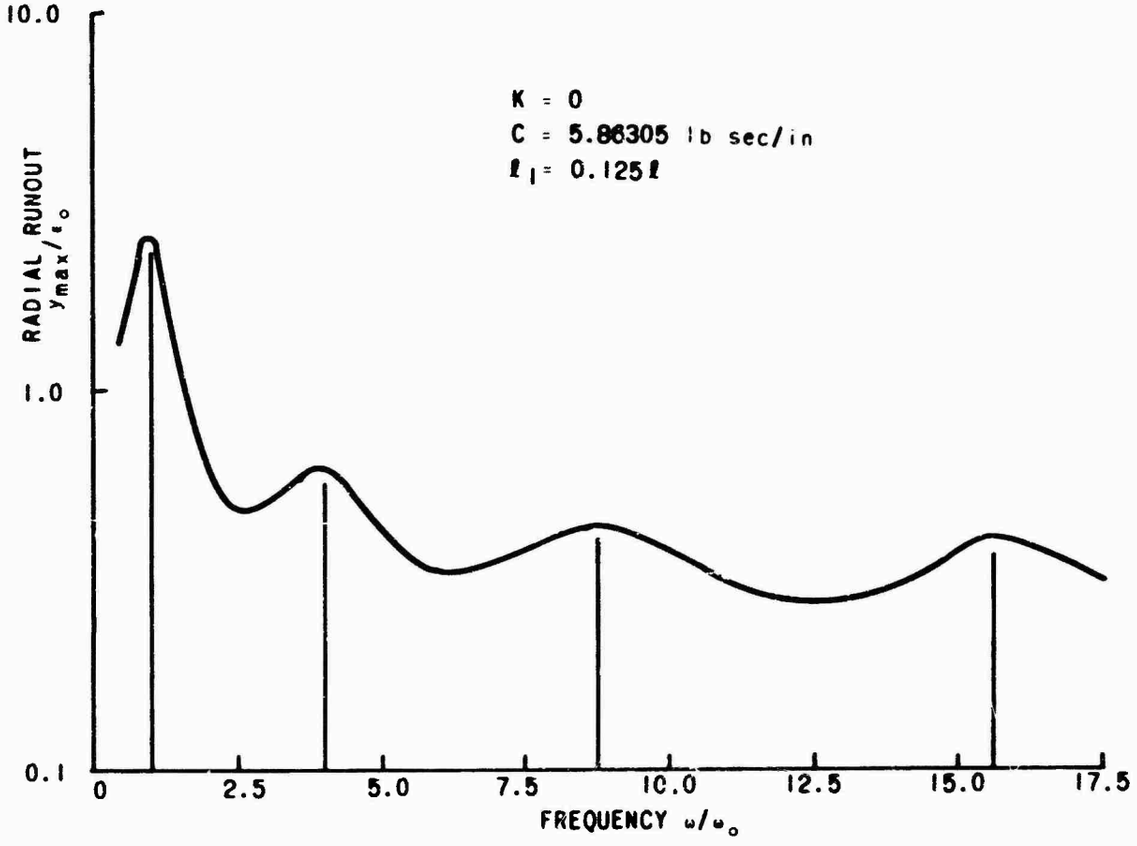

Figure 34. Runout Versus Frequency Curve of a Rotating Shaft for an Intermediate Support at 0.125 Span.

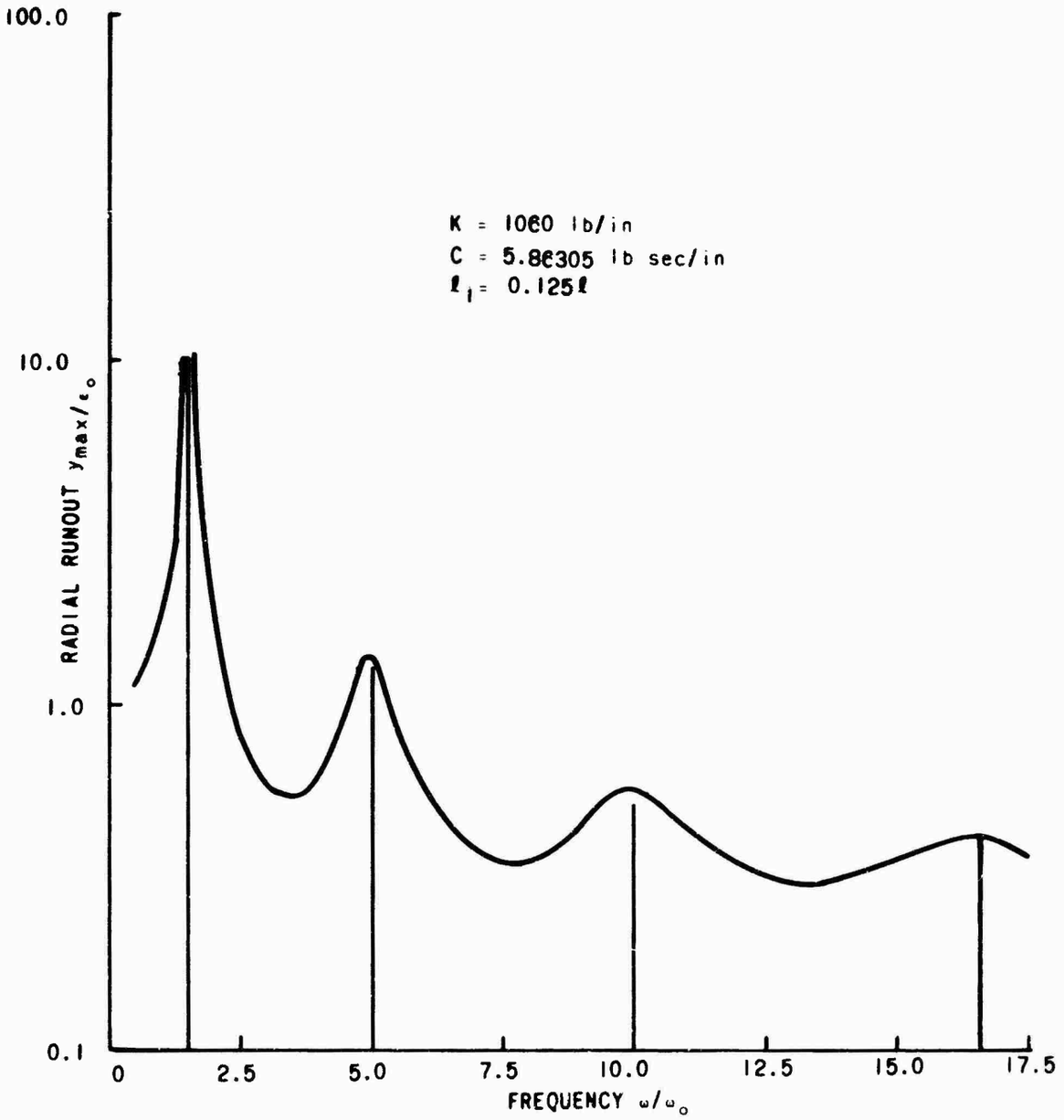

Figure 35. Runout Versus Frequency Curve of a Rotating Shaft for an Intermediate Support at 0.125 Span.

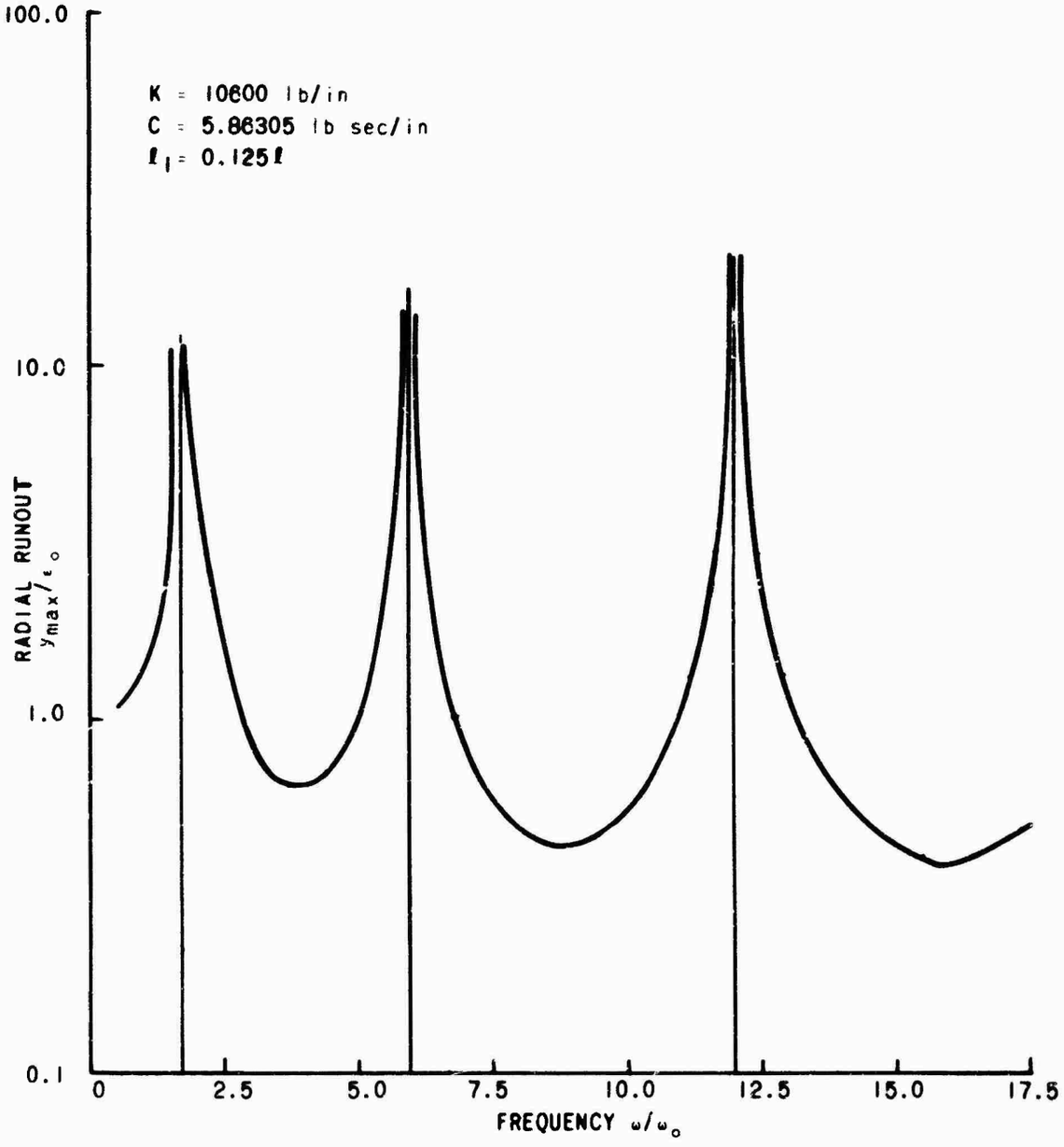

Figure 36. Runout Versus Frequency Curve of a Rotating Shaft for an Intermediate Support at 0.125 Span.

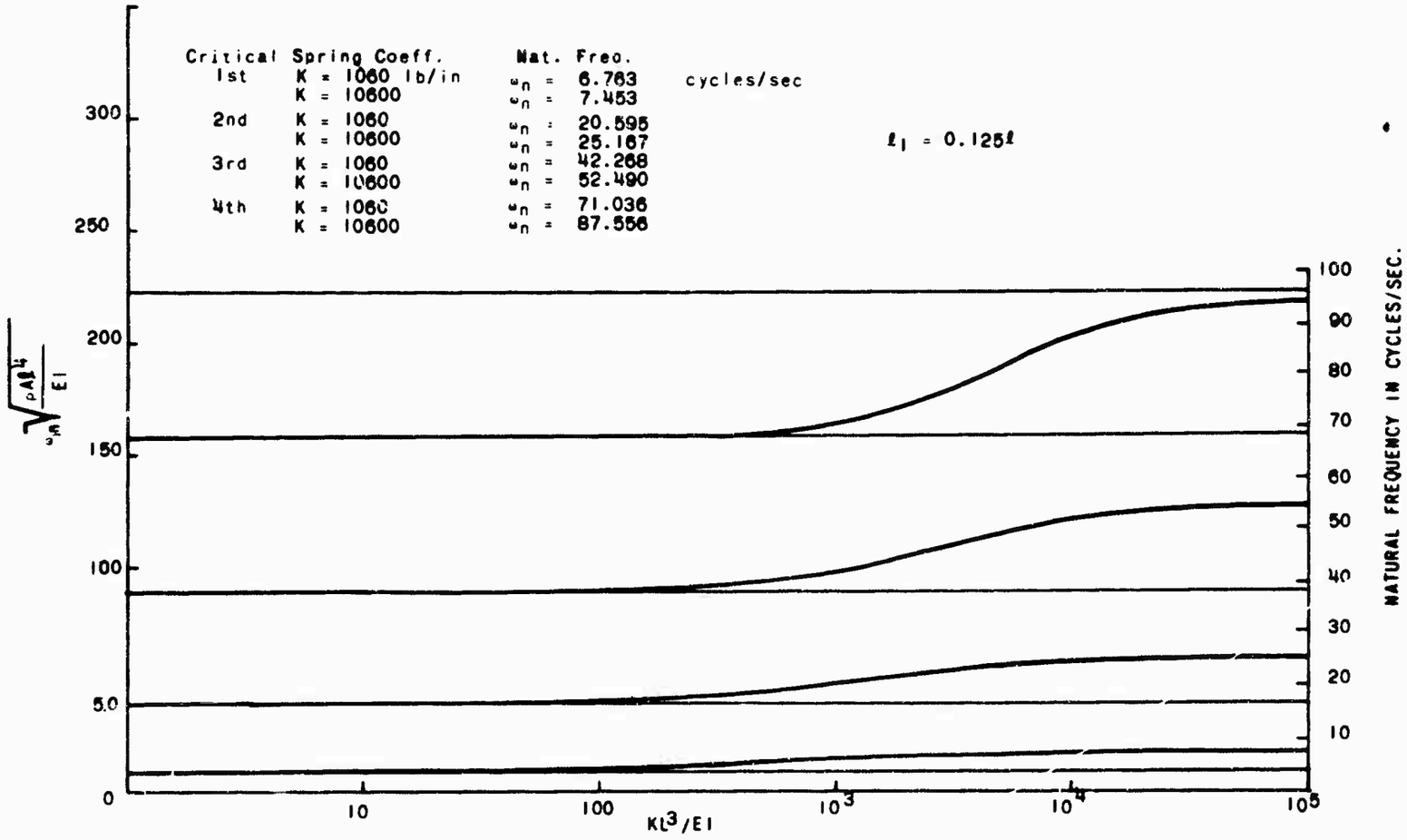

Figure 37. Stiffness Versus Frequency Curve for a Rotating Shaft Having an Intermediate Support at Right Span.

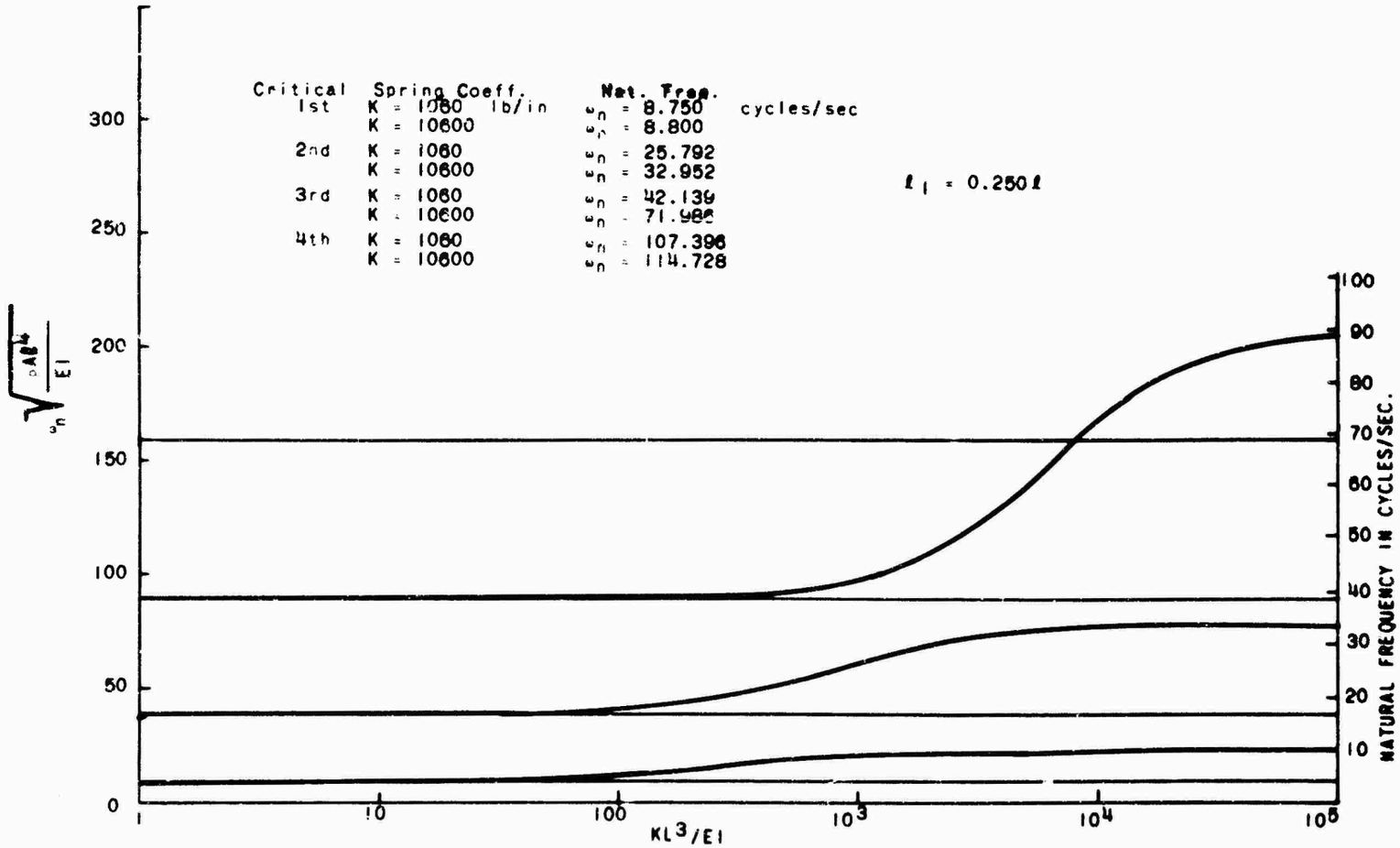

Figure 38. Stiffness Versus Frequency Curve for a Rotating Shaft Having an Intermediate Support at Quarter Span.

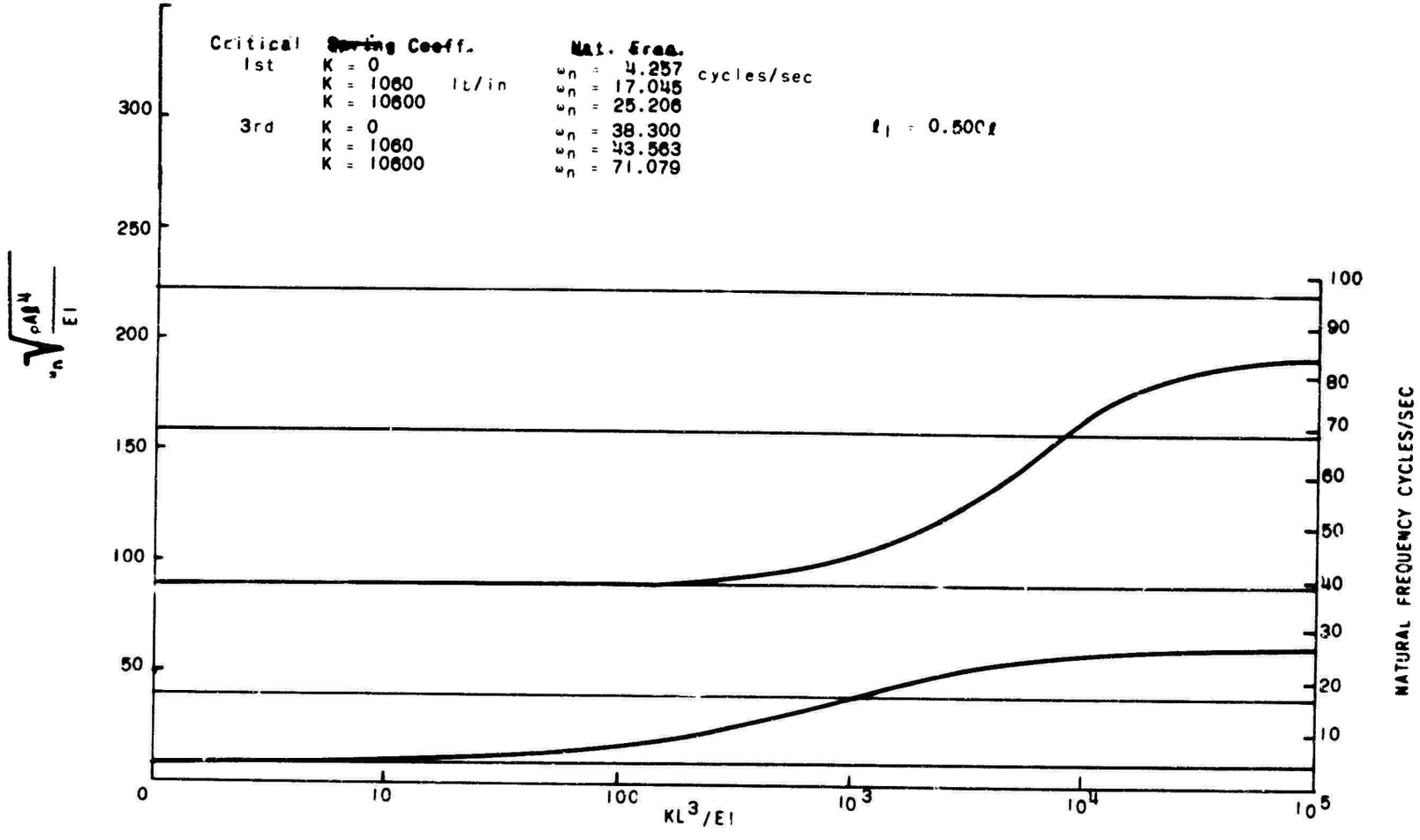

Figure 39. Stiffness Versus Frequency Curve for a Rotating Shaft Having an Intermediate Support at Midspan.

the intermediate support point such that the damping is momentarily lost. At the frequencies immediately adjacent to the third critical frequency, these points do not coincide and damping is available to adequately suppress excessive runouts. For the shaft with the intermediate support at one-eighth span, these spurious runouts are not seen for the first four critical frequencies, but will probably show up with the sixth or seventh critical frequencies.

4. Natural Frequencies of a Flexibly Supported Shaft With Concentrated End Masses [Reference 5]

In this study, the effects of variation in both end spring stiffness and end mass on the natural frequencies of shafts on two flexible supports with end masses are investigated; no intermediate support is being considered. A schematic of this configuration is shown in the upper left corner of Figure 40. The results in this figure are presented both in nondimensional units and units which specifically apply to the Chinook drive shaft. If a stiffness of

$$\frac{E_y I}{\ell^3} = 1.06 \text{ lb./in.}$$

and a natural frequency unit of

$$\frac{E_y I}{\rho A \ell^4} = 2.71 \text{ rad/sec } (0.432 \text{ rev/sec})$$

were used, the nondimensional units (left side and bottom scales of Figure 40) will convert to the dimensional units (right side and top scales of Figure 40) for the Chinook shaft. The above unit conversion factors are on an aluminum shaft with a 4.5-inch-outside-diameter and 4.26-inch-inside-diameter and are unsupported along a 338.5-inch span.

Figure 40 shows that the frequencies of a free-free shaft occur for zero spring stiffness and no end mass and that the frequencies of a pinned-pinned shaft are obtained in the limit as the spring stiffness approaches infinity. (These frequencies are indicated on the left- and right-hand edges of the chart, respectively.)

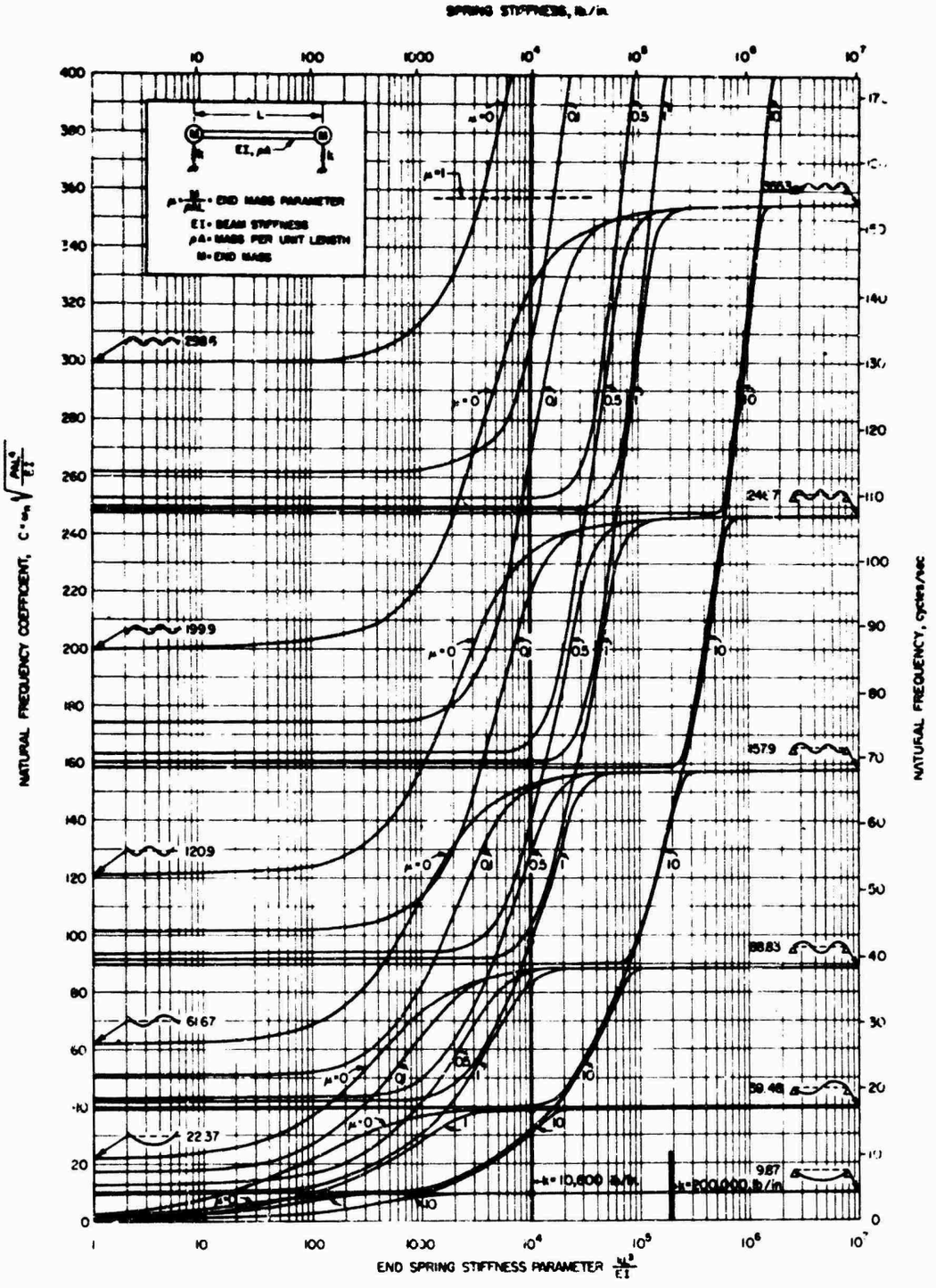

Figure 40. Natural Frequencies of a Beam With Concentrated End Masses Supported on End Spring.

As an example, consider the curves for a shaft with end masses each of which weighs the same as the shaft itself (i.e., $\mu = 1.0$). Physically, these end masses correspond to the gear-boxes at each end of the power transmission shaft. The flexible end supports are provided in the actual system by the fuselage of the helicopter.

If it were assumed that the shaft behaved as a pinned-pinned beam at all rotational speeds in the range of interest (essentially the range of the chart), it may be observed that end springs of stiffness larger than 200,000 pounds per inch would be required. This is a very stiff spring indeed.

A more likely behavior is that indicated for a spring stiffness parameter, $kL^3/EI = 10,000$ ($k = 10,600$ pounds per inch). Studying the natural frequencies of the shaft for this spring condition and $\mu = 1$, the first two critical frequencies are encountered at 4.3 revolutions per second ($9.87 \times 2.71 = 26.8$ radians per second and 17.0 revolutions per second ($39.48 \times 2.71 = 107.2$ radians per second. These frequencies are equal to the first and second pinned-pinned natural frequencies, respectively. Consequently, at these speeds the 10,600 pounds-per-inch spring stiffness is adequate to effectively pin the ends of the shaft. The next two criticals correspond to antisymmetrical and symmetrical modes and occur at speeds of 35.9 and 42.0 revolutions per second, respectively. The mode occurring at 35.9 revolutions per second represents a transition between the first free-free and the third pinned-pinned modes; at 42.0 revolutions per second, the mode represents a transition between the second free-free and the fourth pinned-pinned modes. Note that these critical frequencies bracket that of the third pinned-pinned natural frequency. All subsequent criticals may be considered as "free-free" since the natural frequency values are the same as those which would occur if no end springs were present. As indicated in the chart, these criticals occur at frequencies of 69.5, 107.7 and 154.3 revolutions per second. Although they correspond to the fourth through sixth free-free criticals, the effect of the end mass has been to reduce the critical frequencies to values just slightly larger than the second through sixth pinned-pinned natural frequencies.

Examining the significance of these findings, exceedingly stiff supports are required to insure pinned-pinned behavior for the frequency range of interest. Even in carefully designed experimental rigs, spring stiffnesses in excess of about 100,000 pounds per inch cannot be achieved. Consequently, at the higher frequencies,

pinned-pinned behavior of the shaft cannot exist either for the full-scale power transmission shaft or for modelled experimental investigations.

The results and discussion presented here is directly applicable to a power transmission shaft attached to gearboxes supported on translational springs. Although results are not currently available, there appears to be no reason to believe that the same general conclusions regarding the effect of the boundary conditions would not be valid for other support configurations. For example, suppose that the gearboxes were also mounted against rotation by use of rotational springs; the translational and rotational springs would allow a transition from free-free to pinned-pinned to fixed-fixed boundaries, and again the particular boundary condition most representative of the behavior of the shaft would depend on both the spring coefficients and the rotational speed. The pinned-pinned condition, for example, could not be assumed for the entire frequency range. The analysis for this situation requires a generalization of the computer program and should be performed at some futu date.

The above analysis could serve to explain some of the discrepancies which exist between experimental and theoretical studies on rotating shafts. The predicted and measured shaft performance could be significantly different if the incorrect boundary conditions (end impedances) were assumed. Note, however, that the measured natural frequencies may not indicate an error. For the example discussed ($kL^3/EI = 10,000$, $\mu = 1.0$), all of the natural frequencies have values close to the expected pinned-pinned frequencies. The critical speeds at 35.9 and 42.0 revolutions per second corresponding to the transition modes deviate a little more from the bracketed pinned-pinned frequency. It is possible, however, that this difference would be unnoticed in an experimental run and that one of the two criticals would pass undetected. If so, a logical but false conclusion would be that the supports are pinned. It should be understood that the end impedances for free-free shafts with heavy end masses are totally different from those for pinned-pinned shafts. (The force effect of mass on the shaft is 180 degrees out of phase with the force effect of spring, since the former is associated with acceleration and the latter with displacement; the pinned-pinned condition represents the shaft supported on infinitely stiff springs, not infinitely large masses.)

5. Numerical Comparison Study [Reference 4]

In order to evaluate the significance of the added terms in the governing differential equation, a numerical evaluation is performed between critical speeds obtained by the plain beam equation and the more complete equation of rotating shafts. The specific shaft configuration considered was made of aluminum tubing, 4.5 inches in diameter by 28 feet long and 0.070 inch thick.

A simply supported shaft is selected in the determination of errors between critical frequencies obtained by the vibrating beam equation and those by the more complete equation which includes the gyroscopic, rotary inertia, and shear terms because the ideal boundary conditions permit convenient closed form solutions. It is felt that errors should be similar for the flexibly supported and the simply supported shaft.

Equation 7, the equation of motion for the deflection, y, of a shaft, at position x, vibrating with frequency ω, may also be written in terms of stationary coordinate axes in the following manner.

$$\frac{d^4y}{dx^4} + \eta\omega\left[(\overline{m}+1)\omega - 2i\omega\right]\frac{d^2y}{dx^2} - \omega^2\left[1 - \eta^2\overline{m}\omega\,(\omega - 2i\omega)\right]y = 0 \qquad (27)$$

The unit of distance is the length, ℓ.

The unit of time is $\frac{1}{\Omega_o}$ where $\Omega_o = \frac{1}{\ell^2}\sqrt{EI/\rho A}$.

The unit of mass is the mass of the beam, $\rho A\ell$.

If the parameter $\eta = I/A\ell^2$ vanishes (infinitely slender beam) the simple beam equation results. For nonzero, η, the motion depends also on $\overline{m} = E_y/K'E_s$ and ω, the spin frequency of the beam about its longitudinal axis.

The moment and shear along the beam are given by:

$$M(x) = \frac{d^2y}{dx^2} + \eta\overline{m}\omega^2 y, \quad S(x) = \frac{\frac{d^3y}{dx^3} + \eta\omega\left[(\overline{m}+1)\omega - 2i\omega\right]\frac{dy}{dx}}{1 - \eta^2\overline{m}\omega(\omega - 2i\omega)}. \qquad (28)$$

The general solution of equation 27 is:

$$y(x) = A \cosh \beta x + B \sinh \beta x + C \cos \gamma x + D \sin \gamma x$$

where

$$\beta = \omega e_2 = \left\{ \omega \left(\sqrt{1 + \frac{\eta^2}{4}[(\bar{m} - 1)\omega + 2i\omega} \right] - \frac{\eta}{2}[(\bar{m} + 1)\omega - 2\Omega_o] \right)\}^{1/2} \quad (29)$$

and

$$\gamma = \omega e_1 = \left\{ \omega \left(\sqrt{1 + \frac{\eta^2}{4}[(\bar{m} - 1)\omega + 2i\omega} \right] + \frac{\eta}{2}[(\bar{m} + 1)\omega - 2\Omega_o] \right)\}^{1/2} \quad (30)$$

and A, B, C, and D are constants to be determined by the boundary conditions.

For the simply supported beam, $\sin \gamma = 0$, equation 30 at the critical frequencies becomes

$$\left\{ \omega \left(\sqrt{1 + \left[\frac{(\bar{m} + 1)\eta\omega}{2} \right]^2} + \frac{\eta(\bar{m} - 1)}{2} \omega \right) \right\}^{1/2} = \pi n$$

or

$$\eta^2 m\omega^4 + [1 + \pi^2 n^2 \eta(\bar{m} - 1)]\omega^2 - \pi^4 n^4 = 0 \quad (31)$$

where n is an integer indicating critical mode number. In the evaluation of equation 31 for the critical frequencies of the 4.26-inch-inside-diameter, 4.5-inch-outside-diameter, 0.070-inch wall by 28-foot-long, aluminum rotor, the following numerical values were used:

$$\eta = 1.74 \times 10^{-5}$$

$$\bar{m} = 5.3 \text{ with } K' = 2.$$

The critical frequencies for the rotor, using the equation for which gyroscopics, rotary inertia, are shear and neglected, are simply determined by

$$\omega = n\pi\Omega_o$$

where for the aluminum shaft Ω_o = 2.71 radians per second = .432 rps. From these equations, it was determined that for the ninth critical which occurs in the vicinity of 20,000 rpm, the discrepancy between

critical frequencies is 2.8 percent; for the sixteenth critical, at about 60,000 rpm, the discrepancy is 6.7 percent.

It may be concluded that for the speed range considered, the critical frequencies predicted by the simple vibrating beam equation are reasonably accurate.

MULTIRING SQUEEZE FILM DAMPERS

FREQUENCY DEPENDENT DAMPER [References 1 and 3]

It has been established analytically and experimentally for hypercritical shafts that there is an optimum value of damping for each critical speed.

A damper which will meet these requirements is the multiple concentric ring damper, a device which consists of a number of translating, but nonrotating, rings nestled one into the other (see Figure 41). Damping is derived from the hydrodynamic action of the pressurized oil films between the rings. It has been found experimentally that these rings should be pinned against rotation to prevent hydrodynamic instabilities and consequent excitation of nonsynchronous whirling of the rings.

The damping and spring coefficients, C and K, respectively, are defined by $C = F_T/\rho\omega$ and $K = F_R/\rho$, where F_T and F_R are the tangential and radial components of force which the journal experiences due to ρ, the journal runout, and ω, the circular frequency. A collection of parameters is required to specify a theoretical multiple-ring (MR) assembly; i.e., length, radius, and clearance of each film, the masses of the rings, the ambient pressure, fluid viscosity, operating speed, and radius of journal runout orbit.

The multiple-ring assembly can be regarded as a synthesis of a single-film device. Digital computer programs have been written which compute up to five films bearing properties over a fairly useful range of the characterizing parameters. This includes $0.1 < L/D < 3.0$ and film eccentricities which are not substantially greater than 0.7 to 0.75. These programs are based on the analytic expressions which describe the single-film assembly.

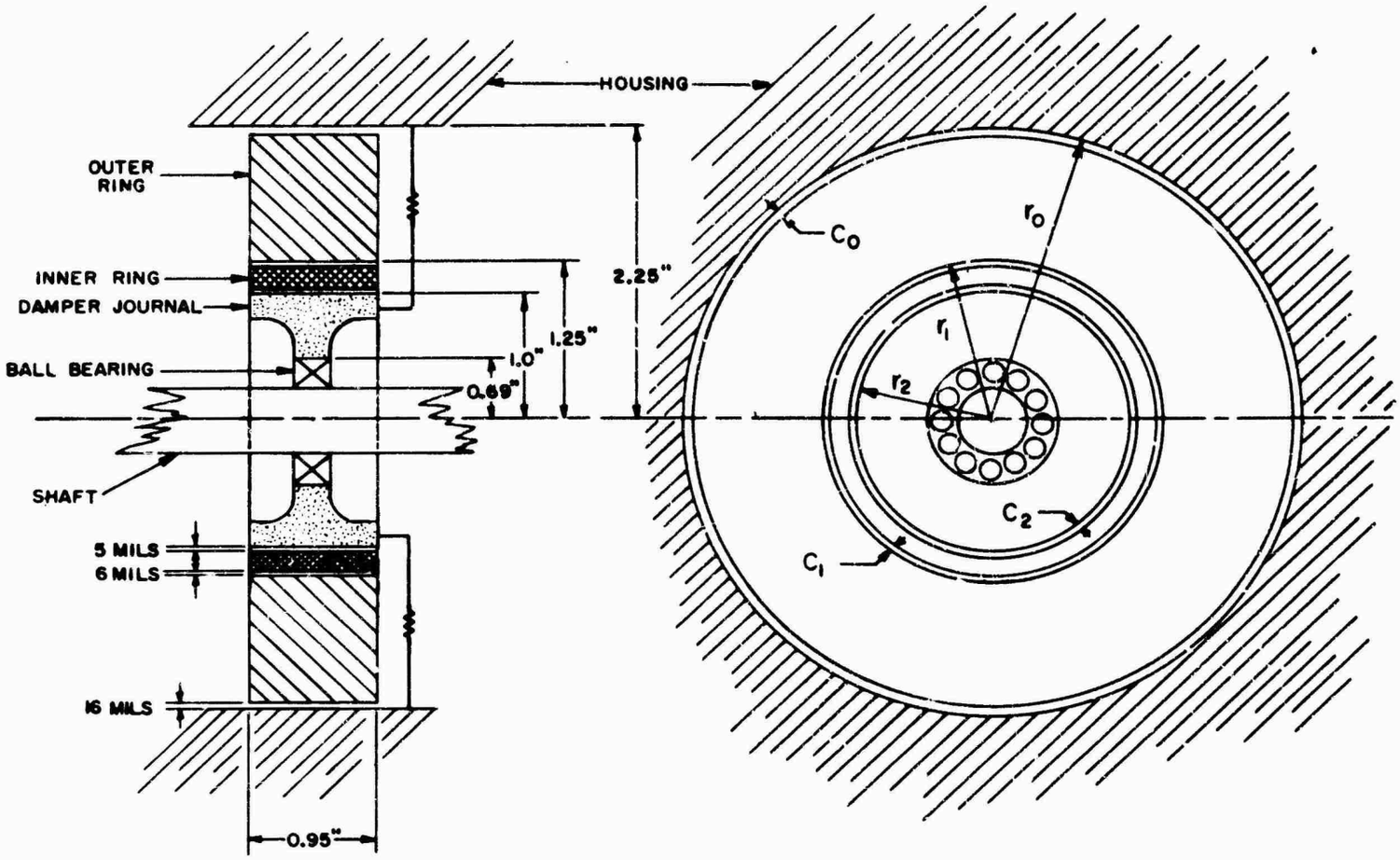

Figure 41. Schematic of Two-Ring Damper.

In the design of dampers for a given range of C, a single-film computation shows that the required clearance is usually too small for the expected runouts. A multiple-ring assembly can be tried in order to achieve a gain in allowable runout.

The values of C for the two films tend to combine roughly like capacitances in series. This simplified picture is approximate but does give, in the case of light rings, a useful way to make qualitative statements about an MR assembly. At high operating speeds, the inertia of heavier rings will restrict their motion and most of the motion will take place in the innermost film. At low speeds, action of all the films will be evident. Thus, at high speeds, the higher C coefficient will be roughly that corresponding to the innermost film, and at low speeds C will correspond to that predicted by the single film of the outer clearance. This, then, is a qualitative explanation of the variation of C with ω in the MR assembly and the reason for its usefulness in frequency responsive damping bearings for supercritical rotors.

The graphs and charts presented here should be regarded as illustrative of the type of results which may be expected for the multiring bearing assembly when applied to the Battelle shaft model. Although there are limitations to the frequency-dependent characteristics of the damping coefficient which can be achieved (some of which are evident in the data presented), these results can be improved with additional manipulation and refinement in the selection of the support parameters.

The basic specifications of this two-ring damper are as follows (refer to Figure 41):

L = length = 0.95 inch

r_o = radius of the bearing = 2.25 inches

r_1 = inner radius of the outer ring = 1.25 inches

r_2 = radius of the journal = 1.0 inch

C_o = radial clearance of the outer film = 16 MILS

C_1 = radial clearance of the middle film = 6 MILS

C_2 = radial clearance of the inner film = 5 MILS

M_o = mass of outer ring = 1335 grams

M_1 = mass of inner ring = 215 grams

μ_o = viscosity of fluid in outer film = .2 POISE

μ_1 = viscosity of fluid in middle film = .1 POISE

μ_2 = viscosity of fluid in inner film = .1 POISE

P_a = ambient pressure = 20 PSI

Tolerances on all the linear dimensions should be held to 5 percent or better. The masses of the rings should be maintained to within about 10 percent of the values specified; the above design is based on the rings made of steel (SP. GR. = 7.8).

The viscosities indicated correspond to Teresso 43, at 100°F for the outer film and 150°F for the middle and inner films. Teresso 43 is, according to the charts, somewhat less viscous than SAE 10W oil. The temperatures chosen are those typically used in some similar calculations; any indication that the operating temperatures are significantly different from these will be a signal for recalculation.

The choice of ambient pressure equal to 20 PSI was based on past experience; this should certainly be enough to effect the fluid exchange required to offset heat generation in the bearing. If the fluid is saturated with gas at ordinary atmospheric pressure, then P_a refers to gauge pressure.

Figures 42 and 43 show damping coefficient versus runout of the journal for constant values of shaft speed. From these figures it may be observed that the damping coefficient remains relatively constant with respect to runout at low runouts or low shaft speeds.

Figure 44 superposes a cross plot of the results from Figure 42 on the curve of desired damping characteristics. Curves of constant runout of 4, 8, and 12 mils are presented. The vertical bars indicate the complete range of damping coefficient experienced at the critical speeds for the values of runout represented in Figure 42.

Table I is also included and gives values of the effective spring coefficients, K, obtained for this two-ring damper assembly. Note that all of these values are negative, and an equivalent mass at the journal can be obtained by dividing the values of K by ω^2.

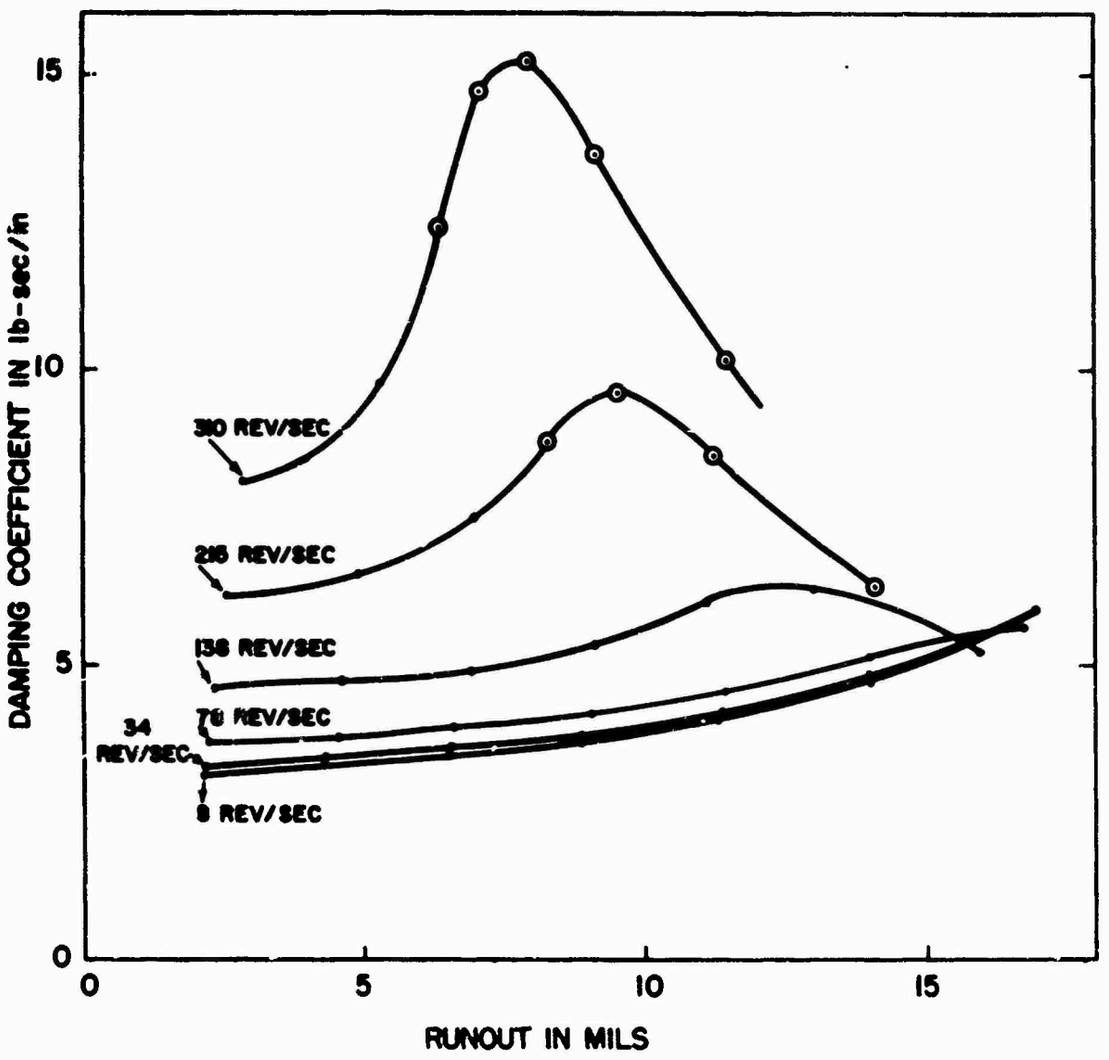

Figure 42. Damping Characteristic of a Two-Ring Damper.

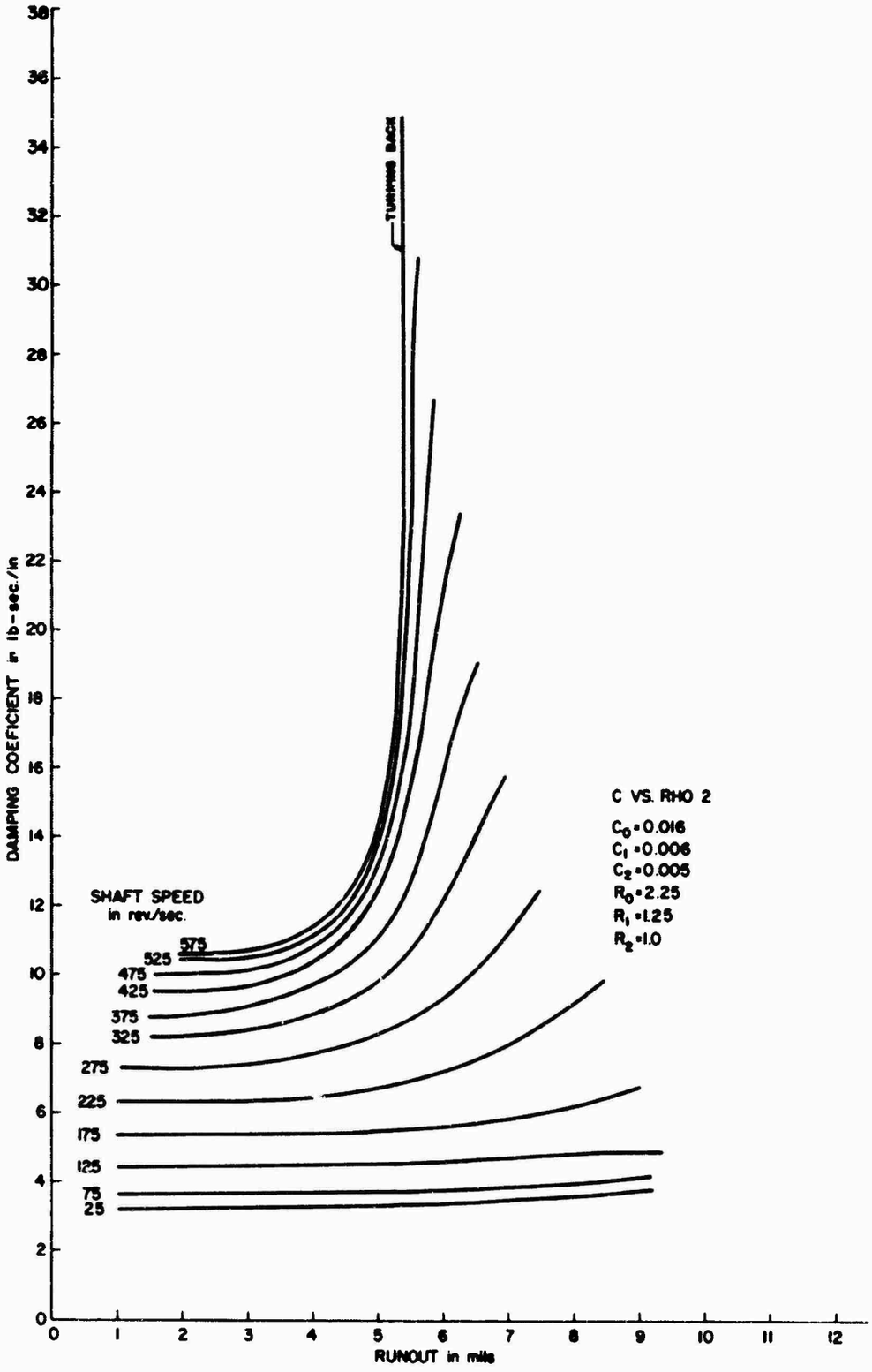

Figure 43. Damping Characteristics of Two-Ring Damper.

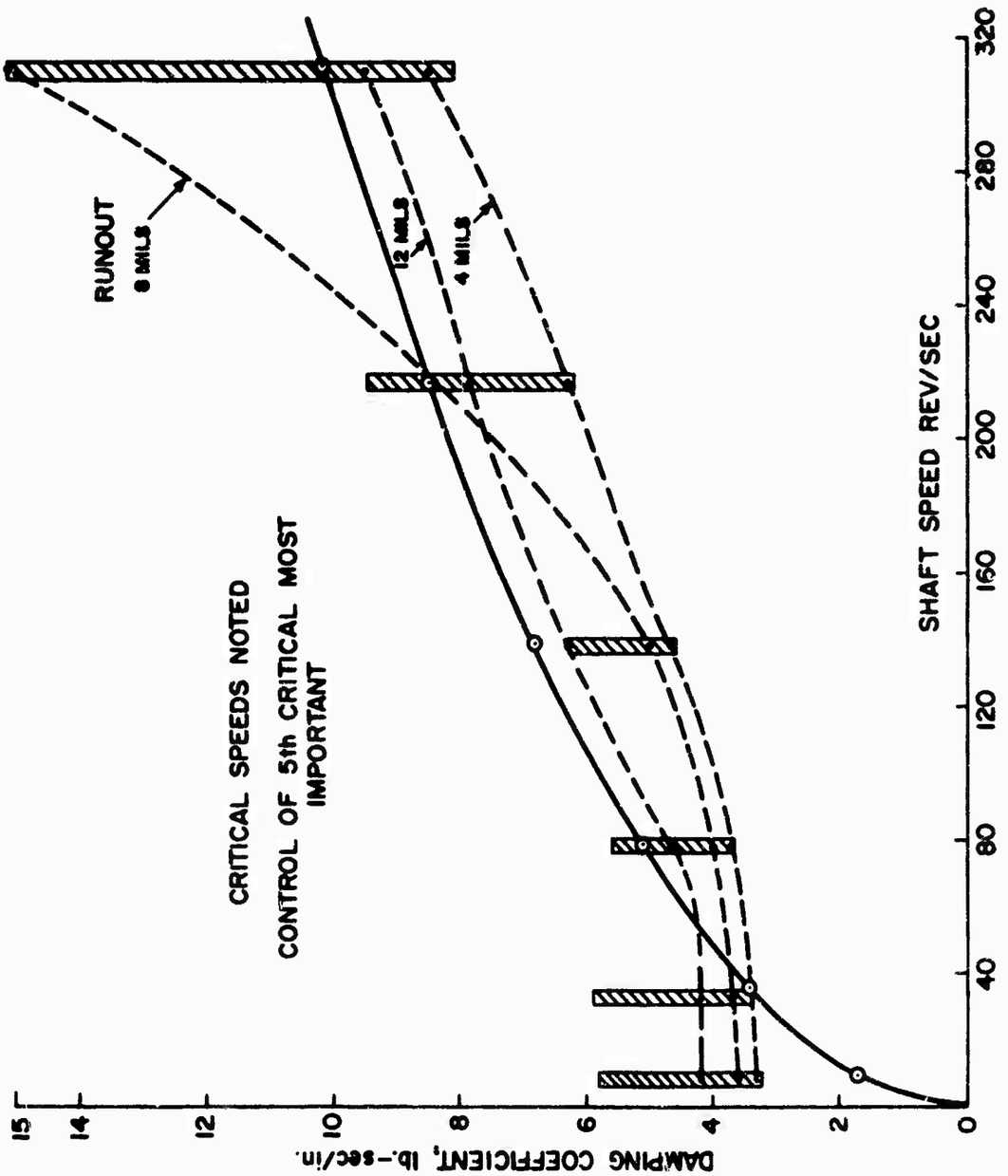

Figure 44. Damping Coefficient Versus Shaft Speed for Battelle Model Shaft.

TABLE 1

EFFECTIVE SPRING COEFFICIENT, K, FOR TWO-RING DAMPER

ω = 8 rev/sec.		ω = 34 rev/sec.		ω = 78 rev/sec.	
RUNOUT (mils)	$-K \times 10^{-2}$ (lb./in.)	RUNOUT (mils)	$-K \times 10^{-2}$ (lb./in.)	RUNOUT (mils)	$-K \times 10^{-2}$ (lb./in.)
2.15	.1306	2.16	2.339	2.21	11.85
4.33	.1291	4.35	2.315	4.43	11.77
6.58	.1266	6.60	2.273	6.70	11.63
8.91	.1230	8.94	2.212	9.03	11.42
11.3	.1184	11.4	2.134	11.4	11.12
14.0	.1129	14.0	2.038	14.0	10.14
16.9	.1066	16.9	1.928	16.7	2.643
ω = 138 rev/sec.		ω = 215 rev/sec.		ω = 310 rev/sec.	
RUNOUT (mils)	$-K \times 10^{-2}$ (lb./in.)	RUNOUT (mils)	$-K \times 10^{-2}$ (lb./in.)	RUNOUT (mils)	$-K \times 10^{-2}$ (lb./in)
2.32	33.8	2.54	69.86	2.89	110.1
4.63	34.0	4.98	69.14	5.30	79.23
6.92	34.16	7.00	61.26	6.38	74.36
9.15	32.69	8.30	58.78	7.10	92.79
11.1	28.92	9.51	60.25	7.95	122.9
13.0	22.71	11.2	56.87	9.17	139.7
15.9	8.737	14.1	36.00	11.5	111.7

TABLE 1 (CONTINUED)

ω = 25 rev / sec.		ω = 75 rev / sec.		ω = 125 rev / sec.	
RUNOUT (mils)	- K x 10^{-2} (lb. /in)	RUNOUT (mils)	-K x 10^{-2} (lb. /in.)	RUNOUT (mils)	- K x 10^{-2} (lb. /in.)
1. 07	1. 274	1. 10	11. 01	1. 14	28. 36
2. 16	1. 269	2. 20	10. 99	2. 29	28. 40
3. 24	1. 264	3. 31	10. 95	3. 44	28. 43
4. 34	1. 256	4. 43	10. 91	4. 58	28. 47
5. 46	1. 245	5. 55	10. 86	5. 72	28. 50
6. 59	1, 232	6. 69	10. 78	6. 87	28. 49
7. 74	1, 217	7. 85	10. 68	8. 02	28. 38
8. 93	1. 199	9. 02	10. 58	9. 16	27. 93
ω = 175 rev / sec		ω = 225 rev / sec.		ω = 275 rev / sec.	
RUNOUT (mils)	-K x 10^{-2} (lb. /in.)	RUNOUT (mils)	- K x 10^{-2} (lb. /in.)	RUNOUT (mils)	- K x 10^{-2} (lb. /in.)
1. 21	50. 29	1. 29	73. 98	1. 38	97. 45
2. 41	50. 56	2. 57	74. 75	2. 74	98. 70
3. 61	50. 95	3. 82	75. 32	4. 08	91. 65
4. 79	51. 42	5. 03	72. 48	5. 24	80. 62
5. 94	51. 08	6. 11	67. 48	6. 05	73. 54
7. 04	49. 52	6. 95	63. 52	6. 61	72. 02
8. 04	47. 20	7. 60	61. 93	7. 07	74. 81
8. 89	44. 98	8. 16	62. 36	7. 49	80. 85

ω = 325 rev / sec.	
RUNOUT (mils)	- K x 10^{-2} (lb. /in.)
1. 49	119. 7
2. 97	114. 0
4. 37	92. 60
5. 31	77. 14
5. 89	71. 62
6. 29	74. 26
6. 62	83. 53
6. 95	97. 75

Operation of this bearing depends upon the provision of a load resisting spring connected between the journal and the bearing housing. A schematic of this arrangement is indicated in Figure 41. This spring should be arranged so as to offset the negative "spring" obtained in the multiring computations.

LIGHTWEIGHT DAMPER [Reference 4]

In the previous section a conceptual design was presented for a multiring damping assembly which could accommodate the Battelle model of the Chinook drive shaft. Although this design provides the necessary damping as a function of frequency, the ring masses required are excessive. Similarly, dampers designed to match the variable damping requirements (Figure 45) of the full-scale, 4.5-inch-diameter, 28-foot-long aluminum Chinook helicopter shaft are also relatively massive (4 to 5 pounds) compared to the lightweight bearings desired.

Presented in this section is a multiring bearing configuration in which the variable damping characteristics have been sacrificed for the sake of lightweight design. One aspect which should still make the multiring damper an attractive means for suppressing shaft criticals is the fact that it will provide high damping coefficients with low-viscosity damping fluids. The low-viscosity fluid recommended is the Dow Corning, 20 centistoke, 200 fluid, which, in comparison to other fluids, is less viscosity sensitive to temperature changes. The variation of viscosity with temperature for this fluid is shown in Figure 46. The higher viscosity fluids needed for shear dampers (50,000 to 100,000 centistokes) are more temperature sensitive and yield less desirable damping coefficients at temperatures lower than operating temperature.

The variable damping characteristics of the multiring damper are obtained by a careful selection of masses and clearances of the rings such that an increase in damping occurs with an increase in rotational speed. The damping coefficient depends primarily on the quantity $M \rho \omega^2$ (where M = mass of outer ring, ρ = journal runout, and ω = angular speed). Consequently, when ρ and ω are relatively small, as in the case of the Chinook shaft, large outer ring masses are required to provide the desired damping profile shown in Figure 45.

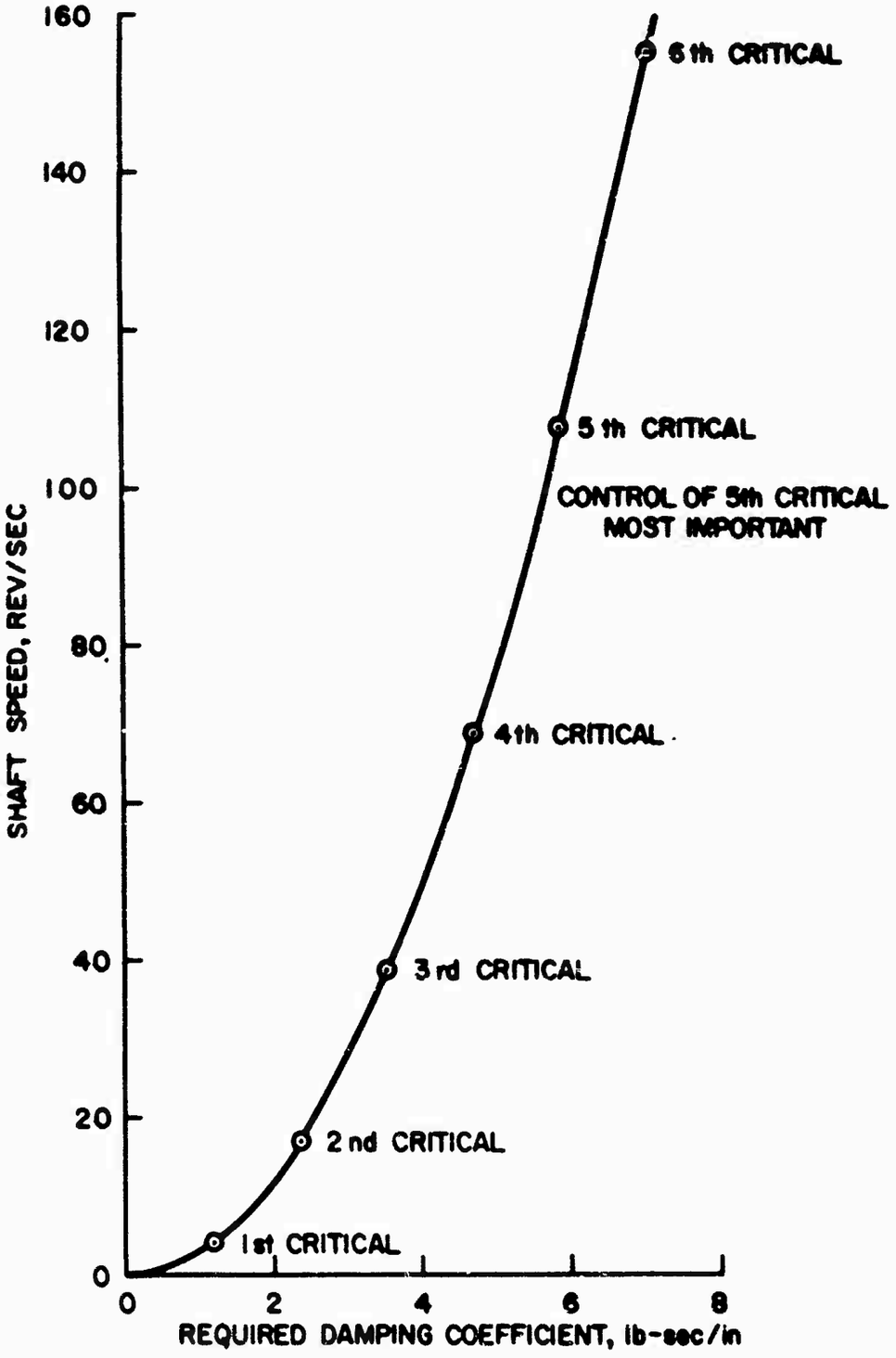

Figure 45. Damping Coefficient Versus Shaft Speed for Full-Scale Shaft of the Vertol Chinook.

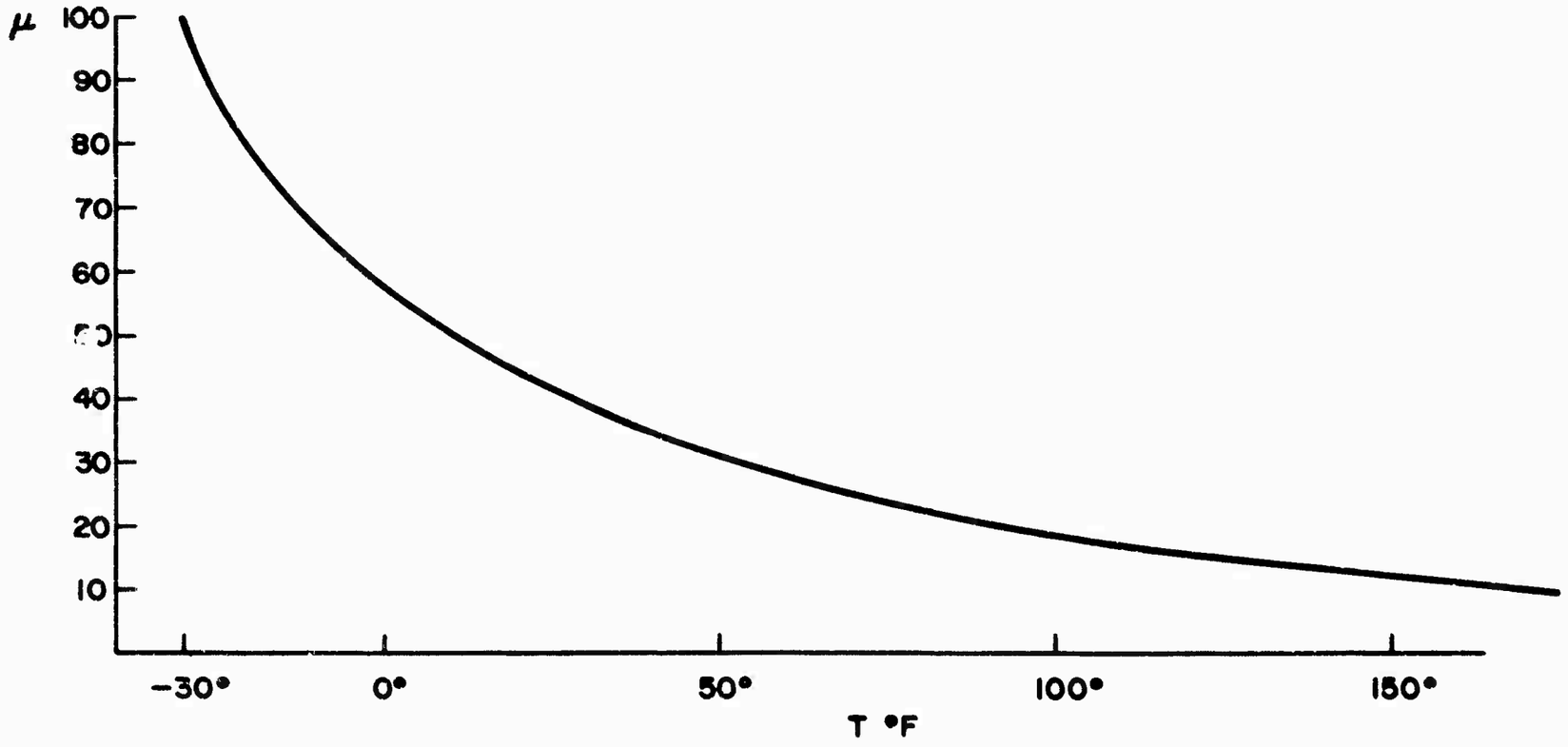

Figure 46. Absolute Viscosity (in Centipoise) Versus Temperature (In °F) for Dow Corning, 20 Centistoke 200 Fluid.

In view of these observations, it was decided to select a lightweight, two-ring damper having a constant damping output with changes in frequency and specifically designed to be optimum for the fifth critical frequency of the Chinook Shaft. In other words, the damper has been designed to deliver a damping coefficient of about 6 pounds per second per inch over the entire speed range operating at a temperature of 160°F.

The design specifications recommended for the damper are as follows:

length of the damper = 1.5 inches
radius of the housing = 2.25 inches
inner radius of the outer ring = 2.125 inches
outer radius of the bearing holder = 2.00 inches
radial clearances of all 3 films = 0.012 inch
mass of outer ring = 0.25 lb (Al), 0.151 lb (Mg), 0.65 lb (Fe)
mass of inner ring = 0.24 lb (Al), 0.141 lb (Mg), 0.62 lb (Fe)
ambient pressure = 15 psi (atmospheric)
viscosity of fluid = refer to Figure 46

Typical results for the damping coefficients at various temperatures are presented in Table 2. Case I represents a bearing in which the entire assembly is of the same material. Case II is for an assembly constructed of different materials arranged to utilize their different coefficients of expansion in a manner which would partially compensate for the viscosity change of the fluid. Consequently, a smaller change in the damping coefficient with temperature is produced.

The value of the damping coefficient at 160°F is optimum for the fifth critical speed as specified in Figure 45. At lower temperatures the results of Table 2 indicate a damping coefficient which is too large. This is due to the increased viscosity of the damping fluid. For Case I at the first critical frequency and a temperature of -30°F, the damping coefficient is 30 times larger than the optimum value. Although an overdamping of this magnitude could result in rough operation at the critical speeds, it is felt that the runouts and bearing loads actually experienced could be tolerated.

TABLE 2

DAMPING COEFFICIENTS IN THE LIGHTWEIGHT TWO-RING DESIGN

TEMPERATURE °F	DAMPING COEFFICIENT LB. SEC/IN.	
	CASE I	CASE II
160	6.0 - 7.0	6.0 - 7.0
90	12.0 - 13.0	10.0 - 11.0
27	23.0 - 24.0	16.0 - 17.0
-4	32.0 - 34.0	21.0 - 22.0
-30	45.0 - 47.0	34.0 - 35.0

Case II illustrates the beneficial effects which can be obtained by utilizing different materials in the bearing assembly. If the rings and housing are constructed of materials of different coefficients of expansion, they can be arranged to bring about an increase of the ring clearances with decreasing temperature. This in turn leads to a lowering of the effective damping coefficient of the damper. With this behavior in mind a number of configurations were investigated using common materials with widely separated coefficients of expansion.

Steel (Fe), $\alpha = 6.5 \times 10^{-6}/^{\circ}F$
Aluminum (Al), $\alpha = 10 \times 10^{-6}/^{\circ}F$
Magnesium (Mg), $\alpha = 15 \times 10^{-6}/^{\circ}F$

The combination which leads to the smallest increase in damping coefficient with lowering temperatures consists of a damper for which the damper holder and both rings are of magnesium and the housing is of steel. The results for this combination are presented in Table 2.

It should be mentioned that the rings and damper holder should be pinned to permit translation but to prohibit rotation, thus preventing hydrodynamic instabilities and consequent excitation of nonsynchronous whirling of the rings. Damping should be derived from true squeeze film action. Furthermore, no external restoring springs are required in the design of the proposed damper. In this particular design, the resultant springs provided by the fluid films are directed radially inward and are of sufficient magnitude to provide adequate centering.

REFERENCES

1. Eppink, R. T., and Tomlin, R., "Brief Physical and Theoretical Description of the Multi-Ring Bearing Assembly," Letter report to John E. Voorhees, Machine Dynamics Group, Battelle Memorial Institute, Columbus, Ohio, November 12, 1963.

2. Eppink, R. T., "An Investigation of the Behavior of Floating Ring Dampers and the Dynamics of Hypercritical Shafts on Flexible Supports," First Quarterly Report, Research Laboratories for the Engineering Sciences, University of Virginia, Charlottesville, Virginia, Report No. CE-3340-101-64U (Revised), February 1964.

3. Eppink, R. T., and Friedericy, J. A., "An Investigation of the Behavior of Floating Ring Dampers and the Dynamics of Hypercritical Shafts on Flexible Supports," Second Quarterly Report, Research Laboratories for the Engineering Sciences, University of Virginia, Charlottesville, Virginia, Report No. CE-3340-102-64U, March 1964.

4. Eppink, R. T., and Friedericy, J. A., "An Investigation of the Behavior of Floating Ring Dampers and the Dynamics of Hypercritical Shafts on Flexible Supports," Third Quarterly Report, Research Laboratories for the Engineering Sciences, University of Virginia, Charlottesville, Virginia, Report No. CE-3340-103-64U, May 1964.

5. Friedericy, J. A., and Eppink, R. T., "Natural Frequencies of Flexibly Supported Hypercritical Shafts with Concentrated End Masses," Letter report to John Mack, Vertol Division of the Boeing Company, Morton, Pennsylvania, June 19, 1964.

6. Nelson, L. W., "Flexural Vibration of Uniform Shafts," Research Laboratories for the Engineering Sciences, University of Virginia, Charlottesville, Virginia, Report No. EP-4422-184-61S, November 1961.

7. Voorhees, John E., Mellor, Jr., C. C., and Dubensky, R. G., "The Control of Shaft Vibrations at their Hypercritical Speeds," Presented at the Design Engineering Conference and Show of the American Society of Mechanical Engineers, New York, New York, May 20-23, 1963.

DISTRIBUTION

US Army Materiel Command	5
US Army Mobility Command	3
US Army Aviation Materiel Command	5
Chief of R&D, D/A.	1
US Army Aviation Materiel Laboratories	25
USAAML Liaison Officer, US Army R&D Group (Europe)	2
US Army Engineer R&D Laboratories	2
US Army Limited War Laboratory	1
US Army Human Engineering Laboratories	1
Army Research Office-Durham	1
US Army Engineer Waterways Experiment Station	1
US Army Transportation School	1
US Army Aviation School	1
US Army Tank-Automotive Center	1
US Army Field Office, AFSC, Andrews AFB	1
Air Force Flight Dynamics Laboratory, Wright-Patterson AFB	1
Air Force Systems Command, Wright-Patterson AFB	2
Air Force Avionics Laboratory, Wright-Patterson AFB	1
Air Force Flight Test Center, Edwards AFB	1
Chief of Naval Research	3
Bureau of Naval Weapons	4
US Naval Air Station, Patuxent River	1
David Taylor Model Basin	1
Marine Corps Liaison Officer, US Army Transportation School	1
Ames Research Center, NASA	1
NASA-LRC, Langley Station	1
Lewis Research Center, NASA	1
Manned Spacecraft Center, NASA	1
NASA Representative, Scientific and Technical Information Facility	2
Research Analysis Corporation	1
NAFEC Library (FAA)	1
Defense Documentation Center	20
US Patent Office	1
US Government Printing Office	1

APPENDIX I

IMPORTANT FUNCTIONS

$$e_3 = -\sqrt{1 + \left[\omega + \left(\frac{e^1 - 1}{2}\right)\omega\right]^2 + \left[\omega + \left(\frac{e^1 - 1}{2}\right)\omega\right]}$$

$$e_1 = -\sqrt{\frac{1}{e_3} + e^1\omega}$$

$$e_2 = \sqrt{\frac{1 + e^1(2\omega - is)}{e_1}}$$

where $\omega = is$

$$C_{11} = \begin{bmatrix} -ie_1e_3 & -ie_2 \\ 1 & -ie_3 \end{bmatrix}, \qquad C_{22} = \begin{bmatrix} ie_3 & -1 \\ e_1 & -e_2e_3 \end{bmatrix}$$

$$C_{12} = \begin{bmatrix} 1 & 0 \\ 0 & -1 \end{bmatrix} C_{11}, \qquad C_{21} = \begin{bmatrix} -1 & 0 \\ 0 & 1 \end{bmatrix} C_{22}$$

$$C_+ = \frac{\begin{bmatrix} ie_3 & 1/e_1 \\ 1 & -e_3/e_2 \end{bmatrix}}{2(1 + e_3^2)}, \qquad C_- = C_+ \begin{bmatrix} 1 & 0 \\ 0 & -1 \end{bmatrix}$$

$$C_y = \omega^n \begin{bmatrix} \omega & 0 \\ 0 & \omega^{3/2} \end{bmatrix}, \qquad C_f = \omega^n \begin{bmatrix} \omega^{3/2} & 0 \\ 0 & \omega \end{bmatrix}$$

where n as used in this context denotes an arbitrary real constant.

APPENDIX II

EVALUATION OF THE REFLECTION MATRIX OF A FIXED END

For a fixed end, at x = 0, the boundary condition is

$$\tilde{Y} = 0.$$

Hence, using equation 9, one may obtain

$$\tilde{Y}(0) = \frac{1}{s} C_y [C_{11} R(0)q + C_{12} R(-0)r] = 0$$

or

$$q = (-C_{11}^{-1} C_{12})r.$$

For an end support which is not specialized,

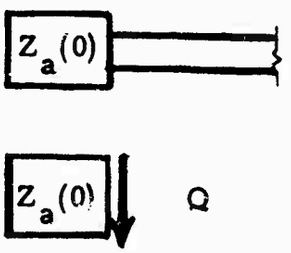

$$\tilde{Y}(x) = \frac{1}{s} C_y [C_{11} R(x)q + C_{12} R(-x)r]$$

$$\tilde{F}(x) = C_f [C_{21} R(x)q + C_{22} R(-x)r] \qquad \text{-------(a)}$$

$$\tilde{Q} = sZ\tilde{Y}$$

at x = 0

$$-\tilde{F}(0) = sZ(0)\tilde{Y}(0) \qquad \text{----------(b)}$$

Combining a and b, we get

$$-C_f [C_{21} q + C_{22} r] = Z_a(0) C_y [C_{11} q + C_{12} r].$$

After some algebraic manipulation, the following relation may be obtained:

$$q = \Gamma_a(0)r.$$

Comparing this expression with

$$q = (-C_{11}^{-1}C_{12})r,$$

it may be concluded that for a fixed end, the reflection matrix is

$$\Gamma_a(0) = C_{11}^{-1}C_{12}.$$

Similarly, it can be proved also that

$$\Gamma_b(\ell) = C_{11}^{-1}C_{12}$$

for a fixed end.

APPENDIX III

FLOW DIAGRAM OF THE RUNOUT PROGRAM

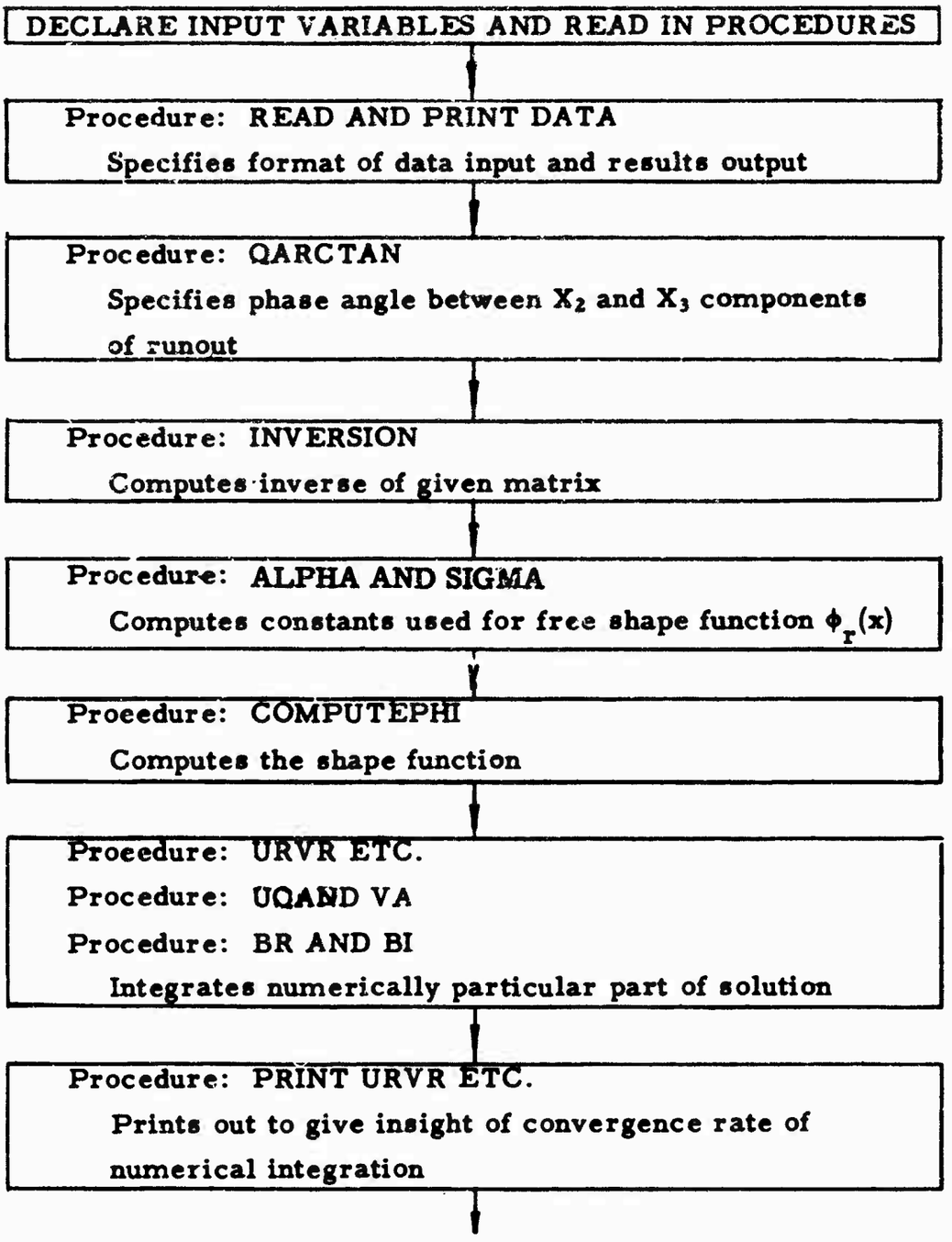

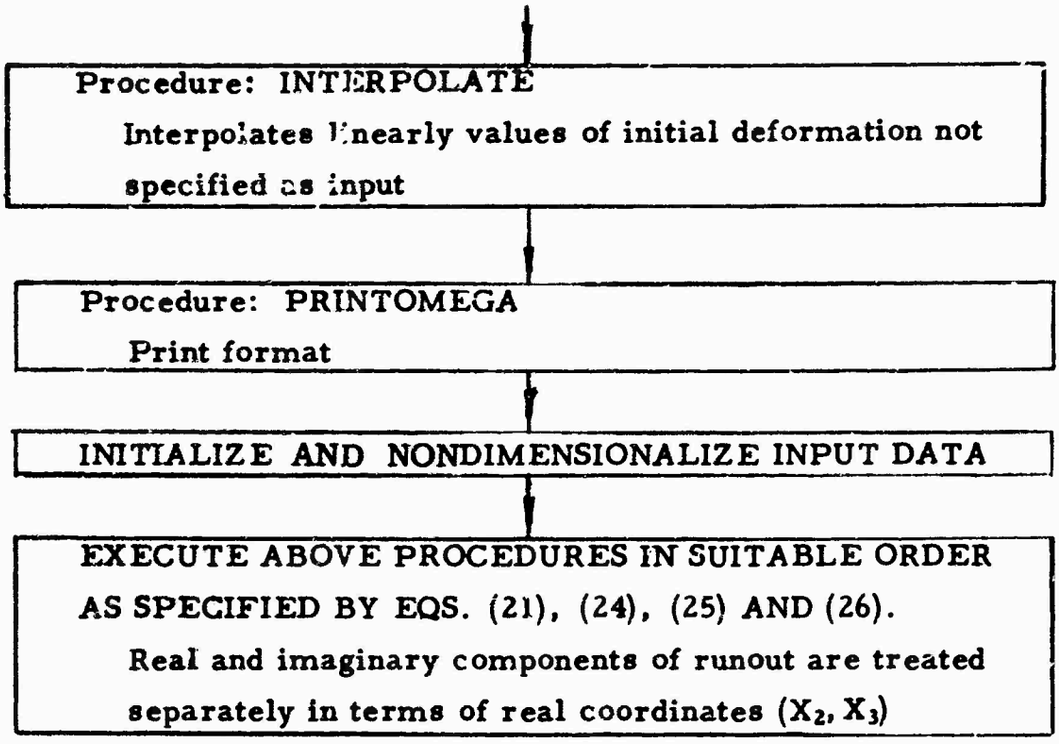
Procedure: INTERPOLATE
Interpolates linearly values of initial deformation not specified as input
Procedure: PRINTOMEGA
Print format
INITIALIZE AND NONDIMENSIONALIZE INPUT DATA
EXECUTE ABOVE PROCEDURES IN SUITABLE ORDER AS SPECIFIED BY EQS. (21), (24), (25) AND (26).
Real and imaginary components of runout are treated separately in terms of real coordinates (X_2, X_3)